Article

# Imidazole propionate is a driver and therapeutic target in atherosclerosis

https://doi.org/10.1038/s41586-025-09263-w

Received: 1 June 2023

Accepted: 9 June 2025

Published online: 16 July 2025

Open access

Check for updates

Annalaura Mastrangelo[1,30], Iñaki Robles-Vera[1,30], Diego Mañanes[1,2], Miguel Galán[1,2], Marcos Femenía-Muiña[1,3], Ana Redondo-Urzainqui[1,2], Rafael Barrero-Rodríguez[1,2], Eleftheria Papaioannou[4,5,6], Joaquín Amores-Iniesta[1], Ana Devesa[1,7,8], Manuel Lobo-González[1], Alba Carreras[9], Katharina R. Beck[9], Sophie Ivarsson[9], Anders Gummesson[9,10], Georgios Georgiopoulos[11,12,13], Manuel Rodrigo-Tapias[1,14], Sarai Martínez-Cano[1,14], Ivan Fernández-López[1], Vanessa Nuñez[1], Alessia Ferrarini[1], Naohiro Inohara[15], Kimon Stamatelopoulos[11], Alberto Benguría[1], Danay Cibrian[1,8,16], Francisco Sánchez-Madrid[1,8,16,17], Vanesa Alonso-Herranz[18], Ana Dopazo[1,8], Coral Barbas[19], Jesús Vázquez[1,8], Juan Antonio López[1,8], Alicia González-Martín[4,5,6], Gabriel Nuñez[15,19,20], Konstantinos Stellos[21,22,23,24], Göran Bergström[9,25], Fredrik Bäckhed[9,25,26,27], Valentín Fuster[1,28], Borja Ibañez[1,8,29] & David Sancho[1]✉

Atherosclerosis is the main underlying cause of cardiovascular diseases. Its prevention is based on the detection and treatment of traditional cardiovascular risk factors[1]. However, individuals at risk for early vascular disease often remain unidentified[2]. Recent research has identified new molecules in the pathophysiology of atherosclerosis[3], highlighting the need for alternative disease biomarkers and therapeutic targets to improve early diagnosis and therapy efficacy. Here, we observed that imidazole propionate (ImP), produced by microorganisms, is associated with the extent of atherosclerosis in mice and in two independent human cohorts. Furthermore, ImP administration to atherosclerosis-prone mice fed with chow diet was sufficient to induce atherosclerosis without altering the lipid profile, and was linked to activation of both systemic and local innate and adaptive immunity and inflammation. Specifically, we found that ImP caused atherosclerosis through the imidazoline-1 receptor (I1R, also known as nischarin) in myeloid cells. Blocking this ImP–I1R axis inhibited the development of atherosclerosis induced by ImP or high-cholesterol diet in mice. Identification of the strong association of ImP with active atherosclerosis and the contribution of the ImP–I1R axis to disease progression opens new avenues for improving the early diagnosis and personalized therapy of atherosclerosis.

Cardiovascular disease (CVD) is a leading cause of death worldwide, with atherosclerosis being its main determinant. Despite advances in prevention and therapy, the increase in CVD-linked morbidity and mortality highlights the need for early interventions in seemingly healthy populations. Atherosclerosis is a complex multifactorial disease whose prevention is based on traditional cardiovascular risk factor-based scores[1] that do not identify individuals at risk for atherosclerotic vascular disease at early stages[2]. Moreover, the main pharmacological interventions are bound to established risk factors (lipid metabolism[4] and recently inflammation[5,6]). This emphasizes the need for exploration of treatments that target other factors in the pathophysiology of atherosclerosis[3], particularly for patients who, despite optimal treatment, still have significant residual cardiovascular risk[6–8].

Crosstalk between the metabolisms of the microbiota and host contributes to CVD[9–11]. However, only a few gut microbiota-dependent metabolites that correlate with late stages of the disease have been described[11,12]. We sought to identify microbial metabolites associated with early stages of atherosclerotic vascular disease that could contribute to atherosclerosis progression.

## Untargeted metabolomics links ImP to atherosclerosis in mice

To screen for microbial metabolites that could affect atherosclerosis progression, we fed atherosclerosis-prone *Apoe*$^{-/-}$ mice different diets with or without antibiotic treatment to deplete the microbiota[13] (Extended Data Fig. 1a). High-cholesterol (HC) diets induced atherosclerosis, which was partially prevented upon antibiotic treatment with HC diet supplemented with choline (HC/HC) (Fig. 1a). Untargeted metabolomics showed a substantial reshaping of the plasma metabolome (Fig. 1b,c) associated with altered gut microbiota composition (Fig. 1d,e and Extended Data Fig. 1b) upon diet and antibiotic administration. First, we validated the metabolomics by demonstrating that the host-microbial co-metabolite, trimethylamine *N*-oxide (TMAO) was induced by the addition of dietary choline and associated

A list of affiliations appears at the end of the paper.

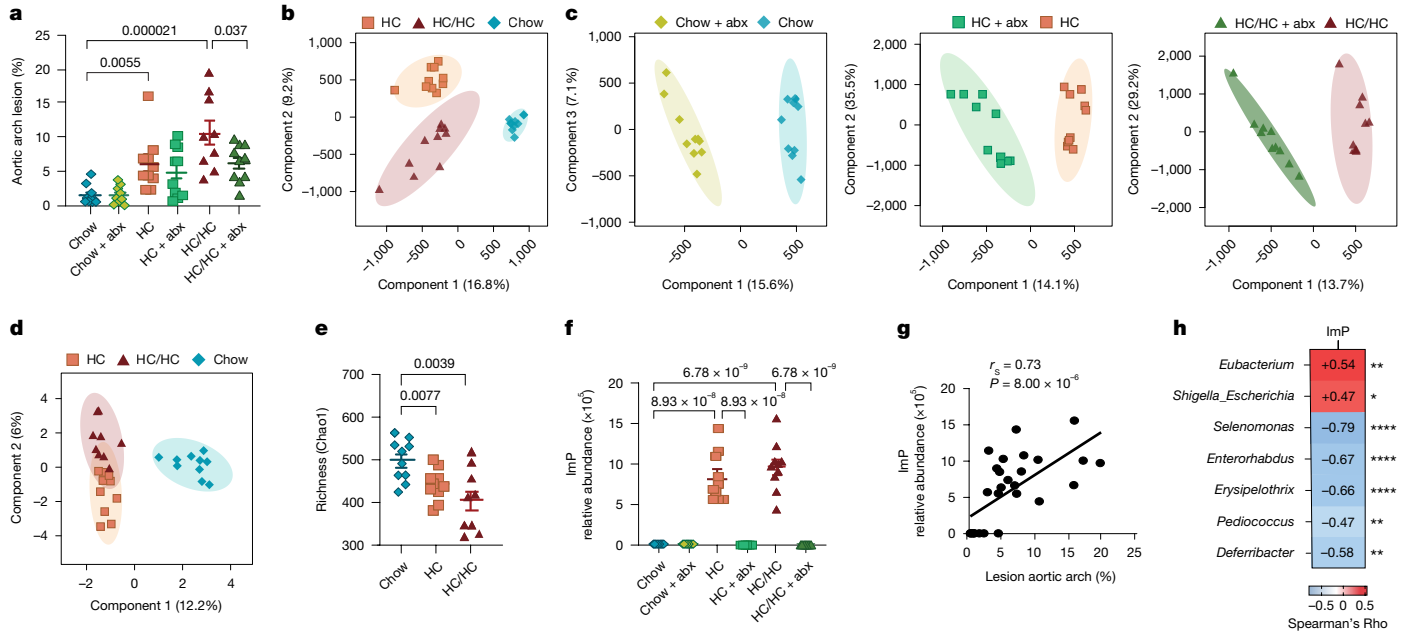


**Fig. 1 | Untargeted metabolomics unveils ImP as a microbiota-dependent metabolite that is associated with atherosclerosis.** *Apoe*$^{-/-}$ mice were fed chow, HC diet or HC/HC diet with or without antibiotics (abx) in the drinking water. **a**, Quantification of atherosclerotic plaque lesion size in the aortic arch by Oil red O staining. Each point represents an individual mouse ($n = 10$ per group for all conditions, except chow-fed mice administered antibiotics and HC/HC-fed mice, $n = 9$). **b**–**d**, Score plots of partial least squares discriminant analysis (PLS-DA) performed on liquid chromatography–mass spectrometry (LC–MS) data of plasma samples collected at endpoint (euthanasia) ($n = 10$ per group) for the three diets (**b**) and the three diets with antibiotics (**c**) and 16S rDNA sequencing analysis of caecal samples collected at endpoint (chow, HC, $n = 10$; HC/HC, $n = 9$) (**d**). **e**, Chao1 richness analysis of microbiota diversity. **f**,**g**, ImP relative abundance in plasma from *Apoe*$^{-/-}$ male mice at endpoint measured by untargeted LC–MS (**f**) and correlation with aortic arch lesion (**g**). **h**, Correlation matrix showing the correlation between ImP and gut microbiota genera (>0.1% of total abundance) in caecal samples from *Apoe*$^{-/-}$ mice fed chow, HC or HC/HC diets for 8 weeks. Data are pooled from two independent experiments (chow, HC, $n = 10$; HC/HC, $n = 9$). **g**,**h**, Correlation coefficient ($r_s$) and $P$ values are calculated by Spearman's rank-order correlation test. **a**,**e**,**f**, Individual data and arithmetic mean ± s.e.m. of each group are shown. Two-sided one-way ANOVA with Tukey post hoc correction. *$P < 0.05$, **$P < 0.01$, ****$P < 0.0001$.

with atherosclerosis in a microbiota-dependent manner[14] (Extended Data Fig. 1c,d). Notably, we identified ImP, a microbiota-dependent metabolite[15], to be highly associated with atherosclerosis upon HC feeding (Fig. 1f,g and Extended Data Fig. 1e). Plasma ImP concentration was also associated with changes in the gut microbial ecology upon dietary intervention, particularly with a relative enrichment of *Escherichia* and *Shigella*, or *Eubacterium* (Fig. 1h). However, identification of specific strains with the capacity to produce ImP requires further investigation.

## ImP is linked to subclinical atherosclerosis in humans

Next, we aimed to investigate whether increased plasma concentration of ImP was also associated with atherosclerosis in humans. We recruited 400 asymptomatic volunteers from the Progression of Early Subclinical Atherosclerosis (PESA)-Centro Nacional de Investigaciones Cardiovasculares (CNIC)-Santander prospective cohort (hereafter the PESA cohort) study[2] (Supplementary Table 1a,b). On the basis of multiterritorial and multimodal imaging (2D or 3D vascular ultrasonography and non-contrast computed tomography), we classified 295 participants with subclinical atherosclerosis and 105 controls without atherosclerosis. Extent of atherosclerosis was defined according to the number of affected vascular sites and the coronary artery calcium (CAC) score. Targeted metabolomics was used to quantify ImP and its related metabolites (histidine and urocanic acid)[15] in plasma samples. Plasma concentrations of ImP, but not histidine or urocanic acid, were selectively increased in individuals with subclinical atherosclerosis compared with controls (Fig. 2a and Extended Data Fig. 2a). Linear and non-linear associations were observed between ImP concentrations and atherosclerosis and extent of atherosclerosis, respectively (Fig. 2b). ImP was subsequently measured in an independent cohort, the impaired glucose tolerance (IGT) cohort (Supplementary Table 2a,b), comprising asymptomatic volunteers, including 529 controls and 1,315 individuals with subclinical atherosclerosis[16]. Notably, the association between ImP and early atherosclerosis was confirmed (Fig. 2c,d and Extended Data Fig. 2a).

We further explored the association between ImP, dietary patterns and the microbiota composition. Among the five main principal component analysis (PCA)-derived dietary patterns in the PESA cohort (Extended Data Fig. 2b), ImP was inversely correlated with a Breakfast1 and a Mediterranean dietary pattern (Fig. 2e), consistent with previous findings[17]. 16S ribosomal DNA (rDNA) sequencing of faecal samples detected a direct correlation of ImP with the relative abundance of *Veillonella* and *Acidaminococcus*, and inverse correlation with *Erysipelotrichaceae* and *Coriobacteriaceae* families (Fig. 2e), which are altered in individuals with CVD[18,19].

Next, we investigated the association between plasma ImP and established cardiovascular risk factors. In both cohorts, ImP directly correlated with fasting glucose and an adverse cardiometabolic profile, including increased high-sensitivity C-reactive protein (hs-CRP), body mass index (BMI), visceral fat, dyslipidaemia and hypertension, and lower high-density lipoprotein (HDL)-cholesterol (Fig. 2e,f and Supplementary Tables 1b and 2b). The prevalence of atherosclerosis endpoints and the CAC score also increased across ascending ImP tertiles (Supplementary Tables 1b and 2b). After adjusting for traditional risk factors in both cohorts, higher ImP levels were independently associated with main atherosclerosis outcomes (Fig. 2g and Supplementary Table 3), suggesting high ImP levels as indicator of increased atherosclerosis risk. Of note, ImP also showed additive value when added to established blood-derived atherosclerosis biomarkers such as

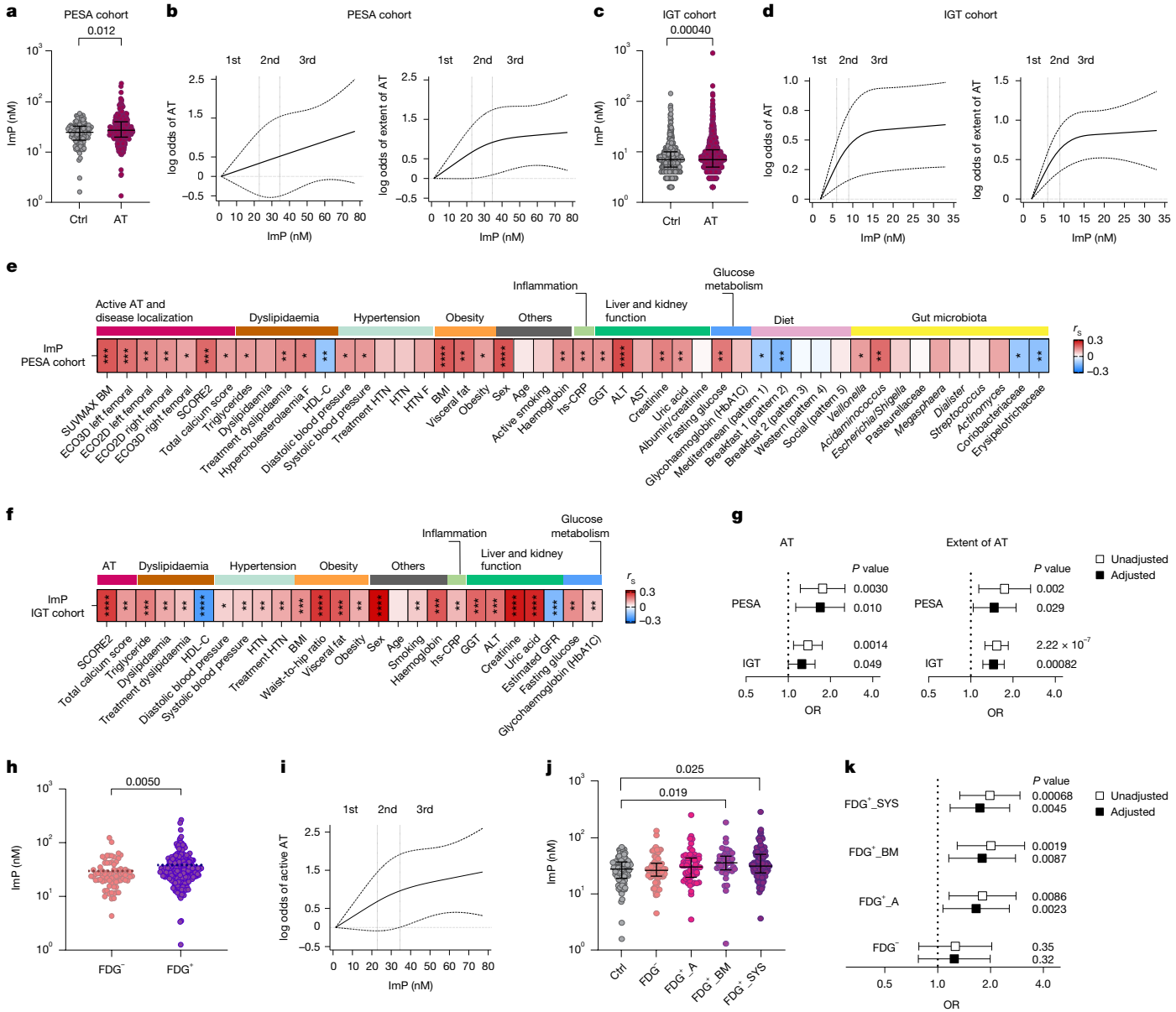


**Fig. 2 | ImP is associated with subclinical atherosclerosis in humans.** **a**,**c**, Plasma ImP in healthy individuals (Ctrl) and individuals with subclinical atherosclerosis (AT) from the PESA (**a**; Ctrl, $n = 105$; AT, $n = 295$) and IGT (**c**; Ctrl, $n = 529$; AT, $n = 1{,}315$) cohorts. **b**,**d**, Dose–response curves of plasma ImP concentration and endpoints in the PESA (**b**) and IGT (**d**) cohorts. **e**,**f**, Spearman correlation matrices between ImP and atherosclerosis traits, diet and microbiota in the PESA (**e**) and IGT (**f**) cohorts. Benjamini–Hochberg adjusted *P* values. ALT, alanine aminotransferase; AST, aspartate aminotransferase; BM, bone marrow; ECO2D, 2D vascular ultrasound; ECO3D, 3D vascular ultrasound; F, familial; GFR, glomerular filtration rate; GGT, gamma-glutamyl transferase; HTN, hypertension. **g**, Adjusted regression models for the association of ImP with atherosclerosis (left) and extent of atherosclerosis (right) in the PESA (top, $n = 400$) and IGT (bottom, $n = 1{,}844$) cohorts. Effect estimates were controlled for age, sex, smoking, creatinine, family history of CVD, haemoglobin, hypertension and LDL-C (PESA cohort) and age, smoking, family history of CVD, hypertension, LDL-C, Hb1Ac, hs-CRP and ALT (IGT cohort). Error bars show 95% confidence intervals. OR, odds ratio. **h**,**j**, Plasma ImP in individuals with inactive atherosclerosis ($FDG^-$, $n = 74$) and active atherosclerosis ($FDG^+$, $n = 221$) (**h**). $FDG^+$ individuals were further stratified according to vascular inflammation (arterial $^{18}$F-FDG uptake, $FDG^+$_A, $n = 57$), bone marrow activation ($^{18}$F-FDG uptake in bone marrow, $FDG^+$_BM, $n = 40$) and systemic inflammation (concurrent arterial and bone marrow $^{18}$F-FDG uptake, $FDG^+$_SYS, $n = 124$) (**j**). $FDG^-$ refers to the group of inactive atherosclerosis. **a**,**c**,**h**,**j**, Horizontal line represents median and error bars show interquartile range (Supplementary Tables 1a, 2a and 4). Two-tailed Mann–Whitney *U*-test. **i**, Dose–response curve for plasma ImP effect on active atherosclerosis for the PESA cohort. **b**,**d**,**i**, Dashed lines represent the 95% confidence interval; vertical lines delineate tertiles. **k**, Multinomial logistic regression for subclinical atherosclerosis in the atherosclerosis subgroups ($FDG^+$_SYS, $FDG^+$_BM, $FDG^+$_A and $FDG^-$) versus controls according to plasma ImP. Odds ratio was adjusted for age, sex, smoking, glucose, hs-CRP and haemoglobin concentration. **g**,**k**, Whiskers indicate 95% confidence intervals (values in Supplementary Tables 3 and 5). ***$P < 0.001$.

low-density lipoprotein (LDL)-cholesterol and hs-CRP in discriminating atherosclerosis prevalence in both cohorts (Extended Data Fig. 2c,d).

In the PESA cohort, individuals with subclinical atherosclerosis were further classified by $^{18}$F-fluorodeoxyglucose ($^{18}$F-FDG) uptake in arteries and/or bone marrow activation into those with metabolically active atherosclerosis ($FDG^+$) or not ($FDG^-$)[20,21]. Increased ImP plasma concentration was observed in the $FDG^+$ group, following a non-linear association with the outcome (Fig. 2h,i). Further stratification by $^{18}$F-FDG uptake (Extended Data Fig. 2e and Supplementary Table 4) revealed higher plasma ImP concentration in the subgroups of bone

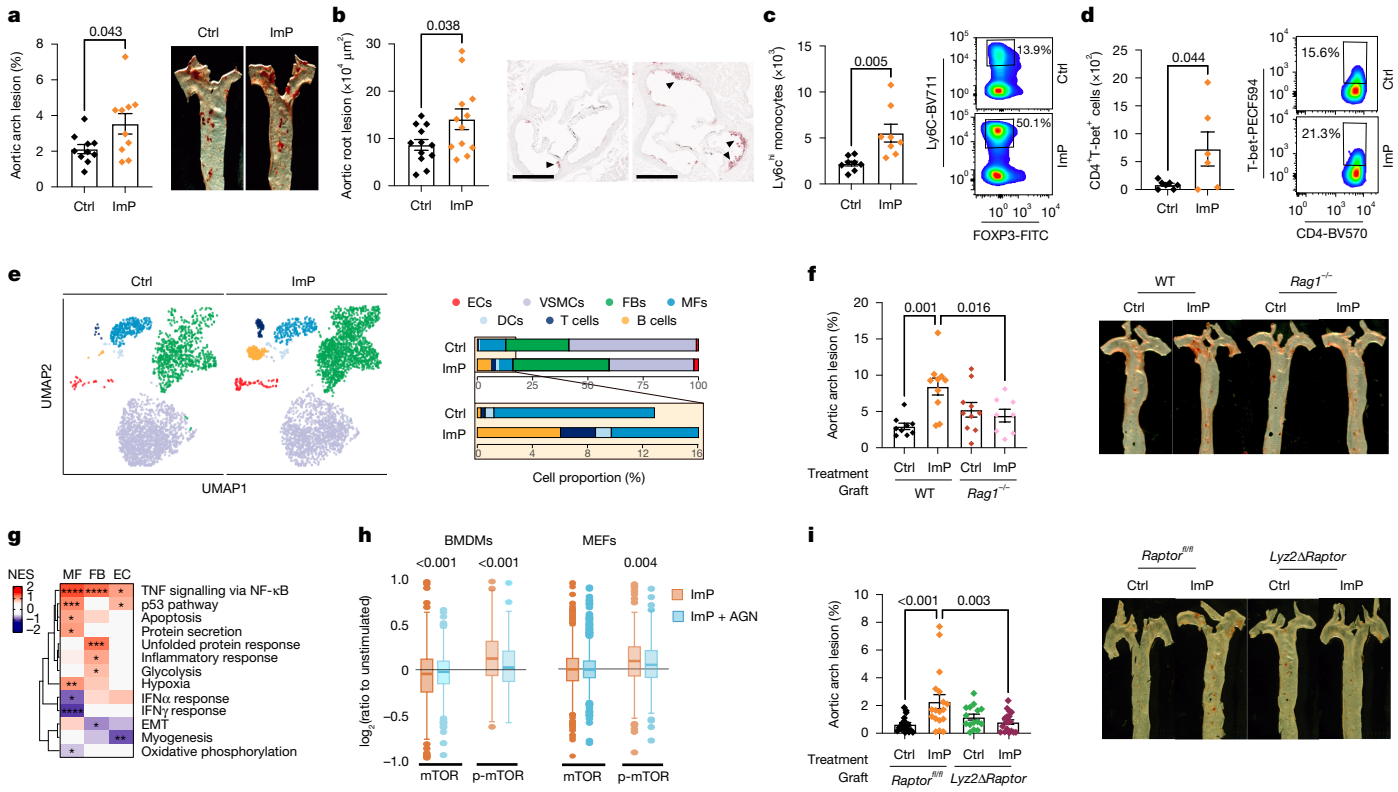


**Fig. 3 | Increased circulating ImP induces atherosclerosis and systemic inflammation in chow-fed atherosclerosis-prone mice. a**, ImP was administered (ImP) or not (Ctrl) to chow-fed *Ldlr*$^{-/-}$ mice. Oil red O staining of aortic arch (left, $n = 10$) and representative images of aorta (right). **b**–**e**, ImP was administered (ImP) or not (Ctrl) to *Apoe*$^{-/-}$ mice. **b**, Quantification (left) and representative images (right) of Oil red O staining of aortic root lesions. $n = 12$. Arrowheads indicate areas with positive Oil red O staining. Scale bars, 500 µm. **c**,**d**, Flow cytometry analysis of Ly6C$^{hi}$ monocytes ($n = 8$) (**c**) and T-bet in CD4$^+$ T cells ($n = 6$) (**d**) in blood at endpoint. Right, representative density plots for Ctrl and ImP. **e**, Uniform manifold approximation and projection (UMAP) embedding (left) and cell proportions (right) labelled by cell type of cells derived from whole aorta, based on transcriptomic profiles. DCs, dendritic cells; ECs, endothelial cells; FBs, fibroblasts; MFs, macrophages; VSMCs, vascular smooth muscle cells. **f**, *Ldlr*$^{-/-}$ mice grafted with bone marrow from wild-type (WT) (Ctrl, $n = 9$; ImP, $n = 10$) or *Rag1*$^{-/-}$ (Ctrl, $n = 10$; ImP, $n = 8$). Atherosclerosis by Oil red O staining of aortic arch (left) and representative images of aorta (right). **g**, Heat map of GSEA comparing ImP versus control for endothelial cells, fibroblasts and macrophages from scRNA-seq data of *Apoe*$^{-/-}$ mice fed chow diet for 4 weeks. EMT, epithelial–mesenchymal transition; NES, normalized enrichment score. **h**, Global abundance of peptides (mTOR) and phosphopeptides (p-mTOR) in BMDMs (left) or MEFs (right) treated with ImP for 3 h with or without AGN192403 (AGN). The $\log_2$ ratio is relative to unstimulated conditions. **i**, *Ldlr*$^{-/-}$ mice grafted with bone marrow from control *Raptor*$^{fl/fl}$ (Ctrl, $n = 17$; ImP, $n = 18$) or *Lyz2ΔRaptor* (Ctrl, $n = 15$; ImP, $n = 18$). Quantification (left) and representative images (**i**) of Oil red O staining of aorta, showing atherosclerosis in aortic arch. **a**–**d**,**f**,**i**, Individual data points and mean ± s.e.m. of at least two pooled independent experiments. **a**–**d**, Two-tailed unpaired Student's *t*-test. **f**,**i**, One-way ANOVA with Tukey post hoc correction. **g**, Two-tailed Kolmogorov–Smirnov test comparing ImP versus unstimulated. **h**, Two-tailed Wilcoxon signed rank test comparing peptide and phosphopeptide abundance in ImP versus ImP plus AGN treatments.

marrow activation (FDG$^+$_BM) and systemic inflammation (FDG$^+$_SYS; Fig. 2j). Notably, after adjusting for conventional risk factors, the association between ImP and increased risk remained significant across all subgroups of metabolically active FDG$^+$ atherosclerosis (Fig. 2k and Supplementary Table 5). Additionally, ImP demonstrated additive discriminative ability for active atherosclerosis over LDL-cholesterol and hs-CRP alone (Extended Data Fig. 2c,d). These findings reveal a strong association between ImP and atherosclerosis, particularly active atherosclerosis, suggesting its potential use as an indicator of early active atherosclerosis before other comorbidities become confounding factors.

## ImP causes atherosclerosis without cholesterol change

To further explore the effect of ImP on atherosclerosis and determine whether it causally contributed to the development of the early stages of the disease, we administered ImP in the drinking water of atherosclerosis-prone mice, including chow-fed *Ldlr*$^{-/-}$ mice, which we treated with ImP for 12 weeks (Fig. 3a and Extended Data Fig. 3a,b) and chow-fed *Apoe*$^{-/-}$ mice, which we treated with ImP for 8 weeks (Fig. 3b and Extended Data Fig. 3c–e). In both models, ImP supplementation increased atherosclerosis development in the aorta and aortic root without affecting circulating cholesterol or glucose concentration (Fig. 3a,b and Extended Data Fig. 3a–e). Feeding with HC diet alone induced ImP production (Fig. 1f). Additional ImP supplementation did not significantly exacerbate atherosclerosis in HC-fed *Apoe*$^{-/-}$ mice, although it further increased atherosclerotic lesions in *Ldlr*$^{-/-}$ mice (Extended Data Fig. 3f,g). Thus, to establish a direct ImP-dependent model of atherosclerosis for subsequent investigations, we administered ImP exclusively to chow-fed mice. Notably, *Apoe*$^{-/-}$ mice treated with ImP for eight weeks showed an expansion of proinflammatory Ly6C$^{hi}$ monocytes, and T helper 1 $T_H1$ and T helper 17 ($T_H17$) cells (Fig. 3c,d and Extended Data Fig. 4a) in the blood, which are associated with a proatherogenic environment[22].

To further understand the specific changes induced by ImP in the aorta, we performed single-cell RNA-sequencing (scRNA-seq) analysis of the whole aorta from chow-fed *Apoe*$^{-/-}$ mice that were administered ImP for four or eight weeks (Extended Data Fig. 4b–e). Mice treated with ImP for four weeks showed a mild increase in aortic arch atherosclerosis (Extended Data Fig. 4f), and some local changes in

cell population frequency in the aorta (Extended Data Fig. 4e), without changes in circulating immune cells (Extended Data Fig. 4g,h). By contrast, scRNA-seq of aortas from mice treated with ImP for eight weeks revealed an increase in the relative number of fibroblasts, endothelial cells and immune cells (Fig. 3e). The increased number of immune cells in the aorta was confirmed by flow cytometry analysis (Extended Data Fig. 4i) and histological analysis of the aortic root, which showed increased T cell infiltration in the intima–media layer and increased MAC2 staining for inflammatory macrophages in the atheroma plaque of ImP-treated mice compared with controls (Extended Data Fig. 4j,k). Remarkably, the ability of ImP to induce atherosclerosis was markedly reduced in *Ldlr*$^{-/-}$ mice grafted with *Rag1*$^{-/-}$ bone marrow, which lacks T and B cells (Fig. 3f and Extended Data Fig. 4l). These data identify ImP as a novel contributor to atherosclerosis aetiology in atherosclerosis-prone mice that is associated with activation of the immune response without affecting the bloodstream concentration of cholesterol.

## In vivo ImP alters the aortic transcriptome

To further dissect cellular targets of ImP in the aorta, we investigated transcriptional changes using scRNA-seq analysis after four weeks of treatment. Gene set enrichment analysis (GSEA) of each cell type showed increased inflammation-associated transcriptional pathways in macrophages, fibroblasts and endothelial cells following ImP treatment (Fig. 3g). Reclustering of each cell type in independent analyses identified four macrophage, five fibroblast and three endothelial cell subclusters (Extended Data Fig. 5a–c). Analysis of the ImP effect in these subclusters (including four- and eight-week data) showed a reduction in the MF1 cluster associated with homeostatic genes[23], and an increase in the MF3 cluster expressing genes associated with lipid metabolism, inflammation and macrophage activation[24–26] (Extended Data Fig. 5d,g). Increased ImP in the circulation induced expansion of aortic FB2, FB3 and FB4 subsets, which were characterized by the expression of genes associated with acetylcholine response, immune response and inflammation, and extracellular matrix organization, respectively (Extended Data Fig. 5e,g). Finally, the EC1 subset, which highly expressed genes regulating endothelial cell function[27], mesenchymal markers[28] and proangiogenesis genes[29–32] was enriched in the aorta after ImP treatment (Extended Data Fig. 5f,g).

Consistent with these results, ImP was able to activate in vitro mouse embryonic fibroblasts (MEFs) by inducing the production of active monocyte chemoattractant protein-1, which increases monocyte recruitment (Extended Data Fig. 5h,i) associated with atherogenesis[33]. Moreover, RNA-sequencing (RNA-seq) analysis showed a rapid induction of many inflammatory and activation pathways following ImP administration, particularly in bone marrow-derived macrophages (BMDMs) and in MEFs, but not in mouse aortic endothelial cells (MAECs) (Extended Data Fig. 5j), suggesting that macrophages and fibroblasts could be main targets of ImP. Of note, phosphoproteomic analysis showed increased global abundance of phosphopeptides belonging to the mTOR pathway in BMDMs and MEFs upon ImP treatment (Fig. 3h and Extended Data Fig. 5k). These results were in agreement with previous findings in primary hepatocytes[15] and the increased phosphorylated-S6 (p-S6) signal (indicative of mTOR activation) that we found in BMDMs and MEFs following ImP treatment (Extended Data Fig. 5l). Further, pre-incubation with the mTOR inhibitor, rapamycin, prevented the induction of TNF production by ImP in BMDMs and MEFs (Extended Data Fig. 5m). *Apoe*$^{-/-}$ mice fed chow diet and administered ImP for 8 weeks also had increased p-S6 in peritoneal macrophages (Extended Data Fig. 5n). Notably, selective deletion of *Raptor*[34] (also known as *Rptor*; associated with mTOR regulation) in myeloid cells of *Ldlr*$^{-/-}$ mice grafted with bone marrow from *Lyz2*Δ*Raptor* versus control *Raptor*$^{fl/fl}$ littermates prevented the induction of atherosclerosis by ImP (Fig. 3i and Extended Data Fig. 5o). These data show that ImP directly activates an mTOR-dependent inflammatory response in myeloid cells, contributing to atherogenesis.

## ImP drives atherosclerosis via I1R in myeloid cells

Since ImP contains an imidazole ring, we hypothesized that it could be sensed by the ubiquitously expressed imidazoline receptors I1R and I2R[35]. We thus treated BMDMs and MEFs with ImP in the presence of AGN192403 (I1R antagonist)[36] or idazoxan (imidazoline receptor antagonist)[35]. Since several imidazoline receptor ligands may also bind $\alpha_2$-adrenoceptors (for example, idazoxan), we included yohimbine (a $\alpha_2$-adrenoceptor antagonist with low affinity for imidazoline receptors)[35]. ImP increased p-S6 and induced TNF in BMDMs and MEFs, and this effect was selectively blocked by AGN192403 (Extended Data Fig. 6a,b). Phosphoproteomic analysis further confirmed that AGN192403 inhibited ImP-induced mTOR pathway activation (Fig. 3h). Silencing of I1R by small inhibitory RNAs (siRNAs) targeting *Nisch* in MEFs blocked ImP-induced p-S6 and TNF production, revealing that ImP signals selectively through I1R for these inflammatory functions. Of note, AGN192403 prevented ImP-induced p-S6 or TNF in control siRNA-treated cells but had no effect in I1R-silenced cells, consistent with the selective effect of this inhibitor on the ImP–I1R axis (Extended Data Fig. 6c,d).

To further analyse the function of ImP in myeloid cells we mated *Lyz2-cre* mice with *Nisch*$^{fl/fl}$ mice to generate *Lyz2ΔNisch* mice. Analysis of *Nisch* expression showed a selective deletion in spleen myeloid cells, in contrast to maintained expression in CD3$^+$ T cells of *Lyz2ΔNisch* mice compared with control *Nisch*$^{fl/fl}$ mice (Extended Data Fig. 6e). Notably, ImP-driven induction of p-S6 and TNF production by BMDMs was fully dependent on *Nisch* (Extended Data Fig. 6f,g), confirming I1R as the host ImP receptor. To determine whether blocking the ImP–I1R axis in myeloid cells would prevent the atherogenic effects of ImP, we administered ImP to *Ldlr*$^{-/-}$ CD45.1 mice grafted with bone marrow from *Nisch*$^{fl/fl}$ or *Lyz2*Δ*Nisch* mice. The absence of I1R in myeloid cells prevented ImP-induced atherosclerosis (Fig. 4a and Extended Data Fig. 6h).

To analyse the potential use of AGN192403 to prevent ImP-induced atherosclerosis we co-administered ImP and AGN192403 in drinking water to chow-fed *Apoe*$^{-/-}$ mice for eight weeks. We observed that treatment with AGN192403 inhibited the formation of ImP-induced atherosclerotic plaques in both male and female mice (Fig. 4b and Extended Data Fig. 7a,b), without affecting total cholesterol or ImP concentration in plasma (Extended Data Fig. 7c,d). AGN192403 treatment prevented ImP-induced expansion of Ly6C$^{hi}$ monocytes and $T_H1$ cells, production of proinflammatory cytokines, increase in circulating B and T cells and ImP-mediated p-S6 in peritoneal macrophages (Fig. 4c–e and Extended Data Fig. 7f). Moreover, AGN192403 treatment affected infiltration of immune cells in the aorta, by locally blocking the ability of ImP to increase the $T_H1$/T regulatory ($T_{reg}$) cell ratio (Fig. 4f and Extended Data Fig. 7g,h) and preventing ImP-induced infiltration of proinflammatory macrophages and B cells (Fig. 4g and Extended Data Fig. 7i,j). These results show that specific I1R deletion in myeloid cells and AGN192403 block ImP-induced atherosclerosis in chow-fed atherosclerosis-prone mice.

## ImP–I1R blockade prevents atherosclerosis progression

To assess the capacity of the ImP–I1R axis inhibition to treat atherosclerosis, we fed *Apoe*$^{-/-}$ mice chow or HC diets for eight weeks and treated or not with AGN192403 in the last four weeks of the HC diet. HC diet induced atherosclerosis and ImP production, and treatment with AGN192403 inhibited the progression of atherosclerosis in male and female mice, without affecting ImP concentration (Fig. 4h and Extended Data Fig. 8a–c). Notably, this treatment also reduced plaque size, necrotic core extension and caspase-3 staining (Fig. 4i and Extended Data Fig. 8d), indicative of reduced plaque complexity in mice[37]. Yet, this protective effect did not affect the increase in cholesterol concentration

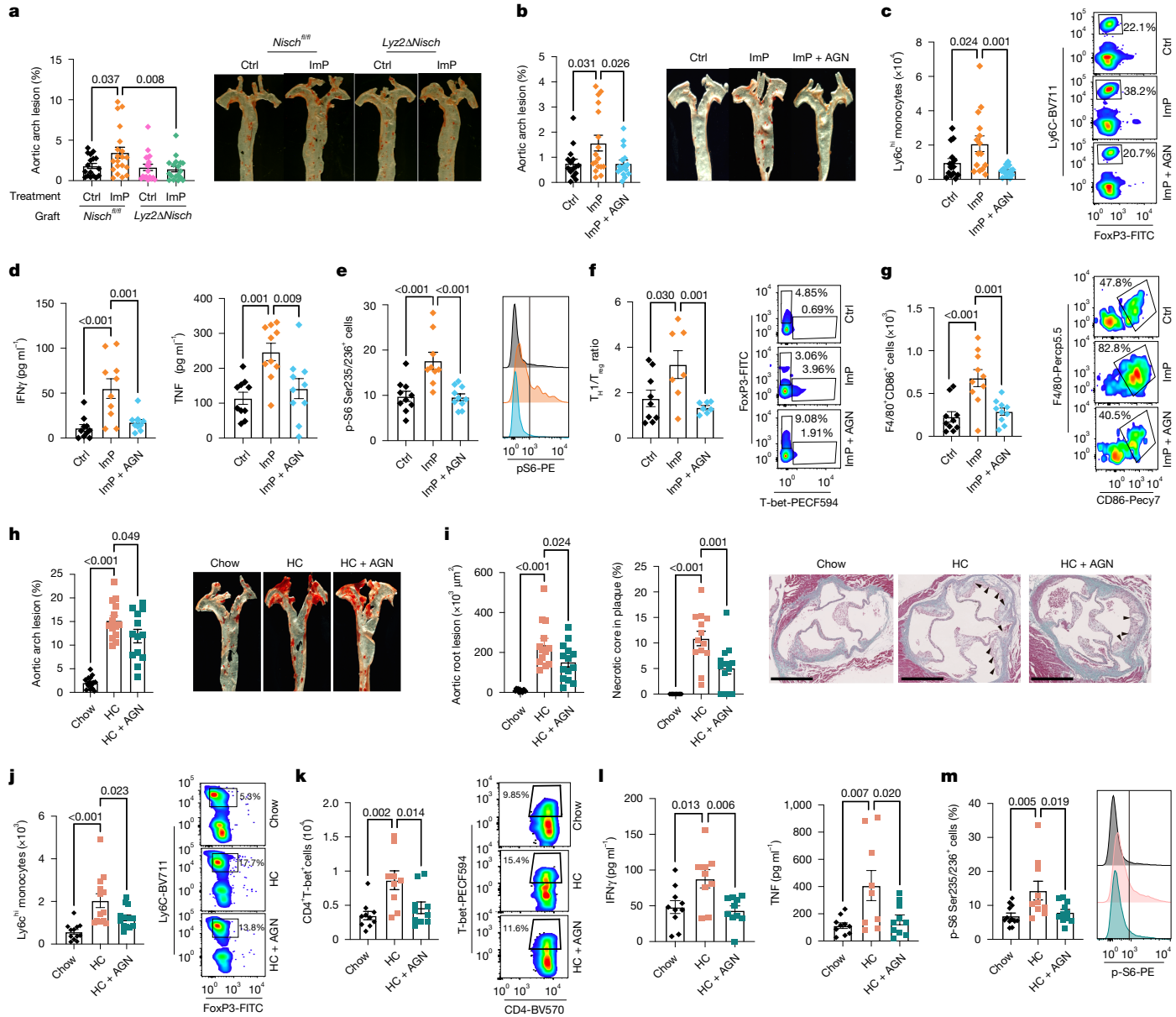


**Fig. 4 | Blockade of I1R prevents atherosclerosis induction by ImP or high-cholesterol diet. a**, *Ldlr*$^{-/-}$ mice grafted with bone marrow from control *Nisch*$^{fl/fl}$ (Ctrl, $n = 17$; ImP, $n = 20$) or *Lyz2ΔNisch* (Ctrl, $n = 19$; ImP, $n = 18$) and fed chow diet for 12 weeks. Oil red O staining of aortic arch (left) and representative images of aorta (right). **b**–**g**, Chow-fed *Apoe*$^{-/-}$ mice were treated as indicated. **b**, Oil red O staining of aortic arch (left) and representative images of aorta (right). Ctrl, $n = 15$; ImP, $n = 17$; ImP + AGN, $n = 16$. **c**, Left, Ly6C$^{hi}$ monocytes in blood at endpoint ($n = 15$). Right, representative density plots. **d**, IFNγ and TNF in plasma. $n = 10$. **e**, Left, p-S6 staining in peritoneal macrophages. Ctrl, $n = 10$; ImP, $n = 9$; ImP + AGN, $n = 10$. Right, representative histograms. **f**, Ratio of $T_H1$ to $T_{reg}$ cells infiltrated in aorta. Ctrl, $n = 9$; ImP, $n = 7$, ImP + AGN, $n = 7$. **g**, F4/80$^+$CD86$^+$ cells infiltrated in aorta. $n = 10$. **f**,**g**, Left, individual data. Right, representative density plots. **h**–**m**, *Apoe*$^{-/-}$ mice were fed a chow diet or HC diet for 8 weeks; AGN192403 was added to the HC group (HC + AGN) in the last 4 weeks. **h**, Oil red O staining of aortic arch (left) and representative images of aorta (right). Chow, $n = 15$; HC, $n = 14$; HC + AGN, $n = 13$. **i**, Masson's trichrome staining of aortic roots. Quantification of lesions in aortic roots (left), necrotic core area (middle) and representative images (right). Arrowheads indicate necrotic areas. Chow, $n = 12$; HC, $n = 13$; HC + AGN, $n = 14$. Scale bars, 500 μm. **j**,**k**, Individual data (left) and representative density plots (right) for flow cytometry quantification of blood Ly6C$^{hi}$ monocytes (**j**; chow, $n = 12$; HC, $n = 13$; HC + AGN, $n = 13$) and T-bet$^+$ CD4$^+$ $T_H1$ cells (**k**; chow, $n = 10$; HC, $n = 9$; HC + AGN, $n = 10$). **l**, Plasma IFNγ and TNF. Chow, $n = 10$; HC, $n = 9$; HC + AGN, $n = 10$. **m**, Individual data (left; chow, $n = 12$; HC, $n = 10$; HC + AGN, $n = 11$) and representative histograms (right) for p-S6 staining in peritoneal macrophages. **a**–**m**, Individual data points and mean ± s.e.m. from at least two pooled independent experiments. One-way ANOVA with Tukey post hoc correction.

in mice fed the HC diet (Extended Data Fig. 8e). Moreover, AGN192403 treatment prevented HC diet-dependent induction of blood Ly6C$^{hi}$ monocytes, $T_H1$ immunity and proinflammatory cytokines (Fig. 4j–l). The treatment also impaired HC diet-driven p-S6 induction in peritoneal macrophages (Fig. 4m). These results demonstrate that the administration of AGN192403, which inhibits the ImP–I1R axis, prevents atherosclerosis linked to immune cell activation without affecting cholesterol concentration in plasma, suggesting a novel approach for atherosclerosis therapy.

## Discussion

The complex aetiology of CVDs and the silent nature of atherosclerosis pose challenges to the detection of early stages of disease.

Previous studies have focused on associations of ImP and other microbiota-dependent metabolites with advanced stages of CVD or mortality[10,38–40]. Specifically, ImP has been related to type 2 diabetes, cardiometabolic disease in people with HIV, coronary artery disease and heart failure[15,38,40–43]. Here, we demonstrate that ImP is associated with atherosclerosis progression in mice and with subclinical active atherosclerosis in an otherwise healthy cohort, in whom atherosclerosis is detected solely through advanced imaging studies that are unavailable in the clinical practice for large population screenings[44]. These findings were independently validated in an additional IGT cohort, despite differences in the median ImP concentration in the PESA cohort, further supporting the association between ImP and early atherosclerosis and suggesting its use as a companion diagnostic and therapeutic target for personalized medicine. Moreover, we demonstrate that ImP induces atherosclerosis without influencing blood cholesterol concentration. Proatherogenic effects of ImP can be pleiotropic and act on multiple cell types[45,46]. We observed that administration of ImP induced local increase in transcriptional activity in macrophages, fibroblasts and—to a lesser extent—endothelial cells. These transcriptional changes were characterized by enhanced immune cell recruitment and inflammation, which could underlie the atherosclerosis-prone effect of ImP. In addition, ImP activated proatherogenic systemic innate and adaptive responses leading to increased infiltration by immune cells of aortic roots, contributing to atherosclerosis progression[46], which further correlates with clinical complications and unstable or vulnerable plaque[47,48]. Although ImP administration does not affect glucose concentration, blood pressure and some renal and liver function parameters, we cannot rule out that other systemic effects could contribute to the pathology, which will have to be addressed in future studies.

We identify I1R as a receptor for ImP that induces p-S6 and proinflammatory cytokine production, consistent with mTOR activation in macrophages contributing to atherosclerosis[37,49]. We find that ImP-induced atherosclerosis is fully dependent on I1R expression in myeloid cells. However, given the expression and transcriptional effects of ImP in other cell types that contribute to atherosclerosis (fibroblasts and endothelial cells), ImP may also affect these cells by boosting atherosclerosis[43]. Pharmacological blockade of I1R inhibits atherosclerosis progression and the inflammatory response induced by ImP or HC diet, independently of changes in cholesterol concentration but dependent on mTOR blocking in macrophages. Notably, I1R blockade also reduced caspase-3 staining and necrotic core at the plaque as readouts for plaque complexity associated with active and unstable plaque[37], which could underlie its association with heart failure[38]. Lipid-lowering therapy is currently used to prevent atherosclerosis progression. However, the rate of cardiovascular events remains high even in patients receiving appropriate lipid-lowering treatments[6–8]. Although other therapies are available, they are not yet established for atherosclerosis treatment and are generally bound to established risk factors[5,50,51]. Thus, we propose the ImP–I1R axis in myeloid cells as an independent target for atherosclerosis therapy that may potentially synergize with current treatments.

## Online content

Any methods, additional references, Nature Portfolio reporting summaries, source data, extended data, supplementary information, acknowledgements, peer review information; details of author contributions and competing interests; and statements of data and code availability are available at https://doi.org/10.1038/s41586-025-09263-w.


1. SCORE2 working group and ESC Cardiovascular risk collaboration. SCORE2 risk prediction algorithms: new models to estimate 10-year risk of cardiovascular disease in Europe. *Eur. Heart J.* **42**, 2439–2454 (2021).
2. Fernández-Friera, L. et al. Prevalence, vascular distribution, and multiterritorial extent of subclinical atherosclerosis in a middle-aged cohort. *Circulation* **131**, 2104–2113 (2015).
3. Libby, P. The changing landscape of atherosclerosis. *Nature* **592**, 524–533 (2021).
4. Brandts, J. & Ray, K. K. Novel and future lipid-modulating therapies for the prevention of cardiovascular disease. *Nat. Rev. Cardiol.* **20**, 600–616 (2023).
5. Ridker, P. M. et al. Antiinflammatory therapy with canakinumab for atherosclerotic disease. *N. Engl. J. Med.* **377**, 1119–1131 (2017).
6. Nelson, K., Fuster, V. & Ridker, P. M. Low-dose colchicine for secondary prevention of coronary artery disease. *J. Am. Coll. Cardiol.* **82**, 648–660 (2023).
7. Sabatine, M. S. et al. Evolocumab and clinical outcomes in patients with cardiovascular disease. *N. Engl. J. Med.* **376**, 1713–1722 (2017).
8. Kaasenbrood, L. et al. Distribution of estimated 10-year risk of recurrent vascular events and residual risk in a secondary prevention population. *Circulation* **134**, 1419–1429 (2016).
9. Chakaroun, R. M., Olsson, L. M. & Bäckhed, F. The potential of tailoring the gut microbiome to prevent and treat cardiometabolic disease. *Nat. Rev. Cardiol.* **20**, 217–235 (2023).
10. Nemet, I. et al. Atlas of gut microbe-derived products from aromatic amino acids and risk of cardiovascular morbidity and mortality. *Eur. Heart J.* **44**, 3085–3096 (2023).
11. Witkowski, M., Weeks, T. L. & Hazen, S. L. Gut microbiota and cardiovascular disease. *Circ. Res.* **127**, 553–570 (2020).
12. Nemet, I. et al. A cardiovascular disease-linked gut microbial metabolite acts via adrenergic receptors. *Cell* **180**, 862–877.e22 (2020).
13. Martínez-López, M. et al. Microbiota sensing by Mincle–Syk axis in dendritic cells regulates interleukin-17 and -22 production and promotes intestinal barrier integrity. *Immunity* **50**, 446–461.e9 (2019).
14. Wang, Z. et al. Gut flora metabolism of phosphatidylcholine promotes cardiovascular disease. *Nature* **472**, 57–63 (2011).
15. Koh, A. et al. Microbially produced imidazole propionate impairs insulin signaling through mTORC1. *Cell* **175**, 947–961.e17 (2018).
16. Royer, P. et al. Plasma proteomics for prediction of subclinical coronary artery calcifications in primary prevention. *Am. Heart J.* **271**, 55–67 (2024).
17. Molinaro, A. et al. Imidazole propionate is increased in diabetes and associated with dietary patterns and altered microbial ecology. *Nat. Commun.* **11**, 5881 (2020).
18. Koren, O. et al. Human oral, gut, and plaque microbiota in patients with atherosclerosis. *Proc. Natl Acad. Sci.* **108**, 4592–4598 (2011).
19. Trøseid, M., Andersen, G. Ø., Broch, K. & Hov, J. R. The gut microbiome in coronary artery disease and heart failure: current knowledge and future directions. *eBioMedicine* **52**, 102649 (2020).
20. Fernández-Friera, L. et al. Vascular inflammation in subclinical atherosclerosis detected by hybrid PET/MRI. *J. Am. Coll. Cardiol.* **73**, 1371–1382 (2019).
21. Devesa, A. et al. Bone marrow activation in response to metabolic syndrome and early atherosclerosis. *Eur. Heart J.* **43**, 1809–1828 (2022).
22. Ma, J., Luo, J., Sun, Y. & Zhao, Z. Cytokines associated with immune response in atherosclerosis. *Am. J. Transl. Res.* **14**, 6424–6444 (2022).
23. Gold, E. S. et al. ATF3 protects against atherosclerosis by suppressing 25-hydroxycholesterol–induced lipid body formation. *J. Exp. Med.* **209**, 807–817 (2012).
24. Wculek, S. K., Dunphy, G., Heras-Murillo, I., Mastrangelo, A. & Sancho, D. Metabolism of tissue macrophages in homeostasis and pathology. *Cell. Mol. Immunol.* **19**, 384–408 (2022).
25. Chen, J. Y., Cortes, C. & Ferreira, V. P. Properdin: a multifaceted molecule involved in inflammation and diseases. *Mol. Immunol.* **102**, 58–72 (2018).
26. Kiss, M. G. & Binder, C. J. The multifaceted impact of complement on atherosclerosis. *Atherosclerosis* **351**, 29–40 (2022).
27. Kan, H. et al. Single-cell transcriptome analysis reveals cellular heterogeneity in the ascending aortas of normal and high-fat diet-fed mice. *Exp. Mol. Med.* **53**, 1379–1389 (2021).
28. Zhao, G. et al. Single-cell transcriptomics reveals endothelial plasticity during diabetic atherogenesis. *Front. Cell Dev. Biol.* **9**, 689469 (2021).
29. Gocheva, V., Chen, X., Peters, C., Reinheckel, T. & Joyce, J. A. Deletion of cathepsin H perturbs angiogenic switching, vascularization and growth of tumors in a mouse model of pancreatic islet cell cancer. *Biol. Chem.* **391**, 937–945 (2010).
30. Shih, S.-C. et al. The L6 protein TM4SF1 is critical for endothelial cell function and tumor angiogenesis. *Cancer Res.* **69**, 3272–3277 (2009).
31. Schneller, D. et al. Cytokine-like 1 is a novel proangiogenic factor secreted by and mediating functions of endothelial progenitor cells. *Circ. Res.* **124**, 243–255 (2019).
32. Dyer, L. A., Pi, X. & Patterson, C. The role of BMPs in endothelial cell function and dysfunction. *Trends Endocrinol. Metab.* **25**, 472–480 (2014).
33. Aiello, R. J. et al. Monocyte chemoattractant protein-1 accelerates atherosclerosis in apolipoprotein E-deficient mice. *Arterioscler. Thromb. Vasc. Biol.* **19**, 1518–1525 (1999).
34. Wang, L., Lawrence, J. C., Sturgill, T. W. & Harris, T. E. Mammalian target of rapamycin complex 1 (mTORC1) activity is associated with phosphorylation of raptor by mTOR. *J. Biol. Chem.* **284**, 14693–14697 (2009).
35. Bousquet, P., Hudson, A., García-Sevilla, J. A. & Li, J.-X. Imidazoline receptor system: the past, the present, and the future. *Pharmacol. Rev.* **72**, 50–79 (2020).
36. Head, G. A. & Mayorov, D. N. Imidazoline receptors, novel agents and therapeutic potential. *Cardiovasc. Hematol. Agents Med. Chem.* **4**, 17–32 (2006).
37. Zhang, X. et al. High-protein diets increase cardiovascular risk by activating macrophage mTOR to suppress mitophagy. *Nat. Metab.* **2**, 110–125 (2020).
38. Molinaro, A. et al. Microbially produced imidazole propionate is associated with heart failure and mortality. *JACC Heart Fail.* **11**, 810–821 (2023).
39. Zhu, W. et al. Gut microbial metabolite TMAO enhances platelet hyperreactivity and thrombosis risk. *Cell* **165**, 111–124 (2016).
40. Wang, Z. et al. Gut microbiota, circulating inflammatory markers and metabolites, and carotid artery atherosclerosis in HIV infection. *Microbiome* **11**, 119 (2023).
41. van Son, J. et al. Plasma imidazole propionate is positively correlated with blood pressure in overweight and obese humans. *Nutrients* **13**, 2706 (2021).
42. Trøseid, M. et al. Gut microbiota alterations and circulating imidazole propionate levels are associated with obstructive coronary artery disease in people with HIV. *J. Infect. Dis.* **229**, 898–907 (2024).
43. Nageswaran, V. et al. Gut microbial metabolite imidazole propionate impairs endothelial cell function and promotes the development of atherosclerosis. *Arterioscler. Thromb. Vasc. Biol.* **45**, 823–839 (2025).

44. Wüst, R. C. I. et al. Emerging magnetic resonance imaging techniques for atherosclerosis imaging. *Arterioscler. Thromb. Vasc. Biol.* **39**, 841–849 (2019).
45. Gimbrone, M. A. & García-Cardeña, G. Endothelial cell dysfunction and the pathobiology of atherosclerosis. *Circ. Res.* **118**, 620–636 (2016).
46. Roy, P., Orecchioni, M. & Ley, K. How the immune system shapes atherosclerosis: roles of innate and adaptive immunity. *Nat. Rev. Immunol.* **22**, 251–265 (2022).
47. Finn, A. V., Nakano, M., Narula, J., Kolodgie, F. D. & Virmani, R. Concept of vulnerable/unstable plaque. *Arterioscler. Thromb. Vasc. Biol.* **30**, 1282–1292 (2010).
48. Wolf, D. & Ley, K. Immunity and inflammation in atherosclerosis. *Circ. Res.* **124**, 315–327 (2019).
49. Zhang, X. et al. Identification of a leucine-mediated threshold effect governing macrophage mTOR signalling and cardiovascular risk. *Nat. Metab.* **6**, 359–377 (2024).
50. Lloyd-Jones, D. M. et al. 2017 focused update of the 2016 ACC expert consensus decision pathway on the role of non-statin therapies for LDL-cholesterol lowering in the management of atherosclerotic cardiovascular disease risk: a report of the American College of Cardiology Task Force on Expert Consensus Decision Pathways. *J. Am. Coll. Cardiol.* **70**, 1785–1822 (2017).
51. Gupta, A. et al. Adverse events associated with unblinded, but not with blinded, statin therapy in the Anglo-Scandinavian Cardiac Outcomes Trial—Lipid-Lowering Arm (ASCOT-LLA): a randomised double-blind placebo-controlled trial and its non-randomised non-blind extension phase. *Lancet* **389**, 2473–2481 (2017).





[1]Centro Nacional de Investigaciones Cardiovasculares Carlos III (CNIC), Madrid, Spain. [2]Escuela de Doctorado, Universidad Autónoma de Madrid, Madrid, Spain. [3]Escuela de Doctorado, Universidad Complutense de Madrid, Madrid, Spain. [4]Institute for Biomedical Research Sols-Morreale (IIBM), Spanish National Research Council–Universidad Autónoma de Madrid, Madrid, Spain. [5]Department of Biochemistry, School of Medicine, Universidad Autónoma de Madrid, Madrid, Spain. [6]Hospital La Paz Institute for Health Research–IdiPAZ, Madrid, Spain. [7]Mount Sinai Fuster Heart Hospital, Icahn School of Medicine at Mount Sinai, New York, NY, USA. [8]CIBER de Enfermedades Cardiovasculares (CIBER-CV), Madrid, Spain. [9]The Wallenberg Laboratory, Department of Molecular and Clinical Medicine, University of Gothenburg, Gothenburg, Sweden. [10]Department of Clinical Genetics and Genomics, Sahlgrenska University Hospital, Gothenburg, Sweden. [11]Department of Clinical Therapeutics, National and Kapodistrian University of Athens Medical School, Athens, Greece. [12]School of Biomedical Engineering and Imaging Sciences, King's College London, London, UK. [13]Department of Physiology, School of Medicine, University of Patras, Patras, Greece. [14]Inmunotek SL, Alcalá de Henares, Spain. [15]Department of Pathology, University of Michigan Medical School, Ann Arbor, MI, USA. [16]Department of Immunology, Instituto de Investigación Sanitaria del Hospital Universitario de La Princesa, Madrid, Spain. [17]Department of Medicine, Universidad Autónoma de Madrid (UAM), Madrid, Spain. [18]Centro de Metabolómica y Bioanálisis (CEMBIO), Facultad de Farmacia, Universidad San Pablo-CEU, Boadilla del Monte, Spain. [19]Rogel Cancer Center, University of Michigan Medical School, Ann Arbor, MI, USA. [20]Center for Infectious Disease Education and Research (CIDER), Osaka University, Osaka, Japan. [21]Department of Cardiovascular Research, European Center for Angioscience (ECAS), Medical Faculty Mannheim, Heidelberg University, Mannheim, Germany. [22]German Centre for Cardiovascular Research (DZHK), Partner Site Heidelberg/Mannheim, Mannheim, Germany. [23]Department of Medicine VI, University Medical Centre Mannheim, Heidelberg University, Mannheim, Germany. [24]Helmholtz-Institute for Translational AngioCardioScience (HI-TAC) of the Max Delbrück Center for Molecular Medicine in the Helmholtz Association (MDC), Heidelberg University, Mannheim, Germany. [25]Department of Clinical Physiology, Sahlgrenska University Hospital, Gothenburg, Sweden. [26]Novo Nordisk Foundation Microbiome Health Initiative, Technical University of Denmark, Kongens Lyngby, Denmark. [27]National Food Institute, Technical University of Denmark, Kongens Lyngby, Denmark. [28]The Zena and Michael A. Wiener Cardiovascular Institute, Icahn School of Medicine at Mount Sinai, New York, NY, USA. [29]Health Research Institute, Fundación Jiménez Díaz, Universidad Autónoma de Madrid (IIS FJD-UAM), Madrid, Spain. [30]These authors contributed equally: Annalaura Mastrangelo, Iñaki Robles-Vera. ✉e-mail: dsancho@cnic.es

# Methods

## Mice

Mice were bred and maintained in groups of five animals per cage at the CNIC under specific pathogen-free conditions. We used proatherogenic background B6.129P2-*Apoe*$^{tm1Unc}$/J mice (The Jackson Laboratory, strain 002052, *Apoe*$^{-/-}$); B6.129S7-*Ldlr*$^{tm1Her}$/J mice (The Jackson Laboratory, strain 002207, *Ldlr*$^{-/-}$) backcrossed with B6.SJL-*Ptprc*$^{a}$ *Pepc*$^{b}$/BoyJ mice expressing the CD45.1 congenic marker (The Jackson Laboratory, strain 002014, B6 CD45.1); B6.129S7-*Rag1*$^{tm1Mom}$/J mice (The Jackson Laboratory, strain 002216, *Rag1*$^{-/-}$); B6.Cg-*Rptor*$^{tm1.1Dmsa}$/J mice (The Jackson Laboratory, strain 013188, *Rap*$^{loxP}$) were mated with B6.129P2-*Lyz2*$^{tm1}$*(cre)Ifo*/J mice (The Jackson Laboratory, strain 004781, *Lyz2-cre*) to generate Lyz2Δ*Raptor* (Cre$^{+}$) and control *Raptor*$^{fl/fl}$ (Cre$^{-}$) littermates used as controls. Sperm from B6.Nisch$^{tm1a(EUCOMM)Hmgu>/H}$ mice (Mary Lyon Centre at MRC Harwell, UK; EM:08808) was used for in vitro fertilization of ROSA-Flpe mice (Gt(ROSA)26Sor$^{tm1(FLP1)Dym}$) to generate *Nisch*$^{fl/fl}$ mice (tm1c). *Nisch*$^{fl/fl}$ mice were mated with *Lyz2-cre* (B6.129P2-*Lyz2*$^{tm1}$*(cre)Ifo*/J) mice to generate *Lyz2*Δ*Nisch* (Cre$^{+}$) and control *Nisch*$^{fl/fl}$ (Cre$^{-}$) littermates used as controls. Mice were 7- to 12-week-old at the initiation of experiments. Littermates of the same sex were randomly assigned to experimental groups. Investigators were blinded to group allocation during data collection and analysis to reduce bias. Animal studies were approved by the local ethics committee at CNIC, UAM and Comunidad de Madrid, PROEX 300.4/21 and PROEX 119.6/22. All animal procedures conformed to European Union Directive 2010/63EU and Recommendation 2007/526/EC regarding the protection of animals used for experimental and other scientific purposes, enforced by Spanish law under Real Decreto 53/2013. Mice were fed different diets, including chow, HC (10% fat, 0.75% cholesterol, SSNIFF S9167-E011) and HC/HC (HC + 1% choline, SSNIFF S9167-E016), as indicated in each experiment. ImP (400 µg per mouse per day, Biogen Cientifica BA-F-3185.0001) was administered in the drinking water. AGN192403 (30 µg per mouse per day, Labclinics B6583-10) was administered in the drinking water.

## Antibiotic administration

For ablation of intestinal bacteria, an antibiotic cocktail of 1 g l$^{-1}$ each of ampicillin (Normon), neomycin sulfate (Sigma Aldrich) and metronidazole (Sanofi), 0.5 g l$^{-1}$ vancomycin (Normon) and 4 mg ml$^{-1}$ sucralose (Sigma Aldrich) dissolved in water was used and replenished every three days as described[52].

## Quantification of lesions in the aorta

For atherosclerotic lesion measurements, *Apoe*$^{-/-}$ or *Ldlr*$^{-/-}$ male or female mice were fed a chow or high-cholesterol diet for 4, 8 or 12 weeks, as indicated in each experiment. Blood was collected from submandibularly punctured mice. Next, mice were perfused with 10 ml phosphate buffered saline (PBS) via cardiac puncture to remove blood contamination from vascular tissue. The aortas were dissected and fixed in formaldehyde 4% w/w (PanReac, AppliChem) at room temperature overnight. Then, the exposed aortas were stained for lipid depositions with Oil Red O (Sigma Aldrich) prior en face assay assessment. In brief, after fixation, aortas were washed with 60% isopropanol and stained for one hour with 2.5 mg ml$^{-1}$ of Oil Red O. After two washing steps of 5 min with isopropanol 60%, aortas were stored in PBS-azide 0.05%. Images were taken with Leica Nikon camera magnifier and atherosclerotic lesions in the aorta were quantified by calculating the ratio of the lesion area to the total surface area. This measurement was carried out using an automated method that quantifies lipid accumulation in the lesions by applying colour thresholding to the Oil red O-positive areas. The threshold was set by the researcher and remained consistent within the same staining batch, as described[53]. Analysis of the images was performed using ImageJ software.

## Aortic roots histology

Perfused hearts were fixed with 4% formaldehyde for 48 h at room temperature. For paraffin sectioning, fixed hearts were incubated overnight in 70% ethanol and embedded in paraffin blocks. Four-micrometre sections of the aortic roots were cut and dried overnight at 37 °C. The trichrome protocol used was a standard Masson's trichrome protocol using Weigert's haematoxylin for nuclei and light green as a collagen stain. Trichrome stain was used to analyse plaque and necrotic core (identified as unstrained regions inside plaque). T cell staining in the heart aortic roots was performed by immunohistochemistry using a CD3 antibody (Invitrogen, MA1-90582). Macrophage staining in the atheroma plaque was performed by immunohistochemestry using a MAC2 antibody (Invitrogen, 14-5302-85). Caspase-3 staining was carried out in the heart aortic roots using anti-caspase-3 antibody (Cell Signaling Technology, 9661). Staining was performed in an automated autostainer (Autostainer Plus, Dako). As secondary antibodies we used anti-rabbit (Dako Envision K4003) for CD3 and caspase-3 staining and rabbit anti-rat (Abcam Ab6734) for MAC2. The digitalized images were obtained using the Carl Zeiss Axio Scan Z1 scanner. Analysis of the images was performed using NDPview 2 and ImageJ software.

## Caecal content collection

At the culling, the caecum was resected and rinsed with PBS to collect its contents, which were stored at −80 °C until sample processing.

## Serum analysis

Blood samples were obtained by cardiac puncture. The serum was collected after blood centrifugation at 1,000*g* for 10 min and frozen at −80 °C. Serum biochemical parameters were analysed with a Dimension RxL Max automated analyser the day after the extraction. Glucose and protein content were measured with Dimension RxL Max automated analyser.

## LC–MS untargeted metabolomics

**Materials.** LC–MS grade acetonitrile was from Fluka Analytical; methanol and water were from Fischer Scientific; ethanol was from Merck and formic acid was from Honeywell Fluka.

**Sample preparation.** Plasma samples (50 µl) were prepared as described[54]. In brief, proteins were removed by adding a cold (−20 °C) mixture of methanol:ethanol (1:1, v/v) in a ratio 5:1 (solvent:sample) and by storing the samples on ice for 20 min. Blank sample was prepared following the same extraction procedure, adding only the solvents to a 1.5 ml Eppendorf tube. Quality control samples (QCs) were prepared by pooling 100 µl plasma samples from independent *Apoe*$^{-/-}$ mice and following the same extraction procedures. Samples, QCs and blank, were centrifuged at 16,400*g* for 20 min 4 °C and the supernatant was transferred in a 1.5 ml Eppendorf tube. Supernatants were subsequently dried-out in speedvac (Savant SPD131DDA concentrator, Savant RVT5105 refrigerated vapour trap and OFP400 vacuum pump, Thermo Fisher Scientific) for 2 h at room temperature. Before LC–MS analysis, the dried samples and QCs were resuspended in 50 µl and 100 µl of a mixture composed of acetonitrile:$H_2O$ (90:10, v:v) by constant shaking at 1,000 rpm for 10 min at 8 °C and then centrifuged at 16,400*g* for 5 min to remove insoluble material. The soluble part was placed in the insert of the LC–MS vial.

**LC–MS analysis.** Metabolomics untargeted analysis was performed using an Ultimate 3000 HPLC system consisting of a degasser, two binary pumps, and autosampler with thermostat, maintained at 8 °C (Thermo Fisher Scientific) coupled to a LTQ Orbitrap XL Hybrid Ion Trap-Orbitrap Mass Spectrometer (Thermo Fisher Scientific). The samples (5 µl) were injected onto a Merck SeQuant ZIC-HILIC column (150 × 1 mm, 3.5 µm), which was maintained thermostatically at 45 °C,

and metabolites were eluted at 180 µl $min^{-1}$ with solvent A composed of water with 0.1% formic acid, and solvent B composed of acetonitrile with 0.1% formic acid. The gradient started from 90% to 25% of B in 15 min, keeping constant for 3 min and returned to starting conditions in 0.1 min, finally by keeping the re-equilibration at 90% of B for 11.9 min. Data were collected in positive ESI ion mode. The mass spectrometer operated in full scan mode from 70 to 1,000 *m/z* at 60,000 resolution. MS/MS spectra were collected in data-dependent mode via collision induced dissociation (CID) in the ion trap. Samples were analysed in a randomized order. QCs were analysed at the beginning, at the end and every six samples.

**Data handling.** Generated data were firstly aligned using Compound Discoverer (Thermo Fisher Scientific); signals were extracted and grouped into features (isotopic traces from a single analyte at a particular charge state) using the Metaboprofiler node in Compound discoverer (open source plug-in freely available from OpenMS; https://openms.de/) as described[55]. Features were then filtered by presence keeping the entities that were present in at least 80% of the samples from the same group. Missing values were imputed using the *k*-nearest neigbours method or by limit of detection (LoD) (1/5 of the minimum positive value of each variable) according to the percentage of missing values of the feature within the group in MetaboAnalyst v.5 (https://www.metaboanalyst.ca/MetaboAnalyst/home.xhtml)[56]. Data were autoscaled and log-transformed. Metabolites were annotated by searching their accurate experimental mass against the Ceu Mass Mediator (http://ceumass.eps.uspceu.es/)[57] and the resulting data matrix handled by Turboputative (https://proteomics.cnic.es/TurboPutative/)[58]. Identification of ImP was then confirmed by using the reference standard (Sigma Aldrich 77951) in a subsequent LC–MS/MS analysis following higher-energy collisional dissociation by using 50 eV as collisional energy.

### Flow cytometry analysis

For blood samples, single-cell suspensions were stained for 30 min at 4 °C with LIVE/DEAD Fixable Aqua Dead Cell Stain Kit (Life Technologies). After washing with PBS, cells were stained in FACS buffer containing anti-CD16/32 (BioXcell), 3% FBS and 0.05% EDTA with the corresponding antibody cocktail for 30 min on ice. Cells were stained with a cocktail of antibodies against CD45-APCCy7 (Biolegend), CD11b-BV605 (Biolegend), CD11c-BV650 (Biolegend), Ly6C-BV711 (Biolegend), LY6G-APC (BD Biosciences), CD8-PE (eBioscience), CD90-BV785 (BD Biosciences), MHCII-AF700 (Biolegend), B220-PerCP5.5 (Biolegend), SiglecH-FITC (eBioscience), CD4-PeCy7 (Biolegend). In another set of experiments, cells were stained with, CD45-APCCy7 (Biolegend), LY6G-V450 (BD Biosciences), CD11b-ef660 (eBioscience), CD11c-PE (Biolegend), B220-PerCP (Biolegend), CD90-UV805 (Fisher scientific), XCR1-BV785 (Biolegend), CD206-eF450 (Biolegend), MHCII-UV737 (BD Biosciences), F4/80-PerCp5.5 (Biolegend), Rorγt-APC (Biolegend), T-bet-PECF594 (BD Biosciences), Ly6C-BV711 (Biolegend), CD86-PECy7 (Biolegend), FOXP3-FITC (Biolegend), CD4-BV570 (Biolegend). Cells were washed again and resuspended in FACS buffer for data acquisition using an LSRFortessa SORP (Becton Dickinson) or a FACSymphony (Becton Dickinson) flow cytometry equipment and analysed with FlowJo software version 10 (TreeStar). The gating strategies used for these analyses are detailed in Supplementary Fig. 1.

To perform flow cytometry analysis of cells infiltrating the aorta, mice were perfused with 10 ml PBS via cardiac puncture to remove blood contamination from vascular tissue. Aortas were kept in cold Dulbecco's modified Eagle medium (DMEM) to be digested. Perivascular fat was removed and the thoracic aorta with arch was opened longitudinally and cut into smaller pieces that were incubated for 30 min at 37 °C in a water bath in digestion buffer (Collagenase A (25 mg $ml^{-1}$), (Roche/Sigma 10103586001), Dispase II (25 mg $ml^{-1}$), (Roche/Sigma 04942078001), DNase I (250 µg $ml^{-1}$) (Roche/Sigma 10104159001) elastase (25 µg $ml^{-1}$) and Libersase TL (0.2 Wünsch units per ml, 5401119001)). After incubation time the digested tissue was mixed by pipetting, filtered through a 70-µm strainer and spinned at 400*g* 5 min at 4 °C. Single cells were stained with a cocktail of antibodies against CD45-APCCy7 (Biolegend), CD11b-BV605 (Biolegend), CD11c-BV650 (Biolegend), Ly6C-BV711 (Biolegend), LY6G-APC (BD Biosciences), CD8-PE (eBioscience), CD90-BV785 (BD Biosciences), MHCII-AF700 (Biolegend), B220-PerCP5.5 (Biolegend), SiglecH-FITC (eBioscience), CD4-PeCy7 (Biolegend). Depending on the experimental setting, cells were stained with CD45-APCCy7 (Biolegend), LY6G-V450 (BD Biosciences), CD11b-ef660 (eBioscience), CD45-APCCy7 (Biolegend), LY6G-V450 (BD Biosciences), CD11b-ef660 (eBioscience), CD11c-PE (Biolegend), B220-PerCP (Biolegend), CD90-UV805 (Fisher scientific), XCR1-BV785 (Biolegend), CD206-eF450 (Biolegend), MHCII-UV737 (BD Biosciences), F4/80-PerCp5.5 (Biolegend), Rorγt-APC (Biolegend), T-bet-PECF594 (BD Biosciences), Ly6C-BV711 (Biolegend), CD86-PECy7 (Biolegend), FOXP3-FITC (Biolegend), CD4-BV570 (Biolegend), CD31-PE (Biolegend) and VCAM-AF594 (Biotechne). Cells were washed and resuspended in FACS buffer for data acquisition using a LSRFortessa SORP (Becton Dickinson) or a FACSymphony (Becton Dickinson) flow cytometry equipment and analysed with FlowJo software version 10 (TreeStar). Gating strategies for B cells, T cells, $T_H1$ and $T_{reg}$ cells are shown in Supplementary Fig. 2, and those for macrophage subsets are shown in Supplementary Fig. 3.

### Study populations

**PESA cohort.** This study was conducted in a subset of participants ($n = 400$) from the PESA study[59]. The PESA-CNIC-Santander (NCT01410318) is an ongoing observational prospective cohort study of 4,184 asymptomatic employees of the Santander Bank in Madrid (from 40 to 54 years of age and free of known CVD at baseline in 2009). In addition to the exclusion criteria followed in the main study[2], participants taking antibiotics in the three months prior to the sample collection, with known type 2 diabetes or those treated for diabetes and/or intestinal disorders were excluded. This enabled us to remove possible confounding effects due to the role of ImP in diabetes and insulin resistance[15] and the modification of gut microbiota possibly affecting the production of ImP. Subclinical atherosclerosis was assessed by imaging studies including 2D and 3D vascular ultrasonography of carotid and iliofemoral arteries and presence of coronary artery calcium assessed by CT scan, as previously described[59]. Participants with subclinical atherosclerosis underwent a whole body $^{18}$F-FDG PET/MRI study to characterize arterial $^{18}$F-FDG uptake and bone marrow metabolic activity, as described[20,21]. The cardiovascular risk score used included the European Society of Cardiology SCORE (Systematic Coronary Risk Evaluation), which calculates 10-year risk of fatal CVD[1]. Fasting blood test included biochemistry and determination of hs-CRP. In this study, hypertension was defined as systolic >130 mmHg and/or diastolic >85 mmHg and/or individuals taking antihypertensive drugs. Dyslipidaemia was defined as total cholesterol ≥240 mg $dl^{-1}$, LDL-cholesterol ≥160 mg $dl^{-1}$, HDL-cholesterol <40 mg $dl^{-1}$, or use of lipid-lowering drugs. Anthropometry and bioelectrical impedance analysis assessments were performed during the same appointment for each participant. Height and weight were measured using calibrated equipment (Tanita BC-545N,) with participants wearing underwear and barefoot. BMI was calculated as weight (in kg) divided by height (in metres) squared. Extent of atherosclerosis was defined by a summed ordinal variable that is calculated by the number of affected vascular sites into a sum of total points as follows: (1) carotid atherosclerosis (points: 0, no plaque; 1, 1 plaque; 2, 2 plaques; 3, 3 or more plaques) as estimated by 3D vascular ultrasonography and summed for both left and right carotid artery; (2) femoral atherosclerosis (points: 0, no plaque; 1, 1 plaque; 2, 2 plaques; 3, 3 or more plaques) as estimated by 3D vascular ultrasonography and summed for both left and right femoral artery; (3) presence of calcification in the ascending or descending

aorta (points: 0, no; 1, yes); (4) CAC score (points: 0, 0; 1, 0.1–99; 2, 100–399; 3, 400–maximum). For the metabolomic analysis, peripheral blood samples collected after overnight fasting were centrifuged at 2,750*g* at room temperature for 10 min to obtain plasma that was further aliquoted and stored at −80 °C. For 16S rDNA amplicon gene sequencing analysis, faeces were collected in collection cups and immediately frozen at −80 °C until further analysis. The institutional ethics committee approved the study protocol, and all participants were provided with written informed consent. Characteristics of the participants are listed in Supplementary Tables 1a,b and 3.

**IGT cohort.** To validate the findings from the PESA study, a subset of the IGT cohort was used (Ethics 560-13). Subject and method design from the validation cohort have been described elsewhere[16]. In brief, the study population comprises men and women aged 50–64 years from the Gothenburg area (Sweden), recruited on a random basis from the Swedish population register and included based on their glucose status. The applied exclusion criteria included: known diabetes, inflammatory diseases (for example, Crohn's disease, ulcerative colitis or rheumatic diseases), treatment with steroids or immunomodulatory drugs, cancer (unless relapse free for the preceding five years), cognitive dysfunction, treatment for infectious diseases and with antibiotics in the past three months, inability to understand written and spoken Swedish as well as individuals born outside Sweden. The participants were invited by letter and gave all informed consent. Atherosclerosis was assessed by ultrasound imaging of carotid arteries, using a standardized protocol including a Siemens Acuson S2000 ultrasound scanner, and by presence of coronary artery calcium assessed by CT scan, as previously described[16]. Systolic blood pressure was measured twice with an automatic device (Omron M10-IT, Omron Health Care Company) and the mean of the measurements was used. A questionnaire was used to collect detailed information on medication and family history. A venous blood sample (100 ml) was collected from participants after an overnight fast and was used for immediate biochemical analysis of glucose, glycated haemoglobin and total cholesterol. SCORE2 (systematic coronary risk evaluation) was calculated as described[1]. Body weight, height, waist and hip circumference were measured on calibrated equipment with participants dressed in light clothing without shoes and according to current WHO recommendations. Extent of atherosclerosis was defined by a summed ordinal variable that is calculated by the number of affected vascular sites into a sum of total points as follows: (1) carotid atherosclerosis (points: 0, no plaque; 1, at least 1 plaque at either left or right carotid; 2, plaques at both vessels); (2) CAC score (points: 0, 0; 1, 0.1–99; 2, 100–399; 3, 400–maximum). Characteristics of the participants are listed in Supplementary Table 2a,b.

### Targeted metabolomics

Plasma levels of ImP, urocanic acid and histidine were quantified using ultra high-performance liquid chromatography (UHPLC) coupled to tandem mass spectrometry (LC–MS/MS). Analyses were performed in two different laboratories in Spain (PESA cohort) and in Sweden (IGT cohort). Both laboratories have used fully validated LC–MS/MS methods.

The determination of ImP in plasma samples from *Apoe*$^{-/-}$ mice fed a chow or high-cholesterol diet with and without ImP (400 µg per mouse per day) and/or AGN192403 (30 µg per mouse per day) in the drinking water was carried out by following the method described below for the human study, specifically for the PESA cohort.

**Working solutions and standards.** For the PESA cohort, individual 1,000 ppm stock solutions of ImP (Sigma Aldrich 77951), urocanic acid (urocanic acid-1,2,3-$^{13}$C3, Sigma Aldrich, 709638) and histidine (L-histidine-$d_3$ hydrochloride monohydrate, Sigma Aldrich, 791318) were prepared in ultrapure water and stored at −20 °C. Their respective dilutions were then prepared in methanol:ethanol (1:1, v/v) and stored at 4 °C. For the IGT cohort, histidine (histidine-$d_5$ $^{15}N_3$, Cambridge Isotope Lab), ImP and urocanic acid (ImP-$^{13}C_3$ and urocanate-$^{13}C_3$, Astra Zeneca) were prepared in acetonitrile.

**Metabolite quantification.** For the PESA cohort, 65 µl of methanol: ethanol (1:1, v/v) were added to 50 µl of plasma sample and 35 µl of isotopically labelled internal standards in methanol:ethanol (urocanic acid and histidine). Samples were vortex-mixed for 10 s and then centrifuged at 13,000 rpm for 20 min at 4 °C. One-hundred microlitres of supernatant were taken and transferred to liquid chromatography vials for the analysis. Quantification of the metabolites was performed by using an UHPLC system 1290 Infinity series coupled to a triple quadrupole (QqQ) 6460 MS from Agilent Technologies. In brief, 1 µl of the sample was injected onto an InfinityLab Poroshell 120 HILIC-Z column (2.7 µm, 150 × 2.1 mm, Agilent Technologies) with a flow rate of 0.50 ml min$^{-1}$. Mobile phase A contained 20 mM ammonium formate in ultrapure water at pH 3, whereas mobile phase B contained 20 mM aqueous ammonium formate at pH 3 in acetonitrile:$H_2O$ (9:1, v/v). The initial conditions at time 0 were 100% B, decreasing to 70% at 11.5 min. The gradient was then increased to 100% B at time 12.0 min and held until the total run time of 15 min. Mass spectrometry data were acquired in positive ionization mode. Raw signals for multiple reaction monitoring transitions were checked and peaks corresponding to all the targeted compounds were integrated by MassHunter Quantitative B.10.00 (Agilent Technologies). Multiple reaction monitoring transitions (collision energy, eV) were as follows: 141>123 (10) and 141>81 (26) for ImP; 139>121 (10) and 139>93 (26) for urocanic acid; 142>124 (10) and 142>41 (26) for labelled urocanic acid; 156>110 (10) and 156>83 (30), for histidine; and 159>113 (10) and 159>86 (30) for labelled histidine. Quantification of ImP concentration was performed by generating a standard curve with known concentrations of this metabolite. Histidine and urocanic acid were instead quantified by using internal standards added to plasma samples as stated above. Metabolite standards were analysed alongside plasma samples using the LC–MS/MS method. Dilution of the plasma during sample preparation was also taken into account for quantification.

For the IGT cohort, determination of ImP, urocanate and histidine levels in plasma were performed as described previously with minor modifications[15]. In brief, 25 µl of plasma samples were extracted using 6 volumes of acetonitrile containing 100 nM of internal standards before drying the samples under a flow of nitrogen. Then, the samples were reconstituted with 5% HCl (37%) in 1-butanol, subjected to *n*-butyl ester derivatization and finally reconstituted in 150 µl water:acetonitrile (9:1). ImP, urocanate and histidine levels were determined by UHPLC–MS/MS analysis using multiple reaction monitoring of the transitions 197.2>81.2, 195>93 and 213.2>110.1, respectively. For the internal standards, the transitions 200.2>82.0, 198.2>95.0 and 220.3>118.1 were used. The analytical system consisted of an Acquity UPLC I-class system coupled to a Xevo TQ-XS triple quadrupole mass spectrometer (Waters). Sample volume (2 µl) was injected onto a C18 BEH column (2.1 × 50 mm with 1.7-µm particles, Waters) and separated using a gradient consisting of water with 0.1% formic acid (A-phase) and acetonitrile with 0.1% formic acid (B-phase). Quantifications were performed using a standard curve with known concentrations of ImP, urocanate and histidine.

### DNA extraction, 16S rDNA amplicon sequencing and microbiota data analysis

For mice caecum samples, total DNA was extracted using the MasterPure Complete DNA & RNA Purification Kit (Epicentre) with some modifications, as previously described[60]. DNA concentrations were normalized using a Qubit 2.0 Fluorometer (Life Technology) and specific amplicon of the 16S rDNA gene (V3–V4 region) was generated following the 16S Metagenomic Sequencing Library Preparation Illumina protocol. The multiplexing step was performed using Nextera XT Index Kit (Illumina) and PCR amplicon-product was checked on a

bioanalyzer DNA 1000 chip (Agilent Technologies). The samples were pooled in equimolar amounts and sequenced with the MiSeq Reagent kit v.3, on a MiSeq Illumina platform (FISABIO sequencing service).

For human samples, faecal DNA was extracted using a commercially available kit (E.Z.N.A stool DNA kit, Omega Biotek)[61]. Next, amplicon library of the V4 region within the 16S rDNA gene were generated and both ends of the fragments were sequenced using an Illumina MiSeq by the Microbiome Core of the University of Michigan[62].

In both studies, to rule out and control for potential reagent contamination, the reagents for DNA extraction and PCR amplification were also sequenced as controls. For data analysis of microbiota from mice and humans, the paired-end sequences were curated, binned into operational taxonomic units at >97% identity level, and annotated with SILVA release v.132 using DADA2[63] for mice data and v.138 and RDP version 18 databases using Mothur (v.1.40.5)[62,64] as previously described[61] for human data. Spearman rank correlation coefficients between ImP level and bacterial abundance were determined using otu.association function of Mothur[62,64].

### Dietary pattern assessment

Dietary intake data were collected via semi-quantitative 136-item food-frequency questionnaire validated for the Spanish population[65]. Foods reported during the dietary assessment were classified into 44 food groups based on the similarity of nutrients profile, averaged over the days to derive habitual intake and normalized by the BMI of each participant. Next, a PCA was performed in SPSS V.23.0 (SPSS) to identify common underlying dimensions (factors or patterns) of food consumption by deriving factor loadings for each predefined food group. Factors were subsequently rotated using a Varimax procedure to maintain uncorrelated factors. Analysis of eigenvalues, scree plot, and the interpretability of the factor solution were used to support a final decision on retaining a 5-factor solution, where each factor had an eigenvalue >0.3. According to the observed factor loadings of the food groups, we named the first factor Mediterranean dietary pattern (enriched in vegetables, whole grains, and fish), the second and third factors as Breakfast dietary patterns (Breakfast1: enriched in cereals, tea, low fat dairy, and Breakfast2: mainly composed of bread, egg and coffee), and the fourth factor the Western dietary pattern (enriched in red meat, sugar, snacks and refined grains) and the fifth factor the Social dietary pattern (enriched in soft drinks and spirits).

### scRNA-seq

*Apoe*$^{-/-}$ 8-week-old male mice were treated in the drinking water with ImP (400 µg per mouse per day) for 4 or 8 weeks. Aortas were collected and digested as described above. To obtain enough cell numbers, three aortas per condition were pooled. Each sample was labelled with a cell multiplexing oligo (CMO) using the CMO labelling for scRNA-seq Protocol from 10X Genomics. Cells labelled with CMOs were washed, labelled with SytoxGreen and Hoechst to ensure cell viability, and live cells were sorted with a FACs Aria cell sorter. Samples were pooled and scRNA-seq was performed following the Chromium Next GEM Single Cell 3′ v.3.1 with feature barcode technology for cell multiplexing protocol (10x Genomics). In brief, cells were first counted and checked their viability using the Countess 3 cell counter (Thermofisher). Next, cells were loaded onto a 10X Genomics chip of the Chromium Controller (10X Genomics). After cDNA amplification, gene expression and CMO libraries were generated and sequenced using an Illumina NextSeq 2000 sequencer.

Raw sequencing data processing was performed from FASTQ file from each port using Cell Ranger (v.6.1.2) with default parameters and the mm10 (GRCm38.p6) mouse genome reference provided by 10X Genomics. Obtained raw unique molecular identifier (UMI) count matrices of valid barcoded cells for each port were loaded into R (v.4.1.2) for further analyses using Bioconductor packages[66] and Seurat (v.4.0.6)[67]. First, cells were filtered out according to the total number of UMI counts (≤1,000 and ≥50,000), total number of detected genes (≤200 and ≥6,000), and percentage of mitochondrial UMI counts (≥7.5%). Then, resulted cells were demultiplexed using the cellhashR R package (v.1.0.2)[68] using htodemux, bff_cluster, gmm_demux, multiseq, and dropletutils methods. Consensus classification was used for further analyses. Once the final set of cells was obtained, transcriptional expression values were normalized to total UMI counts per cell multiplied by a scaling factor of 10,000 and natural log-transformed (NormalizeData function). Highly variable genes were defined using the VST method as implemented in Seurat setting. A total of 2,000 highly variable genes and PCA modelling was used to reduce this dimensional space after scaling log-transformed expression values. In this step, variability associated with total number of counts was regressed out using the ScaleData function with linear models. Elbow plot method was used to determine the number of principal components for downstream analyses (25 principal components). Then, cells were clustered using the Louvain algorithm and visualized using the uniform manifold approximation and projection for dimension reduction (UMAP) algorithm with the first 25 principal components as input. Main clusters were identified by using known markers and computing differentially expressed genes with Wilcoxon rank sum test using the presto R package (v.1.0.0) (Extended Data Fig. 4). Cell proportions were calculated for each condition in every cell population, and a two-proportions Z-test using the prop.test R function was used to determine significance.

Differential expression analyses between conditions were independently performed on every cell population comparing ImP vs control for each timepoint (4 or 8 weeks) using the MAST R package (v.1.20.0). Genes were ranked according to log fold changes, and resulting ranks were used as input for the fgsea R package along with the Hallmark gene sets from the Molecular Signature Data Base (MSigDB; https://www.gsea-msigdb.org/gsea/msigdb). In order to identify specific cell subpopulations within every general cell type, each population was separated and independently analysed using the same workflow explained above. Subclusters were identified by using known markers and calculating differentially expressed genes with the presto R package. Finally, an overrepresentation analysis considering gene markers for every identified subcluster was performed along with the GO database (https://www.geneontology.org/) in order to interpret the transcriptional state of each subpopulation.

### Cell lines

MAECs were isolated from mouse thoracic aortas as described[69]. Cells were cultured in Medium 199 (Gibco, Invitrogen Life Technologies) + 20% fetal bovine serum + penicillin/streptomycin 2 mM + glutamine 2 mM + HEPES 10 mM + endothelial cell growth supplement 30 µg ml$^{-1}$ + Heparin 100 mg ml$^{-1}$, all from Sigma Aldrich, under 5% $CO_2$ at 37 °C. MEF cell lines were isolated from 13.5 days post coitum from embryos using standard protocol. Each embryo was dissected into 10 ml of sterile PBS, voided of its internal organs, head, and legs. After 30 min incubation with gentle shaking at 37 °C with 5 ml 0.1% trypsin, cells were plated in two 100 mm dishes and incubated for 24–48 h. To establish the immortalized MEF lines, early passage MEFs were seeded in 60 mm plates and infected with $10^5$ IU ml$^{-1}$ packaged retrovirus carrying the human papillomavirus (HPV) 16 E6/E7 genes. Selection was performed with 400 µg ml$^{-1}$ of G418 during 10 days.

L929 cell line (ATCC CCL-1TM) used for production of the M-CSF supernatant, was grown on 175 cm$^2$ cell culture flasks (Stemcell) and resuspended in RPMI 1640 (Sigma) supplemented with 10% heat-inactivated fetal calf serum (FCS, Sigma), 1 mM pyruvate (Lonza), 100 µM non-essential aminoacids (Thermo Fisher Scientific), 2 mM L-glutamine, 100 U ml$^{-1}$ penicillin and 100 µg ml$^{-1}$ streptomycin (all three from Lonza), herein called R10. Supernatants were obtained by filtering 15-days long cultures through 0.22 µm Stericup Filter units (Merck Millipore) and were used to subsequently supplement the medium for the generation of BMDMs.

Mouse BMDMs were generated as described[70], with some modifications. Bone marrow cells from WT C57BL/6J mice were cultured in RPMI 1640 supplemented with 30% M-CSF obtained from L929 cell line and 10% FBS, 100 μg ml$^{-1}$ penicillin, 100 μg ml$^{-1}$ streptomycin, 10 mM HEPES, 1 nM sodium pyruvate (all from Gibco) during 5 days in sterile, but not tissue culture-treated, 10-cm Petri dishes.

**Bulk RNA-seq**

Cultured BMDMs, MEFs and MAECs were plated in equal number and rested overnight. Specifically, for BMDMs and MEFs, $6 \times 10^5$ cells per well were plated in 6-well plates (2,000 μl final volume, Corning), and for MAECs $1 \times 10^5$ cells per well were plated in p24 (1,000 μl final volume, Corning). Cells were treated in vitro with or without ImP (10 μg ml$^{-1}$) for 1 or 2 h. Total RNA was isolated from BMDMs, MEFs (QIAamp DNA Mini Kit) and MAECs (miRNeasy Micro Kit). Bulk RNA-seq experiments were performed in the Genomics Unit of the CNIC. For the BMDM and MEF samples, RNA-seq libraries were prepared using the NEBNext Ultra II Directional RNA Library preparation kit (New England Biolabs) according to the manufacturer's instructions. For MAECs samples, libraries were prepared using the NEBNext Single Cell/Low Input RNA Library Prep Kit for Illumina (New England Biolabs) according to the manufacturer's instructions. All libraries were sequenced in a Nextseq 2000 (Illumina). FastQ files for each sample were obtained using bcl2fastq v.2 2.20 software (Illumina). The number of reads per sample was between 11 and 21 million. Reads were preprocessed according to the type of library preparation using cutadapt to trim adapters and FastQC to assess read quality. In the case of directional RNA-seq reads (BMDMs and MEFs), Illumina adaptor sequences were removed, and only reads longer than 30 bp were kept as valid. For MAECs, in addition to Illumina adaptor sequences, adaptors from the low input NEBNext protocol were detected and removed and only reads longer than 30 bp were kept as valid. Resulting reads were mapped to the reference transcriptome GRCm38.102 using STAR[71] and gene expression levels were estimated using RSEM[72]. Further analyses were performed in R (v.4.3.2). In brief, counts per million were calculated, and size factors for inter-sample normalization were determined using the trimmed mean of M values method. Then, log-normalized data considering only genes with ≥20 counts in 3 samples were used for differential expression analysis, making all possible comparisons within the same cell type using the DESeq2 R package[73]. Gene-set enrichment analysis was performed using the fgsea R package comparing 1 h and 2 h after ImP stimulation with 0 h (unstimulated) within each cell type. Genes were ranked in each comparison according to logFC, and fgsea was used along with the Hallmark gene sets from the Molecular Signature Data Base (MSigDB; https://www.gsea-msigdb.org/gsea/msigdb). Finally, normalized enrichment scores of significant selected pathways were represented as a heat map using the ComplexHeatmap R package[74].

**Proteomics and phosphoproteomics by isobaric labelling**

Cultured BMDMs and MEFs were plated at $1 \times 10^6$ cells per well in 6-well plates (Corning), 2 ml final volume, and rested overnight in RPMI 1% medium. Cells were treated in vitro with or without ImP (10 μM) and co-incubated or not with AGN192403 (1 μM, I1R antagonist) for 180 min. Cell culture monolayers were washed with PBS, and protein extracts were obtained with lysis buffer (50 mM Tris-HCl pH 7.6, 2% SDS, 10 mM Tris-(2-carboxyethyl)phosphine (TCEP)) containing protease and phosphatase inhibitor cocktails (Complete Mini EDTA-free and phosSTOP, Roche). Samples were boiled for 5 min and incubated for 20 min at room temperature for solubilization and reduction of the proteins, and after centrifugation at 15,000*g* for 15 min, supernatants were recovered, and protein concentration was determined by using a RC DC Protein Assay Kit (BioRad Laboratories).

Proteome and phosphoproteome analyses were carried out using 18-plex isobaric TMT labelling as described[75]. Statistical analysis of quantitative data was performed using iSanXoT[76], and the comparative analysis between conditions was performed using the normalized values $X_p^m$ and $X_q^m$, which represent the binary logarithm of the ratio between the abundance in sample $m$ and its control for peptide $p$ and protein $q$, respectively. GSEA[77] using $X_p$ values of peptides was used to evaluate the phosphorylation levels in proteins of the mTOR signalling pathway among conditions (that is, cells stimulated with ImP versus unstimulated). In addition, a Wilcoxon signed rank test was performed using paired phosphopeptide abundance $X_p$ values to determine the effects of AGN192403 in the phosphorylation levels of the mTOR pathway among cells treated with ImP and co-incubated or not with AGN192403.

**p-S6 staining by flow cytometry**

Cultured MEFs and BMDMs were plated in equal numbers ($6 \times 10^5$ cells per well) in 6-well plates (2,000 μl final volume, Corning) and rested overnight. Cells were treated in vitro with or without ImP (10 μg ml$^{-1}$) co-incubated with Rapamycin (10 nM), AGN192403 (1 μM, I1R antagonist), Idazoxan (0.29 nM, imidazoline receptor and $\alpha_2$-adrenergic antagonist) or Yohimbine (0.28 nM, $\alpha_2$ antagonist). After 24 h, cells were collected and labelled with p-S6-PE antibody (Cell Signalling 5316) according to the manufacturer protocol and the activation was measured by flow cytometry.

**Peritoneal macrophages collection**

Peritoneum cells were isolated by lavage with 5 ml of cold PBS. Cells were plated and non-adherent cells were washed with PBS 1 h later. Adherent cells were defined as peritoneal macrophages, which were routinely controlled by flow cytometry. p-S6 staining by flow cytometry was assessed as described above.

**TNF measurement**

Cultured MEFs and BMDMs were plated in equal numbers ($1 \times 10^5$ cells per well) in 96-well plates (200 μl final volume, Corning) and rested overnight. Cells were treated in vitro with and without ImP (10 μM) and co-incubated with Rapamycin (10 nM), AGN192403 (1 μM, I1R antagonist), Idazoxan (0.29 nM, imidazoline receptor and $\alpha_2$ antagonist) or Yohimbine (2.8 nM, $\alpha_2$ antagonist). After 24 h, supernatant was collected, and TNF concentration was quantified with mouse TNF DuoSet ELISA (DY410) according to the manufacturer's instructions.

**MCP1 measurement**

Cultured MEFs were plated ($1 \times 10^5$ cells per well) in 96-well plates (200 μl final volume, Corning) and rested overnight. Cells were treated in vitro with and without ImP (10 μM). After 24 h supernatant was collected, and MCP1 concentration was quantified with mouse CCL2/JE/MCP1 DuoSet ELISA (DY479) according to the manufacturer's instructions.

**Transwell**

Migration of circulating monocytes induced by MEFs was assessed in a transwell migration assay. Circulating monocytes from 8-week-old *Apoe*$^{-/-}$ male mice were sorted (CD3$^-$B220$^-$NK1.1$^-$LY6G$^-$CD49$^-$SIGLECF$^-$CD45$^+$CD11B$^+$Ly6C$^{+/-}$). Initially, MEFs were placed on the lower chamber of the transwell with DMEM 1% FBS. Sorted monocytes were placed onto the upper chamber of the transwell with RPMI 1% FBS. MEFs were stimulated with ImP 10 μM. After 24 h, the medium under transwell was collected and cells in the supernatant were quantified using LSRFortessa SORP (Becton Dickinson).

**Serum cytokines measure**

Blood was collected as described above. Amount of TNF and IFNγ in the serum was measured according to the manufacturer protocol using mouse TNF DuoSet ELISA (DY410) and mouse IFNγ DuoSet ELISA (DY485), respectively.

### ImP treatment in grafted mice

*Ldlr*$^{-/-}$ CD45.1 mice were lethally irradiated with two doses of 550 rad (5.5 Gy), separated by at least 3 h, for a total radiation dose of 1,100 rad, followed by intravenous injection of $2 \times 10^6$ bone marrow cells from CD45.2$^+$ *Lyz2*Δ*Raptor* or control *Raptor*$^{fl/fl}$ littermates. In parallel experiments, $2 \times 10^6$ $\alpha_2$-adrenoceptor cells from *Rag1*$^{-/-}$ or control C57BL/6J wild-type mice were transferred. In another set of experiments, *Ldlr*$^{-/-}$ CD45.1 mice were lethally irradiated as described above followed by intravenous injection of $2 \times 10^6$ bone marrow cells from CD45.2$^+$ *Lyz2*Δ*Nisch* or control *Nisch*$^{fl/fl}$ littermates. Grafted mice were injected with 25 μg g$^{-1}$ of cefovecin subcutaneously to prevent infection upon bone marrow graft. Upon reconstitution of bone marrow after 45 days, mice were treated or not with ImP (400 μg per mouse per day, Biogen Cientifica BA-F-3185.0001) for 12 weeks in the drinking water.

### I1R siRNA silencing

I1R silencing in vitro was performed using *Nisch* siRNA (Santa Cruz sc-61202), a pool of 3 target-specific 19–25 nt siRNAs designed to knock down *Nisch* gene expression or control siRNA (Santa Cruz sc-36869) consisting of a scrambled sequence conjugated to 10–20 fluorescein that does not lead to the specific degradation of any cellular mRNA. Cultured MEFs were plated ($2 \times 10^5$ cells per well) in a 6-well tissue culture plate in 2 ml of antibiotic-free normal growth medium supplemented with FBS. After 24 h, cells were washed with siRNA Transfection Medium (Santa Cruz sc-3686860) and siRNA duplex solution (A + B) was added after mixing by pipetting and incubating the mixed solution for 30 min at room temperature (A: 60 pmol siRNA into 100 μl siRNA Transfection Medium; B: 6 μl of siRNA Transfection Reagent (Santa Cruz sc-29528) into 100 μl siRNA Transfection Medium). MEFs were incubated with the mixed solution. After 5 h transfection, medium was removed and 2 ml of RMPI 10% FBS with antibiotics was added. After 24 h, cells were treated in vitro with and without ImP (10 μM) and co-incubated or not with AGN192403 (1 μM, I1R antagonist).

### Quantitative PCR with reverse transcription

To determine *Nisch* expression, spleen cells were sorted as CD45$^+$CD11b$^+$ and CD45$^+$CD3$^+$ cells, and RNA extracted with the RNeasy Mini Kit and reverse transcribed using the High-Capacity cDNA Reverse Transcription Kit with random hexamers following manufacturer's instructions. Quantitative PCR was performed using the GoTaq qPCR Master Mix in a 7900HT Fast Real-Time PCR System. The sequence of primers used for qPCR were: *Nisch* sense 5′-TATGTTGTGGCACAGAAGATGG-3′; anti-sense 5′-TTCAGGCAATGGATAGTGGAT-3′; *Gapdh* sense 5′-TGAAGCAGGCATCTGAGGG-3′; anti-sense 5′-CGAAGGTGGAAGAGTGGGAG-3′.

### Statistics

Data analysis was carried out using GraphPad Prism software v.9.0 (GraphPad Software) and Stata version 18 (StataCorp). Variables were presented as mean ± s.e.m or mean ± s.d. unless otherwise stated. The Kolmogorov–Smirnov test and Shapiro–Wilk normality test were used to determine the normal distribution of samples. Nominal variables were presented as percentages and frequencies. Comparisons between two groups were performed using two-tailed unpaired Student's *t*-tests (normal distribution) or Mann–Whitney *U*-tests (non-normal distribution) for continuous variables or Fisher exact test for categorical variables. Unless otherwise stated, comparisons across multiple groups were assessed using one-way ANOVA (normal distribution) followed by Tukey's post hoc test, or Kruskal–Wallis test (non-normal distribution) followed by Dunn's test as indicated in each figure legend. Continuous variables were compared across tertiles of ImP by ANOVA or non-parametric Kruskall Wallis tests as appropriate, whereas nominal variables by applying the Cohran–Armitage test (dichotomous variables) and the Jonckheere–Terpstra test (ordinal variable) for trend. Only significant differences are indicated. For untargeted metabolomics data, *P* values were corrected with a Benjamini–Hochberg post hoc method ($q = 0.05$) and supervised (PLS-DA) analyses were applied to select the variables responsible for the separation showed by models in MetaboAnalyst (https://www.metaboanalyst.ca/MetaboAnalyst/home.xhtml)[56] (Fig. 1b,c). The models were statistically validated by cross-validation tool, using the leave-1/3-out approach to exclude model overfitting.

For the human cohorts (PESA and IGT), no sample size calculation was conducted, as samples were retrospectively collected from observational studies. Instead, sample sizes were determined based on the availability of well-characterized patients with complete clinical, imaging, and biosamples from ongoing prospective observational studies. The cohorts were assembled with the goal of maximizing biological and phenotypic depth rather than targeting a predefined effect size. The inclusion of two independent cohorts with complementary phenotypes enabled replication and validation across datasets. Post hoc power considerations indicated that the sample size of the derivation cohort (PESA cohort, $n = 400$) was adequately powered at the 0.85 level to detect a minimum 5 nM difference in ImP levels between the group of individuals without atherosclerosis and individuals with atherosclerosis. A ratio of 1:3 between patients without and with atherosclerosis was selected to reflect the distribution of atherosclerosis in the PESA cohort, and measures of dispersion (s.d.) were derived from the group of participants without atherosclerosis in the PESA cohort. Respectively, the IGT cohort was adequately sized to detect with 0.85 power a difference of 2 nM in ImP levels between participants without and with atherosclerosis. Power considerations were based on the Mann–Whitney test for two independent groups. Type I error was prespecified at 0.05 for power calculations. Power analysis was performed with G*Power 3.1.9.6 (University of Kiel, Germany). Restricted cubic splines (natural splines, RCS) with three knots across ImP distribution were applied to produce dose–response curves and to flexibly model the potential non-linear association of continuous ImP with the main endpoints, as previously described[78,79]. In both cohorts, the three knots for RCS were fixed at the 10th, 50th and 90th percentile of the ImP distribution. Number of knots was selected on the basis of improvement in log likelihood among regression models with 3- or 4-knot RCS. To enhance visual clarity, plots with RCS were truncated at values exceeding the 95th percentile of the ImP distribution. We evaluated the non-linear relationships of ImP with log odds ratio of the main atherosclerosis outcomes by examining (Wald test) the non-linear terms (RCS)[80]. Dose–response curves in both cohorts were controlled for a set of confounders, constructed by combining LASSO regression and variables with biological plausibility. LASSO for logistic regression was used for multivariable model selection with respect to the outcome presence of atherosclerosis. Adaptive LASSO with cross-validation was employed to select the value of the LASSO penalty parameter lambda[81]. Adjusted differences in levels of ImP across groups of interest were estimated by multivariable linear regression analysis. To evaluate the association between ImP levels and the presence and activity of atherosclerosis within the PESA cohort multinomial logistic regression was performed and the model was adjusted on a set of confounders (age, sex, smoking status, fasting glucose, hs-CRP and haemoglobin concentration) based on previous evidence[21]. The proportional odds assumption was tested with the Brant Wald test. Correlation analysis of ImP, atherosclerosis traits and risk factors, gut microbiome and dietary patterns was investigated using non-parametric Spearman's test and the resulting *P* values corrected with a Benjamini–Hochberg post hoc method ($q = 0.05$). Finally, the discriminatory capability of ImP for prevalence of subclinical or active atherosclerosis on top of traditional risk factors, including LDL-cholesterol and hs-CRP, was assessed by comparing area under the curve from corresponding receiver operating characteristic analysis. Areas under the curve were compared using the DeLong test[82]. Bootstrapping with 1,000 replicates was used to derive

95% bias-corrected confidence interval. All tests were two-tailed and the level of statistical significance was pre-specified at $P < 0.05$.

### Reporting summary

Further information on research design is available in the Nature Portfolio Reporting Summary linked to this article.

## Data availability

Metabolomics data are deposited in the Metabolomics workbench (ST003928, ST003929, ST003932 and ST003938). The bulk RNA-seq and scRNA-seq data generated in this study are available in the NCBI GEO database under BioProject IDs GSE297831 and GSE298392, respectively. The proteomics and phosphoproteomics data have been deposited to the ProteomeXchange Consortium via the PRIDE partner repository with the dataset identifier PXD063955. Source data are provided with this paper.


52. Rakoff-Nahoum, S., Paglino, J., Eslami-Varzaneh, F., Edberg, S. & Medzhitov, R. Recognition of commensal microflora by toll-like receptors is required for intestinal homeostasis. *Cell* **118**, 229–241 (2004).
53. Centa, M., Ketelhuth, D. F. J., Malin, S. & Gisterå, A. Quantification of atherosclerosis in mice. *J. Vis. Exp.* https://doi.org/10.3791/59828 (2019).
54. Mastrangelo, A. et al. Insulin resistance in prepubertal obese children correlates with sex-dependent early onset metabolomic alterations. *Int. J. Obes.* **40**, 1494–1502 (2016).
55. Lorenzo, C. et al. ALDH4A1 is an atherosclerosis auto-antigen targeted by protective antibodies. *Nature* **589**, 287–292 (2021).
56. Pang, Z. et al. Using MetaboAnalyst 5.0 for LC–HRMS spectra processing, multi-omics integration and covariate adjustment of global metabolomics data. *Nat. Protoc.* **17**, 1735–1761 (2022).
57. Gil-de-la-Fuente, A. et al. CEU Mass Mediator 3.0: a metabolite annotation tool. *J. Proteome Res.* **18**, 797–802 (2019).
58. Barrero-Rodríguez, R. et al. TurboPutative: a web server for data handling and metabolite classification in untargeted metabolomics. *Front. Mol. Biosci.* **9**, 952149 (2022).
59. Fernández-Ortiz, A. et al. The Progression and Early detection of Subclinical Atherosclerosis (PESA) study: rationale and design. *Am. Heart J.* **166**, 990–998 (2013).
60. Sanguinetti, E. et al. Microbiome-metabolome signatures in mice genetically prone to develop dementia, fed a normal or fatty diet. *Sci. Rep.* **8**, 4907 (2018).
61. Caruso, R., Ono, M., Bunker, M. E., Núñez, G. & Inohara, N. Dynamic and asymmetric changes of the microbial communities after cohousing in laboratory mice. *Cell Rep.* **27**, 3401–3412.e3 (2019).
62. Kozich, J. J., Westcott, S. L., Baxter, N. T., Highlander, S. K. & Schloss, P. D. Development of a dual-index sequencing strategy and curation pipeline for analyzing amplicon sequence data on the MiSeq Illumina sequencing platform. *Appl. Environ. Microbiol.* **79**, 5112–5120 (2013).
63. Callahan, B. J. et al. DADA2: high-resolution sample inference from Illumina amplicon data. *Nat. Methods* **13**, 581–583 (2016).
64. Schloss, P. D. et al. Introducing mothur: open-source, platform-independent, community-supported software for describing and comparing microbial communities. *Appl. Environ. Microbiol.* **75**, 7537–7541 (2009).
65. de la Fuente-Arrillaga, C., Ruiz, Z. V., Bes-Rastrollo, M., Sampson, L. & Martinez-González, M. A. Reproducibility of an FFQ validated in Spain. *Public Health Nutr.* **13**, 1364–1372 (2010).
66. Amezquita, R. A. et al. Orchestrating single-cell analysis with Bioconductor. *Nat. Methods* **17**, 137–145 (2020).
67. Hao, Y. et al. Integrated analysis of multimodal single-cell data. *Cell* **184**, 3573–3587.e29 (2021).
68. Boggy, G. J. et al. BFF and cellhashR: analysis tools for accurate demultiplexing of cell hashing data. *Bioinformatics* **38**, 2791–2801 (2022).
69. Toral, M. et al. Carnitine palmitoyltransferase-1 up-regulation by PPAR-β/δ prevents lipid-induced endothelial dysfunction. *Clin. Sci.* **129**, 823–837 (2015).
70. Garaude, J. et al. Mitochondrial respiratory-chain adaptations in macrophages contribute to antibacterial host defense. *Nat. Immunol.* **17**, 1037–1045 (2016).
71. Dobin, A. et al. STAR: ultrafast universal RNA-seq aligner. *Bioinformatics* **29**, 15–21 (2013).
72. Li, B. & Dewey, C. N. RSEM: accurate transcript quantification from RNA-seq data with or without a reference genome. *BMC Bioinformatics* **12**, 323 (2011).
73. Love, M. I., Huber, W. & Anders, S. Moderated estimation of fold change and dispersion for RNA-seq data with DESeq2. *Genome Biol.* **15**, 550 (2014).
74. Gu, Z., Eils, R. & Schlesner, M. Complex heatmaps reveal patterns and correlations in multidimensional genomic data. *Bioinformatics* **32**, 2847–2849 (2016).
75. Romero-Becerra, R. et al. p38γ/δ activation alters cardiac electrical activity and predisposes to ventricular arrhythmia. *Nat. Cardiovasc. Res.* **2**, 1204–1220 (2023).
76. Rodríguez, J. M. et al. iSanXoT: a standalone application for the integrative analysis of mass spectrometry-based quantitative proteomics data. *Comput. Struct. Biotechnol. J.* **23**, 452–459 (2024).
77. Subramanian, A. et al. Gene set enrichment analysis: a knowledge-based approach for interpreting genome-wide expression profiles. *Proc. Natl Acad. Sci. USA* **102**, 15545–15550 (2005).
78. Stamatelopoulos, K. et al. Amyloid-β (1–40) and mortality in patients with non-ST-segment elevation acute coronary syndrome. *Ann. Intern. Med.* **168**, 855–865 (2018).
79. Stamatelopoulos, K. et al. Cathepsin S levels and survival among patients with non-ST-segment elevation acute coronary syndromes. *J. Am. Coll. Cardiol.* **80**, 998–1010 (2022).
80. Wald, A. Sequential tests of statistical hypotheses. *Ann. Math. Stat.* **16**, 117–186 (1945).
81. Hastie, T., Tibshirani, R. & Wainwright, M. *Statistical Learning with Sparsity: The Lasso and Generalizations* (Chapman & Hall, 2015).
82. DeLong, E. R., DeLong, D. M. & Clarke-Pearson, D. L. Comparing the areas under two or more correlated receiver operating characteristic curves: a nonparametric approach. *Biometrics* **44**, 837–845 (1988).



**Acknowledgements** The authors thank M. C. Collado for mouse gut microbiota analysis; M. O. Garmendia for assistance with the metadata from volunteers; members of the D.S. laboratory for help with discussions and critical reading of the manuscript; and the CNIC facilities, foremost the animal, cellomics, histology, metabolomics, genomics, microscopy, clinical trial and bioinformatics facilities, and personnel for assistance. I.R.-V. is funded by FJC2021-048099-I funded by MCIN/AEI/10.13039/501100011033 and European Union NextGenerationEU/PRTR. D.M. is funded by grant PRE2020-092578 MCIN/AEI/10.13039/501100011033. M.G. is funded by beca de formación de profesorado Universitario fellowship 20/01418. M.F.-M. is funded by INPhINIT Retaining 2024 from Caixa Foundation LCF/BQ/DR24/12080010. A.R.-U. is supported by Community of Madrid (PIPF-2022/SALGL-24581). R.B.-R. is funded by Beca de Formación de Profesorado Universitario Fellowship 20/03365. A. Devesa is scientifically supported by the Thrasher Research Fund and acknowledges the support of Sociedad Española de Cardiología (grant SEC/PRS-MOV-INT20/002). Work in the D.S. laboratory is funded by the CNIC; the European Union's Horizon 2020 Research and Innovation Program under grant agreement ERC-2016-Consolidator Grant 725091; Ministerio de Ciencia, Innovación y Universidades (MICIU) PID2022-137712OB-I00, CPP2021-008310 and CPP2022-009762 MICIU/AEI/10.13039/501100011033 Agencia Estatal de Investigación, Unión Europea NextGenerationEU/PRTR; Comunidad de Madrid (P2022/BMD-7333 INMUNOVAR-CM); Scientific Foundation of the Spanish Association Against Cancer (AECC- PRYGN246642SANC); Worldwide Cancer Research WWCR-25-0080; European Union ERC-2023-PoC; a research agreement with Inmunotek S.L.; and la Caixa Foundation (LCF/PR/HR23/52430012 and LCF/PR/HR22/52420019). Work in the B.I. laboratory is supported by the European Commission (H2020-HEALTH 945118 and ERC-CoG 819775); the PID2022-140176OB-I00, PID2019-107332RB-I00 MCIN/AEI /10.13039/501100011033; and the Comunidad de Madrid RENIM P2022/BMD-7403. F.B. is funded by grants from the Swedish Heart Lung Foundation (20240882) and is a Wallenberg Fellow and recipient of an ERC-Advanced grant 2022 (101096705-IMPACT). K. Stellos was supported by the Deutsche Forschungsgemeinschaft (DFG, German Research Foundation — Project ID 394046768 — SFB1366 'Vascular control of organ function' C07), the European Research Council (ERC) under the European Union's Horizon 2020 research and innovation programme (MODVASC, grant agreement 759248), the German Centre for Cardiovascular Research (DZHK) and the Helmholtz-Institute for Translational AngioCardioScience (HI-TAC) of the Max Delbrück Center for Molecular Medicine in the Helmholtz Association (MDC) at Heidelberg University, Heidelberg, Germany. Metabolomics Workbench is supported by NIH grant U2C-DK119886 and OT2-OD030544 grants. The CNIC is supported by the Instituto de Salud Carlos III (ISCIII), the MICIU and the Pro CNIC Foundation, and is a Severo Ochoa Center of Excellence (CEX2020-001041-S funded by MICIU/AEI /10.13039/501100011033). The PESA study is funded by the CNIC and Santander Bank. This study was partially funded by an intramural grant CNIC-Severo Ochoa to B.I. and D.S.


**Author contributions** A.M., I.R.-V. and D.S. conceptualized and designed the study. A.M., I.R-V., D.M., J.A.-I., S.M.-C., V.N., I.F.-L., N.I., A.B., M.G., M.R.-T., M.F.-M., A.R.-U., R.B.-R., J.A.L., S.I., K.R.B. and V.A.-H. performed the experiments and analysed the data. A.C., K.R.B., S.I., A.F., I.F.-L., A. Dopazo, C.B., J.V., G.N., F.B., E.P., A.G.-M., D.C. and F.S.-M. supported the experiments and provided equipment and reagents. V.F., B.I., A. Devesa, M.L.-G., G.B. and A.G. developed clinical cohorts, including recruitment of patients, and assisted in the analysis of their results. K. Stamatelopoulos and K. Stellos contributed to data interpretation and provided conceptual input during manuscript revision. G.G. conducted the cohort study analyses and together with A.M., K. Stamatelopoulos and K. Stellos interpreted the human findings. D.S. and B.I. acquired funding. D.S. supervised the project. A.M., I.R.-V. and D.S. wrote the manuscript with input from all of the authors. All authors edited and approved the final manuscript.

**Competing interests** F.B. receives research funding from Biogaia AB and Novo Nordisk A/S, is co-founder and shareholder of Roxbiosens Inc., and is on the scientific advisory board of Bactolife A/S. F.B., K.R.B. and A.C. are co-founders and shareholders of Implexion Pharma AB. A.M., I.R.-V., D.S., B.I., V.F. and D.M. are inventors on a patent application titled *Antagonists of the I1R for use in the Prevention and/or Treatment of an Autoinflammatory or Autoimmune Disease*, publication number WO2025002914 (2025). The other authors declare no competing interests.

**Additional information**


**Supplementary information** The online version contains supplementary material available at https://doi.org/10.1038/s41586-025-09263-w.



**Correspondence and requests for materials** should be addressed to David Sancho.



**Peer review information** *Nature* thanks Soraya Taleb and the other, anonymous, reviewer(s) for their contribution to the peer review of this work. Peer reviewer reports are available.

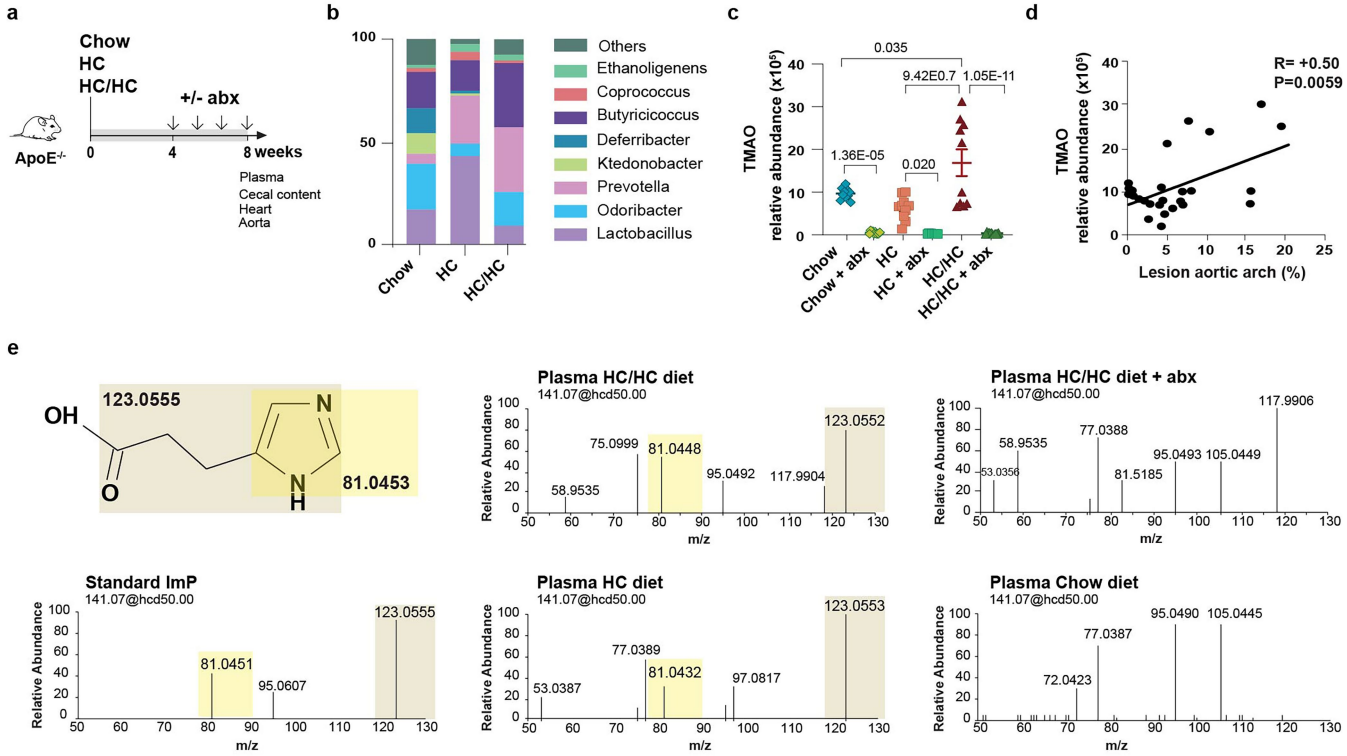


**Extended Data Fig. 1 | High cholesterol diets and antibiotics modulate gut microbiota and plasma metabolites in *ApoE*$^{-/-}$ mice. a**, Experimental setup corresponding to Fig. 1 and Extended Data Fig. 1. *ApoE*$^{-/-}$ mice were fed different diets (chow, high cholesterol (HC), HC and high choline (HC/HC)) for 8 weeks. At 4 weeks post diet initiation, mice were treated or not with a cocktail of antibiotics (abx) in the drinking water. At sacrifice, aorta, heart, cecal content and plasma samples were collected and analysed. **b**, Stacked barplots showing the relative abundance of 16S rDNA sequences, at the genus level ( > 1% of total abundance), that are significantly different in cecal samples of the indicated groups. Genera shown are all significantly different between chow and HC diets by two-sided Kruskal-Wallis with Dunn's correction test. n = 9. **c**, Relative abundance of TMAO in plasma measured by untargeted LC-MS. n = 10. **d**, Correlation of TMAO's relative abundance with aortic arch lesion. Correlation coefficient (R) and p-value are calculated as the Pearson's parametric correlation test. n = 29 (chow and HC n = 10 and HC/HC n = 9). **e**, Tandem mass spectrometry fragmentation by higher-energy collisional dissociation (HCD) using 50 eV as collisional energy of the imidazole propionate (ImP) standard (left) and endogenous m/z = 141.06535 mass from plasma *of ApoE*$^{-/-}$ mice fed different diets as indicated. **b**-**d**, data are pooled from two independent experiments. **c**, Arithmetic mean ± SEM of each group is shown. Two-sided one-way ANOVA with Tukey post-hoc correction.

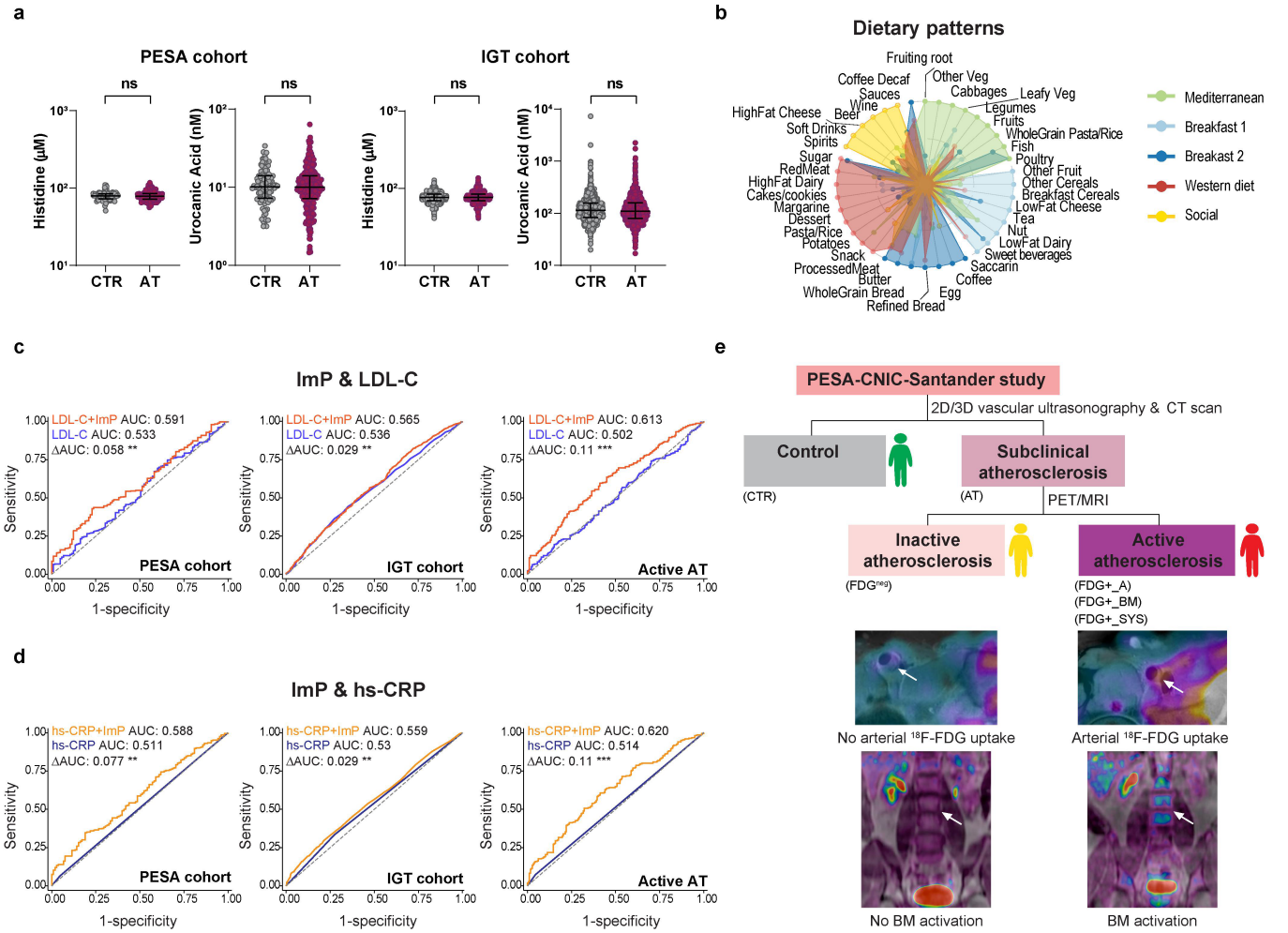


**Extended Data Fig. 2 | Metabolic and dietary features of asymptomatic volunteers from the PESA and IGT cohorts. a**, Plasma concentration of histidine and urocanic acid in healthy subjects (CTR) and subjects with subclinical atherosclerosis (AT) from the PESA cohort (left, CTR n = 105, AT n = 295, plasma concentration for both metabolites) and the IGT cohort (right, CTR n = 529, AT n = 1315, plasma concentration for both metabolites). Data on a base-10 Log scale. Median with interquartile range for each group is shown. ns: non-significant. **b**, Radar graph of loadings factors for each dietary pattern. **c**, ROC analysis for the additive value of ImP over LDL-C alone to discriminate subclinical total AT (left and center) and active AT (right). Left, PESA cohort: $AUC_{ImP+LDL-C}$ 0.591 (CI: 0.524-0.639) vs. $AUC_{LDL-C}$ 0.533 (CI: 0.488-0.590), ΔAUC = 0.058 (CI: 0.01-0.127) p = 0.006. Center, IGT cohort: $AUC_{ImP+LDL-C}$ 0.565 (CI:0.535-0.590) vs. $AUC_{LDL-C}$ 0.536 (CI: 0.508-0.565), ΔAUC = 0.029 (CI: 0.014-0.05) p = 0.008. Right, active AT: $AUC_{ImP+LDL-C}$ 0.613, (CI: 0.554-0.659) vs. $AUC_{LDL-C}$ 0.502 (CI: 0.479-0.524), ΔAUC = 0.11 (CI: 0.061-0.189) p = 0.00042. **d**, ROC analysis for the additive value of ImP on the top of high-sensitivity C Reactive Protein (hs-CPR) to discriminate early AT (left and center) and active AT (right). Left, PESA cohort: $AUC_{ImP+hs-CRP}$ 0.588 (CI: 0.525-0.651) vs. $AUC_{hs-CRP}$ 0.511 (CI:0.501-0.532), ΔAUC = 0.077 (CI 0.014-0.133, p = 0.006. Center, IGT cohort: $AUC_{ImP+hs-CRP}$ 0.559 (CI:0.530-0.584) vs. $AUC_{hs-CRP}$ 0.530 (CI:0.10-0.552), ΔAUC = 0.029 (CI:0.06-0.053) p = 0.003. Right, active AT: $AUC_{ImP+hs-CRP}$ 0.620, (CI: 0.567-0.674) vs. $AUC_{hs-CRP}$ 0.514 (CI:0.501-0.536), ΔAUC = 0.11 (CI 0.054-0.155) p = 0.00042. **e**, Schematic representation of the distribution of volunteers from the PESA study. Based on multiterritorial/multimodal imaging (i.e. 2D/3D vascular ultrasound and non-contrast computed tomography), we classified 295 participants with subclinical atherosclerosis and 105 controls without atherosclerosis (green). Subjects with subclinical atherosclerosis were further stratified according to their uptake of Fluorodeoxyglucose ($^{18}$F-FDG): those without any uptake considered as inactive atherosclerosis ($FDG^{neg}$, yellow); those with metabolic activity in bone marrow (FDG + _BM, n = 40), arteries (FDG + _A, n = 57), or in both compartments (FDG + _SYS, n = 124) considered as active atherosclerosis (FDG + , red). Pictures are representative images of uptake in arteries and bone marrow.

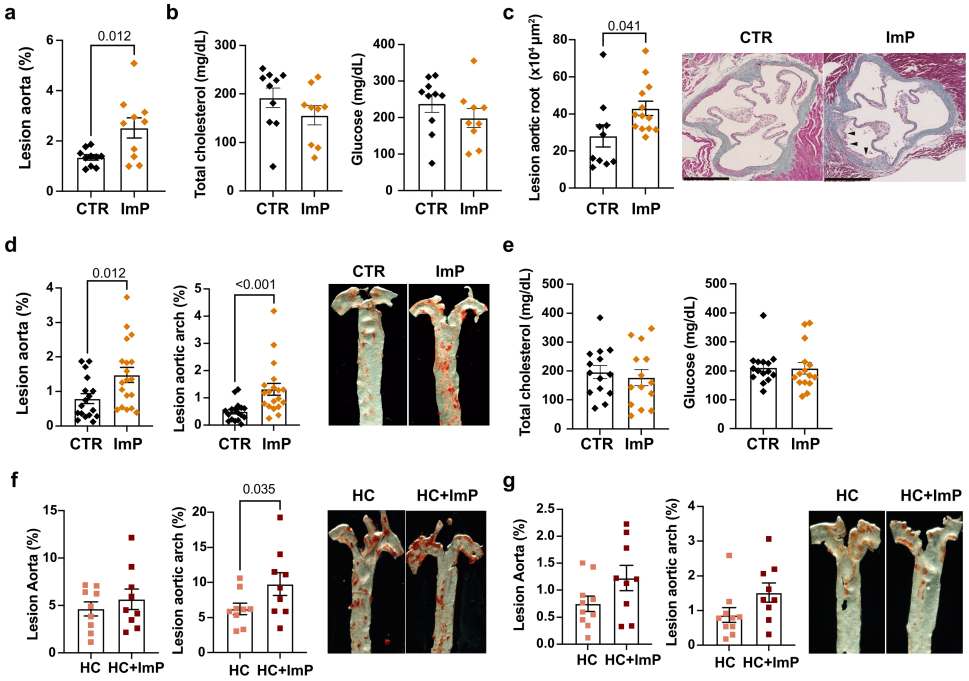


**Extended Data Fig. 3 | The induction of atherosclerosis by ImP supplementation in chow-fed atherosclerosis-prone mice is independent of changes in cholesterol and glucose concentration. a,b**, Chow-fed *Ldlr*$^{-/-}$ mice were administered ImP (ImP) or not (CTR) in the drinking water for 12 weeks, followed by sacrifice and analysis. **a**, Oil red O en face staining of the aorta showing quantification of atherosclerotic lesions in whole aorta (left) and representative images (right). n = 10. **b**, Total cholesterol and glucose concentration in plasma. CTR = 10; ImP=9. **c,d**, Chow-fed *ApoE*$^{-/-}$ mice were treated with ImP or not (CTR) in the drinking water for 8 weeks. **c**, Masson's trichrome staining of the aortic roots showing quantification of lesion area (left) and representative images (right). CTR = 10; ImP=13. Bar size= 500 µm. **d**, Quantification of atherosclerotic lesions by Oil red O en face staining of the aorta showing quantification in aorta (left), aortic arch (middle) and representative images of aorta (right). CTR = 17; ImP=19 **e**, Total cholesterol (n = 14) and glucose concentration (n = 15) in plasma. **f**, HC-fed *Ldlr*$^{-/-}$ mice were administered ImP (ImP) or not (CTR) in the drinking water for 12 weeks, Oil red O en face staining of the aorta showing quantification of atherosclerotic lesions in aorta (left) and representative images (right). n = 9. **g**, HC-fed *Apoe*$^{-/-}$ mice were administered ImP (ImP) or not (CTR) in the drinking water for 4 weeks, followed by sacrifice and analysis Oil red O en face staining of the aorta showing quantification of atherosclerotic lesions in aorta (left) and representative images (right). HC = 10; HC+ImP=9 **a-g**, Individual data and mean ± SEM from at least two pooled independent experiments. **a,b,c,e,g**, Two-tailed unpaired Student's t test. **d**, Two-tailed Mann–Whitney U test. **f**, One-tailed unpaired Student's t test.

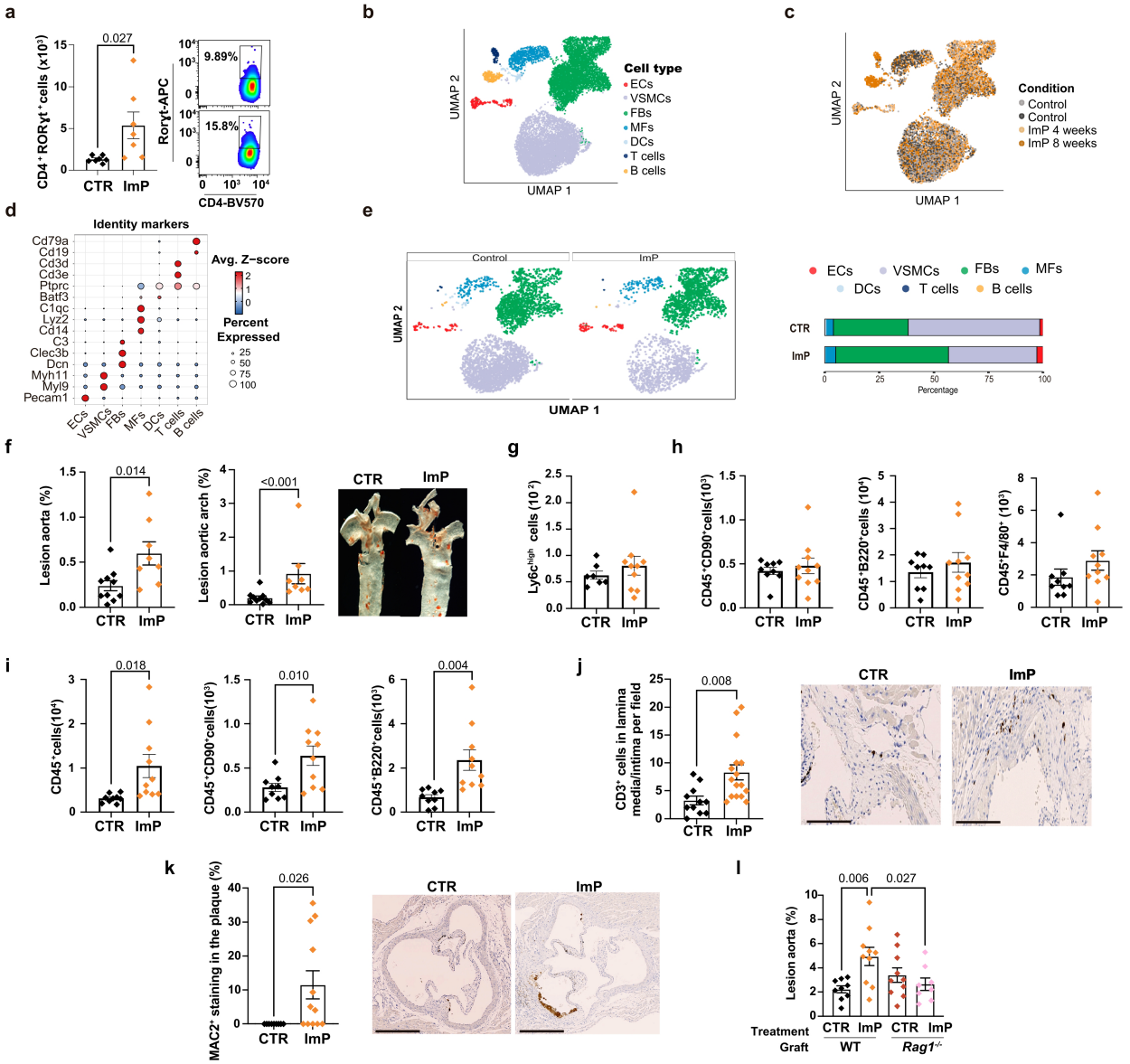


**Extended Data Fig. 4 | Increased ImP in circulation induces atherosclerosis and systemic inflammation in chow-fed atherosclerosis-prone mice.** **a-k**, Chow-fed *ApoE*$^{-/-}$ mice were administered ImP for 4 or 8 weeks as indicated. **a**, Numbers of RORγt in CD4$^+$ T cells in blood at sacrifice. Left: n = 7. Right: representative density plots for CTR (top) and ImP (bottom). **b,c** UMAP embeddings of whole aorta-derived cells profiled by scRNAseq colored by cell type, regardless of treatment duration (**b**) and by treatment and time (**c**). **d**, Dot plot of cell type markers used to identify main cell populations. **e**, UMAP embedding (left) and cell proportions (right) labelled by cell type of whole aorta-derived cells based on transcriptomic profiles from chow-fed *ApoE*$^{-/-}$ mice after 4 weeks of ImP administration. **f**, Quantification of atherosclerotic lesions by Oil red O en face staining of the aorta, showing quantification in whole aorta (left), aortic arch (middle) and representative images (right) following 4 weeks of ImP administration. CTR = 10; ImP=8. **g-i**, Numbers of circulating Ly6C$^{high}$ monocytes CTR = 7; ImP=10 (**g**), CD90$^+$ T cells, B220$^+$ B cells and F4/80$^+$ Macrophages CTR = 9; ImP=10 (**h**) after 4 weeks of ImP administration determined by flow cytometry. **i**, Total numbers of CD45$^+$ cells, CD90$^+$ T cells and B220$^+$ B cells infiltrated in aorta after 8 weeks of ImP administration by flow cytometry analysis. CTR = 9; ImP=10. **j**, Staining of CD3$^+$ cells in intima/media layer in aortic roots showing quantification (left) and representative images (right) of infiltrated T cells after 8 weeks of ImP administration. CTR = 11; ImP=16. Bar size = 500 µm. **k**, MAC2 staining inside atheroma plaque showing MAC2$^+$ area quantification (left) and representative images (right) after 8 weeks of ImP administration. CTR = 9; ImP=12, Bar size = 500 µm. **l**, ImP was administered (ImP) or not (CTR) to *Ldlr*$^{-/-}$ mice grafted with BM from WT (CTR = 9, ImP=10) or *Rag1*$^{-/-}$ (CTR = 10, ImP=8) and fed chow diet for 12 weeks. Quantification of atherosclerotic lesions by Oil red O en face staining of the aorta, showing quantification in whole aorta. **f-l**, Individual data and mean ± SEM from at least two pooled independent experiments. **a, f (left),h-k**, Two-tailed Unpaired Student's t test. **f (right), g, h (left)**, Two-tailed Mann–Whitney U test. **l**, One-way ANOVA with Tukey post-hoc correction.

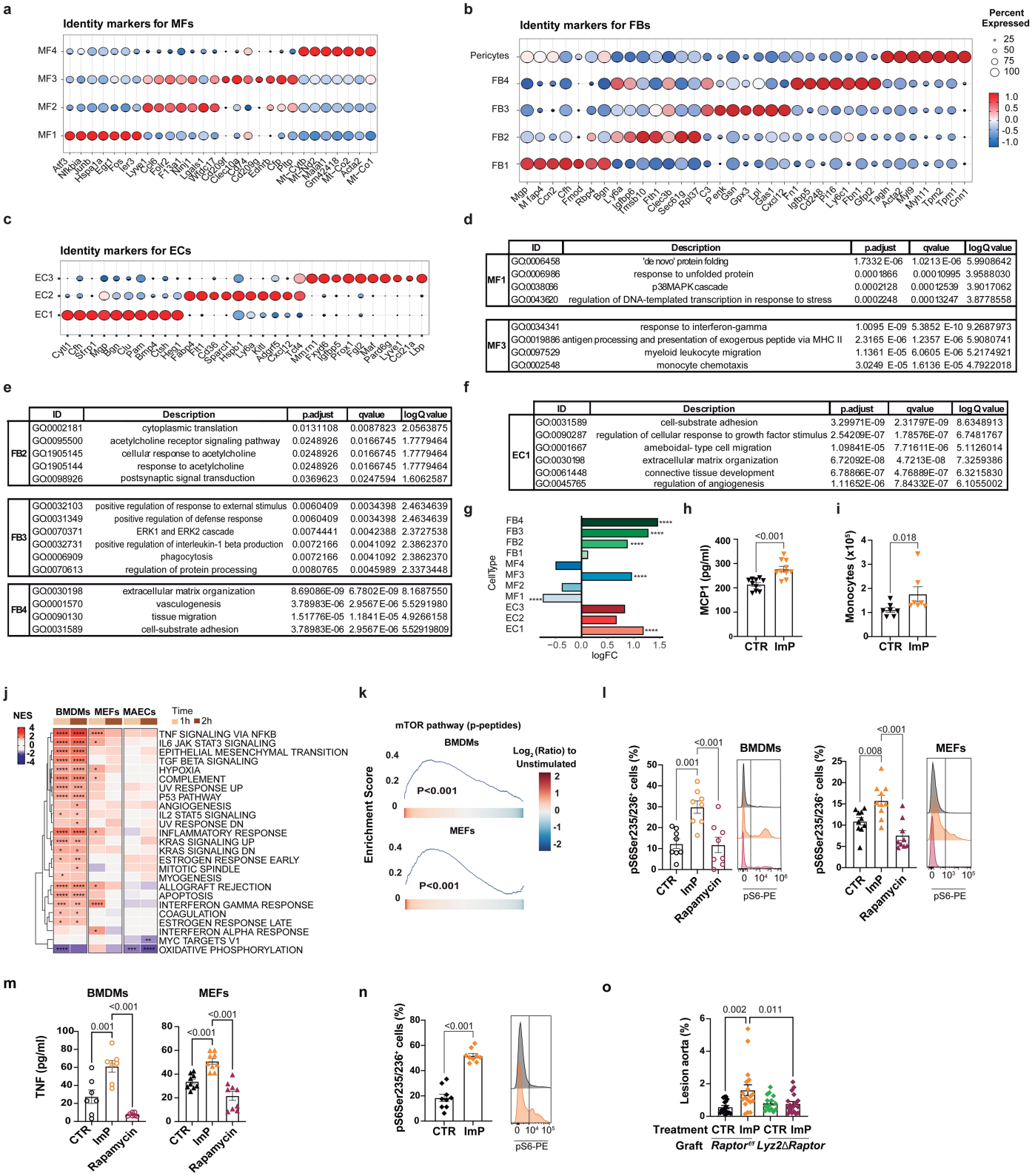


| | ID | Description | p.adjust | qvalue | log Q value |
|---|---|---|---|---|---|
| MF1 | GO:0006458 | 'de novo' protein folding | 1.7332 E-06 | 1.0213 E-06 | 5.9908642 |
| | GO:0006986 | response to unfolded protein | 0.0001866 | 0.00010995 | 3.9588030 |
| | GO:0038066 | p38MAPK cascade | 0.0002128 | 0.00012539 | 3.9017062 |
| | GO:0043620 | regulation of DNA-templated transcription in response to stress | 0.0002248 | 0.00013247 | 3.8778558 |
| MF3 | GO:0034341 | response to interferon-gamma | 1.0095 E-09 | 5.3852 E-10 | 9.2687973 |
| | GO:0019886 | antigen processing and presentation of exogenous peptide via MHC II | 2.3165 E-06 | 1.2357 E-06 | 5.9080741 |
| | GO:0097529 | myeloid leukocyte migration | 1.1361 E-05 | 6.0605 E-06 | 5.2174921 |
| | GO:0002548 | monocyte chemotaxis | 3.0249 E-05 | 1.6136 E-05 | 4.7922018 |

| | ID | Description | p.adjust | qvalue | log Q value |
|---|---|---|---|---|---|
| FB2 | GO:0002181 | cytoplasmic translation | 0.0131108 | 0.0087823 | 2.0563875 |
| | GO:0095500 | acetylcholine receptor signaling pathway | 0.0248926 | 0.0166745 | 1.7779464 |
| | GO:1905145 | cellular response to acetylcholine | 0.0248926 | 0.0166745 | 1.7779464 |
| | GO:1905144 | response to acetylcholine | 0.0248926 | 0.0166745 | 1.7779464 |
| | GO:0098926 | postsynaptic signal transduction | 0.0369623 | 0.0247594 | 1.6062587 |
| FB3 | GO:0032103 | positive regulation of response to external stimulus | 0.0060409 | 0.0034398 | 2.4634639 |
| | GO:0031349 | positive regulation of defense response | 0.0060409 | 0.0034398 | 2.4634639 |
| | GO:0070371 | ERK1 and ERK2 cascade | 0.0074441 | 0.0042388 | 2.3727538 |
| | GO:0032731 | positive regulation of interleukin-1 beta production | 0.0072166 | 0.0041092 | 2.3862370 |
| | GO:0006909 | phagocytosis | 0.0072166 | 0.0041092 | 2.3862370 |
| | GO:0070613 | regulation of protein processing | 0.0080765 | 0.0045989 | 2.3373448 |
| FB4 | GO:0030198 | extracellular matrix organization | 8.69086E-09 | 6.7802E-09 | 8.1687550 |
| | GO:0001570 | vasculogenesis | 3.78983E-06 | 2.9567E-06 | 5.5291980 |
| | GO:0090130 | tissue migration | 1.51776E-05 | 1.1841E-05 | 4.9266158 |
| | GO:0031589 | cell-substrate adhesion | 3.78983E-06 | 2.9567E-06 | 5.52919809 |

| | ID | Description | p.adjust | qvalue | log Q value |
|---|---|---|---|---|---|
| EC1 | GO:0031589 | cell-substrate adhesion | 3.29971E-09 | 2.31797E-09 | 8.6348913 |
| | GO:0090287 | regulation of cellular response to growth factor stimulus | 2.54209E-07 | 1.78576E-07 | 6.7481767 |
| | GO:0001667 | ameboidal- type cell migration | 1.09841E-05 | 7.71611E-06 | 5.1126014 |
| | GO:0030198 | extracellular matrix organization | 6.72092E-08 | 4.7213E-08 | 7.3259386 |
| | GO:0061448 | connective tissue development | 6.78866E-07 | 4.76889E-07 | 6.3215830 |
| | GO:0045765 | regulation of angiogenesis | 1.11652E-06 | 7.84332E-07 | 6.1055002 |

**Extended Data Fig. 5** | See next page for caption.

**Extended Data Fig. 5 | ImP induces transcriptional changes in fibroblasts, macrophages and endothelial cells. a-g**, Chow-fed *ApoE*$^{-/-}$ mice were administered ImP and the aorta-derived cells from the scRNAseq were analysed. **a-c**, Dot plot of expression levels of cell type markers used to identify cell subclusters for macrophages (MFs) (**a**), fibroblasts (FBs) (**b**), and endothelial cells (ECs) (**c**). **d-f**, Table of representative gene ontology (GO) terms enriched in the subclusters of MFs (**d**), FBs (**e**) and ECs (**f**). All shown GO terms are significant (adjusted p-value ≤ 0.05). **g**, Relative abundance (log-ratio) of the subcluster cell proportions comparing ImP treatment vs CTR, regardless of the treatment duration. **h**, MCP1 concentration measured by ELISA in the supernatant of MEFs treated with ImP for 24 h. n = 10. **i**, Number of post-migration monocytes collected in the bottom chamber in response to supernatant from (**h**) and quantified by flow cytometry. n = 7. **j**, Heat map of gene set enrichment analysis (GSEA) from RNAseq analysis of bone marrow-derived macrophages (BMDMs), mouse embryonic fibroblasts (MEFs) and mouse aortic ECs (MAECs) comparing ImP stimulation after 1 h and 2 h vs unstimulated conditions within each cell type. **k**, GSEA enrichment plots of phosphopeptides related to the mTOR pathway from BMDMs (top) and MEFs (down) after ImP treatment for 180 min compared with unstimulated cells. Global abundances of all peptides related to the mTOR pathway were used for the analysis. **l,m**, BMDMs (left) and MEFs (right) after ImP stimulation for 24 h with or without rapamycin co-incubation. **l**, Flow cytometry staining for pS6 ribosomal protein. Left: BMDM n = 8; MEF CTR = 10; ImP=10; ImP + AGN = 9; Right: representative histograms for CTR (top), ImP (middle) and ImP + rapamycin (bottom). **m**,TNF production measured by ELISA. BMDM n = 7; MEF n = 9 **n**, Flow cytometry staining for pS6 in peritoneal macrophages harvested from chow-fed *ApoE*$^{-/-}$ mice administered ImP for 8 weeks. Left: n = 9. Right: representative histograms for CTR (top), ImP (bottom). **o**, ImP was administered (ImP) or not (CTR) to *Ldlr*$^{-/-}$ mice grafted with BM from control *Raptor*$^{f/f}$ (CTR = 17; ImP=18) or *Lyz2*Δ*Raptor* (CTR = 15; ImP=18) and fed chow diet for 12 weeks. Quantification of atherosclerotic lesions by Oil red O en face staining of the aorta, showing quantification in whole aorta. **a-c**, Wilcoxon rank sum test comparing cell clusters. Adjusted p-value < 0.05. **g**, Two-proportions Z-test. **h,i**, Data are pooled from n = 7 independent experiments. **h**, Two-tailed Unpaired Student's t test. **i**, Two-tailed Mann–Whitney U test. **j**, Kolmogorov Smirnov test. **k**, Nominal p-values were calculated using a 1000-permutation test. **l,m,o**, Individual data (each one represent an independent experiment) and mean ± SEM. One-way ANOVA with Tukey post-hoc correction. **n**, Individual data and mean ± SEM of at least two pooled independent experiments. Two tailed unpaired Student's t test between CTR and ImP. *p < 0.05; **p < 0.01; ***p < 0.005; ****p < 0.001.

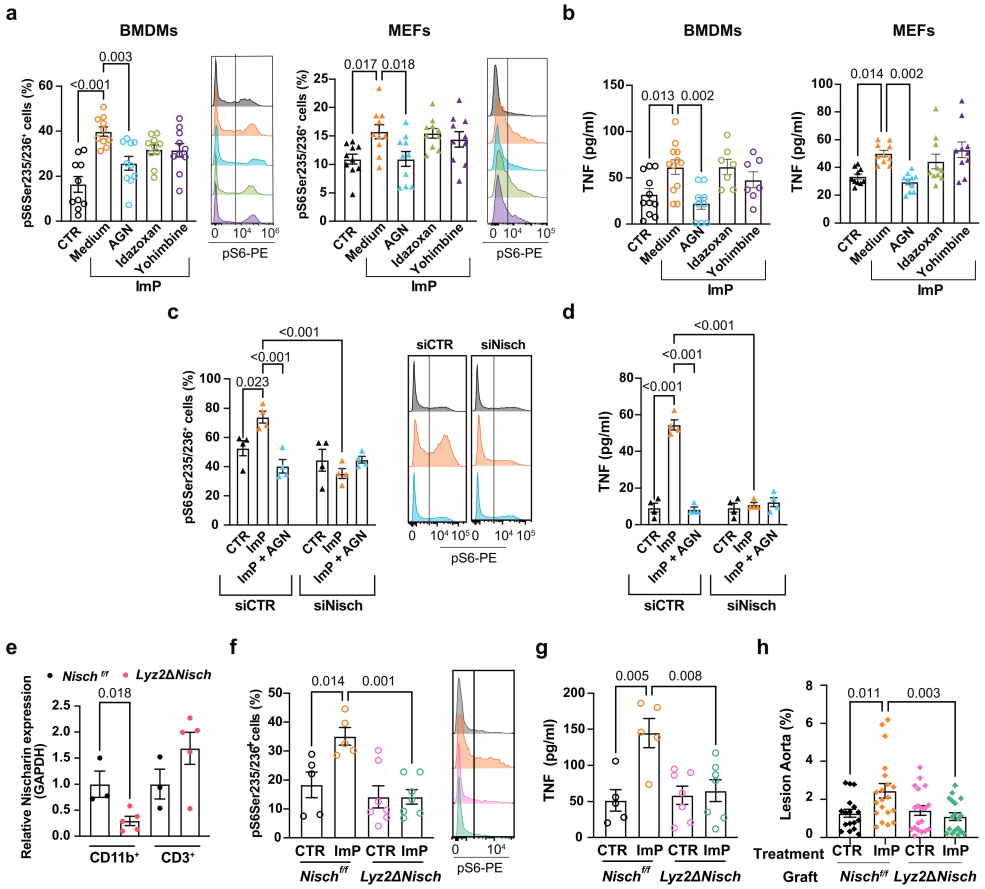


**Extended Data Fig. 6 | Imidazoline-1 receptor mediates functional responses that are induced by ImP. a,b**, Bone marrow-derived macrophages (BMDMs) and mouse mouse embryonic fibroblasts (MEFs) were treated in vitro with ImP (or not, CTR) and co-incubated with AGN192403 (AGN, I1R antagonist), Idazoxan (IR and adrenoreceptor (α2) antagonist) or Yohimbine (α2 antagonist). **a**, Flow cytometry staining for pS6 (left, n = 10) and representative histograms (right) corresponding to each treatment matched by color. **b**, TNF production in 24 h culture supernatant by ELISA (BMDMs: CTR = 11, ImP+medium=12, ImP+AGN = 9, ImP+idazoxan=7, ImP+yohimbine=7; MEF: n = 10 for all groups). **c,d** MEFs were transfected with I1R siRNA (siNisch) or control siRNA (siCTR) and stimulated with ImP or not (CTR) and co-incubated or not with AGN192403 (AGN) as indicated. **c**, Flow cytometry staining for pS6, showing quantification of percentage of pS6 positive cells (left, n = 4) and representative histograms (right) corresponding to each treatment indicated and matched by color. **d**, TNF production in 24 h culture supernatant by ELISA. n = 4. **e**, $CD45^+CD11b^+$ and $CD45^+CD3^+$ splenic cells were isolated to analyse *Nisch* mRNA relative expression by qRT-PCR. $CD11b^+$ $Nisch^{f/f}$ = 3, $CD11b^+$ *Lyz2ΔNisch* = 5; $CD3^+$ $Nisch^{f/f}$ = 3, $CD3^+$ *Lyz2ΔNisch* = 5; **f,g** BMDMs were generated from $Nisch^{f/f}$ or Lyz2Δ*Nisch* mice and treated or not (CTR) with ImP in vitro. **f**, Flow cytometry staining for pS6, showing quantification of percentage of pS6 positive cells (left) and representative histograms (right) corresponding to each treatment matched by color. $Nisch^{f/f}$ CTR = 5, $Nisch^{f/f}$ ImP=5, *Lyz2ΔNisch* CTR = 7, *Lyz2ΔNisch* ImP=7. **g**, TNF production in 24 h culture supernatant by ELISA. $Nisch^{f/f}$ CTR = 5, $Nisch^{f/f}$ ImP=5, *Lyz2ΔNisch* CTR = 7, *Lyz2ΔNisch* ImP=7. **h**. ImP was administered (ImP) or not (CTR) to $Ldlr^{-/-}$ mice grafted with BM from control $Nisch^{f/f}$ or *Lyz2ΔNisch* and fed chow diet for 12 weeks. Quantification of atherosclerotic lesions in the aorta by Oil red O en face staining of the aorta. n = 17-20 **a,b**, Arithmetic mean ± SEM and individual data from biological replicates. One-way ANOVA with Tukey post-hoc correction. **c,d**, Arithmetic mean ± SEM and individual data from n = 4 pooled independent experiments. One-way ANOVA with Tukey post-hoc correction. **e**, Arithmetic mean ± SEM and individual data from biological replicates. Two tailed unpaired Student's t test between $Nisch^{f/f}$ and *Lyz2*ΔNisch. **f,g**, Arithmetic mean ± SEM and individual data. One-way ANOVA with Tukey post-hoc correction. **h**, One-way ANOVA with Tukey post-hoc correction $Nisch^{f/f}$ (CTR = 17, ImP=20) or *Lyz2ΔNisch* (CTR = 19 ImP=18). In all panels, n indicates biological replicates.

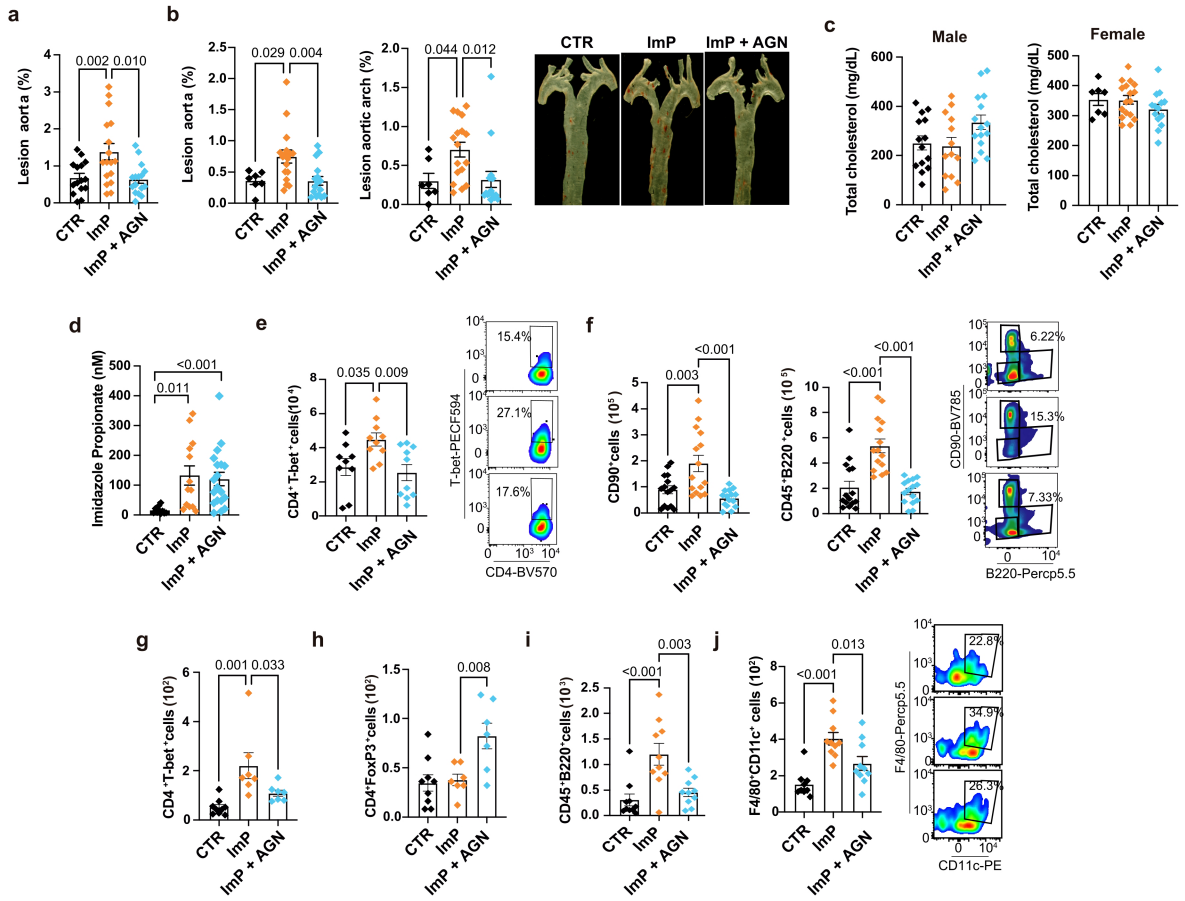


**Extended Data Fig. 7 | Inhibition of the ImP/I1R axis with AGN192403 prevents ImP-induced immune and inflammatory response without affecting circulating ImP and cholesterol concentration. a-i**, ImP was administered (or not, CTR) in the presence of AGN192403 (AGN) or not (ImP) in drinking water to *ApoE*$^{-/-}$ mice fed chow diet for 8 weeks, followed by sacrifice and analysis. **a**, Oil red O en face staining of the aorta showing quantification of atherosclerotic lesions in whole aorta in male mice. CTR = 15; ImP=17; ImP + AGN = 16. **b**, Oil red O en face staining of the aorta showing quantification of atherosclerotic lesions in whole aorta (left), aortic arch (middle) and representative images (right) in female mice. CTR = 7; ImP=17; ImP + AGN = 16. **c**, Total cholesterol concentration in plasma. Male mice (left), CTR = 14; ImP=13; ImP + AGN = 15, and female mice (right), CTR = 7; ImP=17; ImP + AGN = 14. **d**, Imidazole Propionate concentration in plasma of male mice at sacrifice. CTR = 10; ImP=13; ImP + AGN = 17. **e,f**, Number of T-bet in CD4$^+$ T cells. (**e**), and CD90$^+$ T and B220$^+$ B cells (**f**) in blood at sacrifice by flow cytometry. CTR = 9; ImP=10; ImP + AGN = 10 (**e**) and n = 15 (**f**). **g-j** Number of aorta infiltrated T-bet$^+$ Th1. CTR = 9; ImP=7; ImP + AGN = 7 (**g**) and FoxP3$^+$ Treg cells CTR = 9; ImP=7; ImP + AGN = 7 (**h**), B220$^+$ B cells. n = 10 (**i**) and F4/80$^+$ Cd11c$^+$ cells. CTR = 9; ImP=10; ImP + AGN = 10 (**j**) by flow cytometry. **e,f,j**, Right: representative density plots for CTR (top), ImP (middle) and ImP+AGN (bottom). **a-j**, Arithmetic mean ± SEM and individual data from at least two pooled independent experiments. One-way ANOVA with Tukey post-hoc correction.

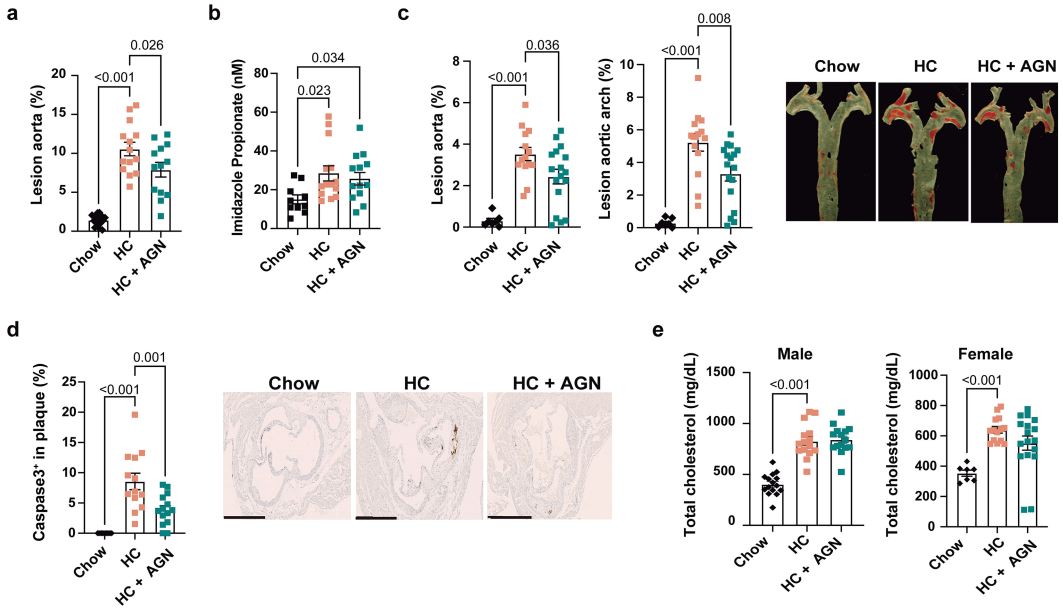


**Extended Data Fig. 8 | Inhibition of the ImP/I1R axis with AGN192403 prevents HC-induced atherosclerosis without affecting circulating ImP and cholesterol concentration. a-e**, *ApoE*$^{-/-}$ mice were fed a chow diet or high cholesterol (HC) diet for 8 weeks. At 4 weeks post-diet initiation, AGN192403 was administered (AGN) or not in the drinking water to mice fed HC diet until week 8, followed by sacrifice and analysis. **a**, Oil red O en face staining of the aorta in male mice showing quantification of atherosclerotic lesions in the whole aorta. Chow=15; HC = 14; HC + AGN = 13. **b**, ImP concentration in plasma of male mice at sacrifice. Chow=10; HC = 14; HC + AGN = 13. **c**, Oil red O en face staining of the aorta in female mice showing quantification of atherosclerotic lesion in the whole aorta (left), aortic arch (middle) and representative images (right). Chow=8; HC = 15; HC + AGN = 18. **d**, Caspase 3 staining of aortic roots. Quantification of caspase-3$^{+}$ (left) and representative images of caspase-3 staining (right). Bar size= 500 µm. Chow=12; HC = 13; HC + AGN = 14. **e**, Total cholesterol concentration in plasma in male (left), n = 15, and female mice (right), Chow=7; HC = 14; HC + AGN = 17, at sacrifice. **a-e**, Arithmetic mean ± SEM and individual data from at least two pooled independent experiments. One-way ANOVA with Tukey post-hoc correction.

nature portfolio

Corresponding author(s): David Sancho

Last updated by author(s): Jun 3, 2025

# Reporting Summary

Nature Portfolio wishes to improve the reproducibility of the work that we publish. This form provides structure for consistency and transparency in reporting. For further information on Nature Portfolio policies, see our Editorial Policies and the Editorial Policy Checklist.

## Statistics

For all statistical analyses, confirm that the following items are present in the figure legend, table legend, main text, or Methods section.

| n/a | Confirmed | |
|---|---|---|
| ☐ | ☒ | The exact sample size (*n*) for each experimental group/condition, given as a discrete number and unit of measurement |
| ☐ | ☒ | A statement on whether measurements were taken from distinct samples or whether the same sample was measured repeatedly |
| ☐ | ☒ | The statistical test(s) used AND whether they are one- or two-sided<br>*Only common tests should be described solely by name; describe more complex techniques in the Methods section.* |
| ☐ | ☒ | A description of all covariates tested |
| ☐ | ☒ | A description of any assumptions or corrections, such as tests of normality and adjustment for multiple comparisons |
| ☐ | ☒ | A full description of the statistical parameters including central tendency (e.g. means) or other basic estimates (e.g. regression coefficient) AND variation (e.g. standard deviation) or associated estimates of uncertainty (e.g. confidence intervals) |
| ☐ | ☒ | For null hypothesis testing, the test statistic (e.g. *F*, *t*, *r*) with confidence intervals, effect sizes, degrees of freedom and *P* value noted<br>*Give P values as exact values whenever suitable.* |
| ☒ | ☐ | For Bayesian analysis, information on the choice of priors and Markov chain Monte Carlo settings |
| ☒ | ☐ | For hierarchical and complex designs, identification of the appropriate level for tests and full reporting of outcomes |
| ☒ | ☐ | Estimates of effect sizes (e.g. Cohen's *d*, Pearson's *r*), indicating how they were calculated |

*Our web collection on statistics for biologists contains articles on many of the points above.*

## Software and code

Policy information about availability of computer code

| | |
|---|---|
| Data collection | Untargeted metabolomics data was collected by an Ultimate 3000 HPLC system coupled to a LTQ Orbitrap XL™ Hybrid Ion Trap-Orbitrap Mass Spectrometer. Targeted metabolomics data was collected for ImP quatification for APOEKO mice and for the PESA cohort by an HPLC system 1290 Infinity series coupled to a triple quadrupole 6460 MS, whereas for the IGT cohort by Acquity UPLC I-class system coupled to a Xevo TQ-XS triple quadrupole mass spectrometer. Fluorescence-Activated Cell Sorting data was collected by LSRFortessa SORP (Becton Dickinson) or a FACSymphony (Becton Dickinson). 16S rRNA amplicon sequencing data was collected by MiSeq Illumina platform. Single-cell and bulk RNA data was collected by Illumina NextSeq 2000 sequencer. Proteomics and phosphoproteomics data was collected by liquid chromatography with tandem mass spectrometry (LC–MS/MS) using Q Exactive HF Orbitrap MS. Other data were collected with Microsoft Excel 2019. |
| Data analysis | Heatmap and all charts were generated using GraphPad Prism software v.9.0 (GraphPad Software, San Diego, CA). SPSS version 23.0 and Stata version 18 (StataCorp LP, College Station, TX) were used for statistical analysis. Partial least squares discriminant analysis (PLS-DA) and receiver operating characteristic (ROC) analyses were performed in MetaboAnalyst V5 (https://www.metaboanalyst.ca/MetaboAnalyst/home.xhtml) and Stata. The Kolmogorov-Smirnov test and Shapiro–Wilk normality test were used to determine the normal distribution of samples. Nominal variables were presented as percentages and frequencies. Comparisons between two groups were performed using two-tailed unpaired Student's t-tests (normal distribution) or Mann–Whitney U-tests (non-normal distribution) for continous variables or Fisher exact test for categorical variables. Unless otherwise stated, comparisons across multiple groups were assessed using one-way ANOVA (normal distribution) followed by Tukey's post hoc test, or Kruskal–Wallis test (non-normal distribution) followed by Dunn's test as indicated in each figure legend. Continuous variables were compared across tertiles of ImP by ANOVA or non-parametric Kruskall Wallis tests as appropriate, whereas nominal variables by applying the Cohran-Armitage test (dichotomous variables) and the Jonckheere-Terpstra test (ordinal variable) for trend. Restricted cubic splines (natural splines, RCS) with 3 knots across ImP distribution were applied to produce a dose-response curves and to flexibly model the potential nonlinear association of continuous ImP with the main endpoints, as previously described (PMID: 29799975; PMID: 36049808). In both cohorts, the 3 knots for RCS were fixed at the 10th, 50th and 90th percentile of the ImP |

distribution. Number of knots was selected on the basis of improvement in log likelihood among regression models with 3- or 4-knot RCS. To enhance visual clarity, plots with RCS were truncated at values exceeding the 95th perecentile of the ImP distribution. We evaluated the non-linear relationships of ImP with log odd ratio (OR) of the main atherosclerosis outcomes by examining (Wald test) the non-linear terms (RCS). Dose–response curves in both cohorts were controlled for a set of confounders, constructed by combining LASSO regression and variables with biological plausibility. LASSO for logistic regression was used for multivariable model selection with respect to the outcome presence of atherosclerosis. Adaptive LASSO with cross validation was employed to select the value of the lasso penalty parameter lambda. Adjusted differences in levels of ImP across groups of interest were estimated by multivariable linear regression analysis. To evaluate the association between ImP levels and the presence and activity of atherosclerosis within the PESA cohort multinomial logistic regression was adjusted on a set of confounders (i.e. age, sex, smoking status, fasting glucose, high-sensitivity C Reactive Protein (hs-CRP), and hemoglobin concentration) based on previous evidence (PMID: 35567559)). The proportional odds assumption was tested with the Brant Wald test. The discriminatory capability of ImP for prevalence of subclinical or active atherosclerosis on top of traditional risk factors, including LDL-cholesterol and high-sensitive C Reactive Protein, was assessed by comparing Area(s) Under the Curve (AUC) from corresponding Receiver Operating Characteristic (ROC) analysis. AUCs were compared using the DeLong test (PMID: 3203132). Bootstrapping with 1,000 replicates was used to derive 95% bias-corrected confidence interval (CI) around AUCs.All tests were two tailed and the level of statistical significance was pre-specified at $P<0.05$.

For untargeted metabolomics data: generated data was firstly aligned using Compound Discoverer (ThermoFisher Scientific); signals were extracted and grouped into features (isotopic traces from a single analyte at a particular charge state) using the Metaboprofiler node in Compound discoverer (the open source plug-in freely available from OpenMS, http://www.openms.de/downloads/). For targeted metabolomics data: Raw signals for multiple reaction monitoring (MRM) transitions were checked and peaks corresponding to all the targeted compounds were integrated by MassHunter Quantitative B.10.00 (Agilent Technologies).
For 16S rRNA gene sequencing analysis from both mice and human samples, the paired-end sequences were curated, binned into operational taxonomic units at >97% identity level, and annotated with SILVA release v.132 using DADA2 for mice data and v.138 and RDP version 18 databases using Mothur (v.1.40.5) for human data.
For dietary pattern assessment a factor analysis was performed in SPSS V.23.0 (SPSS Inc., Armonk, NY, USA) to identify common underlying dimensions (factors or patterns) of food consumption by deriving factor loadings for each predefined food group. Factors were subsequently rotated using a Varimax procedure to maintain uncorrelated factors. Analysis of eigenvalues, scree plot, and the interpretability of the factor solution were used to support a final decision on retaining a 5-factor solution, where each factor had an eigenvalue > 0.3.
For single-cell RNA seq data raw sequencing data processing was performed from FASTQ file from each port using Cell Ranger (v6.1.2) with default parameters and the mm10 (GRCm38.p6) mouse genome reference provided by 10x Genomics. Obtained raw unique molecular identifier (UMI) count matrices of valid barcoded cells for each port were loaded into R (v4.1.2) for further analyses using Bioconductor packages and Seurat (v4.0.6). Cells were clustered using the Louvain algorithm for modularity optimization using KNN graph as input and visualized using the Uniform Manifold Approximation and Projection for Dimension Reduction (UMAP) algorithm with the first 25 principal components as input. Main clusters were identified by using known markers and calculating differentially expressed genes with Wilcoxon-rank sum test using presto R package (v1.0.0)). Cell proportions were calculated for each condition and time point in every cell population, and a two-proportions Z-test using the prop.test() R function was chosen to determine significance. Differential expression analyses between conditions were performed using the MAST R package (v1.20.0). Genes were ranked according to the calculated logFCs, and resulting ranks were used as input for the FGSEA algorithm along with the Hallmark gene sets from the Molecular Signature Data Base (MSigDB; https://www.gsea-msigdb.org/gsea/msigdb). Finally, overrepresentation analysis was performed along with the GO database (www.geneontology.org/).
For RNA-seq resulted reads were mapped to the reference transcriptome GRCm38.102 using STAR25 and gene expression levels were estimated using RSEM26. Further analyses were performed in R (v 4.3.2). In brief, counts per million (CPM) were calculated, and size factors for inter-sample normalization were determined using the trimmed mean of M values (TMM) method. Then, log-normalized data considering only genes with ≥ 20 counts in three samples were used for differential expression analysis, making all possible comparisons within the same cell type using the DESeq2 R package. Gene-set enrichment analysis was performed using the fgsea R package comparing 1h and 2h after ImP stimulation with 0h (unstimulated) within each cell type. Genes were ranked in each comparison according to logFC, and fgsea was used along with the Hallmark gene sets from the Molecular Signature Data Base (MSigDB; https://www.gsea-msigdb.org/gsea/msigdb). Finally, normalized enrichment scores of significant selected pathways were represented as a heatmap using the ComplexHeatmap R package.
Proteome and phosphoproteome analyses were accomplished using 18-plex isobaric TMT labeling as described previously. The statistical analysis of quantitative data was made using iSanXoT, and the comparative analysis between conditions was performed using the normalized values X_p^m and X_q^m, which represent the binary logarithm of the ratio between the abundance in sample m and its control for peptide p and protein q, respectively. Gene Set Enrichment Analysis (GSEA) using X_p values of peptides was employed to evaluate the phosphorylation levels in proteins of the mTOR signalling pathway among conditions (i.e. cells stimulated with ImP vs unstimulated). In addition, a Wilcoxon Signed Rank Test was performed using paired phosphopeptide abundance X_p values to determine the effects of AGN192403 in the phosphorylation levels of the mTOR pathway among cells treated with ImP and co-incubated or not with AGN192403.

For manuscripts utilizing custom algorithms or software that are central to the research but not yet described in published literature, software must be made available to editors and reviewers. We strongly encourage code deposition in a community repository (e.g. GitHub). See the Nature Portfolio guidelines for submitting code & software for further information.

## Data

Policy information about availability of data

All manuscripts must include a data availability statement. This statement should provide the following information, where applicable:

- Accession codes, unique identifiers, or web links for publicly available datasets
- A description of any restrictions on data availability
- For clinical datasets or third party data, please ensure that the statement adheres to our policy

Metabolomics data are deposited in Metabolomics workbench (ST003928, ST003929, ST003932 and ST003938). The bulk RNA-seq and scRNA-seq data generated in this study are available in the NCBI GEO database under BioProject IDs GSE297831 and GSE298392, respectively. The proteomics and phosphoproteomics data have been deposited to the ProteomeXchange Consortium via the PRIDE partner repository with the dataset identifier PXD063955. Source data are provided with this paper.

# Research involving human participants, their data, or biological material

Policy information about studies with human participants or human data. See also policy information about sex, gender (identity/presentation), and sexual orientation and race, ethnicity and racism.

| | |
|---|---|
| Reporting on sex and gender | The current study is focused on subclinical atherosclerosis and explore the blood concentration of imidazole propionate, urocanic acid and histidine in middle-aged asymptomatic participants (56±4 years). Considering the delayed onset of subclinical atherosclerosis that is approximately 10 years later in women (PMID: 34543072 and PMID: 25882487), our cohort included 400 participants of which 310 (78%, by sex) were male participants. The information regarding the sex of each participant was collected by self-reporting via a questionnaire. These data are indicated in Extended Data Table 1a and 2b and Table 3.<br>The IGT cohort that was used to validate the results in an independent cohort comprises men and women aged 50-64 years from the Gothenburg area (Sweden). In this case the cohort included 1844 participants of which 841 (46%, by sex), were male participants thus including an higher the percentage of women. The participants were recruited on a random basis from the Swedish population register and information regarding the sex of each participant was collected by self-reporting via a questionnaire. These data are indicated in Extended Data Table 2a and 2b. |
| Reporting on race, ethnicity, or other socially relevant groupings | This study was conducted in a subset of participants from the PESA study (Progression of Early Subclinical Atherosclerosis), an ongoing observational prospective cohort study of caucasian asymptomatic employees of the Santander Bank in Madrid (PMID: 34238438). The information regarding race and other socially relevant groupings of each participant was collected by self-reporting via a questionnaire and was not used as exclusion factor.<br>In the IGT study, the population includes men and women aged 50-64 years from the Gothenburg area (Sweden), recruited on a random basis from the Swedish population register. Among the exclusion criteria, cognitive dysfunction and inability to understand written and spoken Swedish as well as subjects born outside Sweden were included. |
| Population characteristics | This study was conducted in a subset of participants (n=400) from the PESA-CNIC-Santander. Based on multiterritorial/ multimodal imaging (i.e. 2D/3D vascular ultrasonography and non-contrast computed tomography), we classified 295 participants with subclinical atherosclerosis and 105 controls without atherosclerosis. Extent of atherosclerosis was defined according to the number of affected vascular sites and the coronary artery calcium (CAC) score. Subjects with subclinical atherosclerosis were further stratified by Fluorodeoxyglucose (18F-FDG) uptake and bone marrow activation in: inactive atherosclerosis (FDGneg, n=74), arterial 18 F-FDG uptake (FDG+_A, n=57), bone marrow activation (FDG+_BM, n=40), and both arterial uptake and bone marrow activation (FDG+_SYS, n=124) as indicatives of metabolically active atherosclerosis (FDG+, n=221). Detailed population characteristics and group allocation are presented in Extended Data Table 1a,b and Table 3 and Extended Data Fig. 2c.<br>The IGT study population is composed of men and women aged 50-64 years from the Gothenburg area (Sweden), recruited on a random basis from the Swedish population register and included based on their glucose status. The applied exclusion criteria included: known diabetes, inflammatory diseases (e.g. Crohn's disease, ulcerative colitis, rheumatic diseases), treatment with steroids or immunomodulatory drugs, cancer (unless relapse free for the preceding 5 years), cognitive dysfunction, treatment for infectious diseases and with antibiotics in the past three months, inability to understand written and spoken Swedish as well as subjects born outside Sweden.<br>Atherosclerosis in the carotid arteries was assessed by ultrasound imaging using a standardized protocol including a Siemens Acuson S2000 ultrasound scanner and by presence of coronary artery calcium assessed by CT scan. Systolic blood pressure (SBP) was measured twice with an automatic device (Omron M10-IT, Omron Health care Co, Kyoto, Japan) and the mean of the measurements was used. A questionnaire was used to collect detailed information on medication and family history. A venous blood sample (100 mL) was collected from participants after an overnight fast and was used for immediate biochemical analysis of glucose, glycated haemoglobin and total cholesterol. SCORE2 (Systematic Coronary Risk Evaluation) was calculated as previously. Body weight, height waist and hip circumferences were measured on calibrated equipment with subjects dressed in light clothing without shoes and according to current WHO recommendations. Characteristics of the participants are listed in Extended Data Table 2,b. |
| Recruitment | Participants were recruited following the inclusion criteria of the main PESA-CNIC-Santander study (NCT01410318, https://clinicaltrials.gov/ct2/show/NCT01410318). Exclusion criteria included those previously used for the main study and those that could affect imidazole propionate production or associations previously described (e.g. type 2 diabetes): 1. Active treatment for inflammation or cardiovascular disease. 2. Participants with family history inflammatory illness 3. Active treatment for cancer, history of transplant with active immunosuppressive or immunomodulator treatment. 4. Employees who are pregnant or breast-feeding. 5. Clinically relevant renal or hepatic insufficiency. 6. Unable to consent 7. Any other clinically significant condition that may jeopardize the study or be dangerous for the participant. 8. Active drug or alcohol abuse. 9. Participants taking antibiotics in the three months prior to the collection of the faecal samples. 10. Participants taking proton pump inhibitors, laxatives, and non-steroidal anti-inflammatory drugs 3 days prior to the collection of the faecal sample. 11.Subjects with known Type 2 diabetes or treated for diabetes. 12. Subjects with intestinal disorders.<br><br>IGT cohort (Ethics Dnr 560-13) was recruited n a random basis from the Swedish population register and included based on their glucose status. The applied exclusion criteria included: known diabetes, inflammatory diseases (e.g. Crohn's disease, ulcerative colitis, rheumatic diseases), treatment with steroids or immunomodulatory drugs, cancer (unless relapse free for the preceding 5 years), cognitive dysfunction, treatment for infectious diseases and with antibiotics in the past three months, inability to understand written and spoken Swedish as well as subjects born outside Sweden. The participants were invited by letter and gave all informed consent.<br><br>Despite the application of rigorous recruitment and exclusion criteria, several potential sources of bias should be acknowledged. First, self-selection bias may be present, as participation was voluntary; individuals who chose to enroll may differ systematically from those who declined, potentially leading to a study population with higher health literacy or distinct risk profiles compared to the general population. In the PESA-CNIC-Santander subset, participants were all employees of Santander Bank in Madrid, which may introduce a "healthy worker effect" and limit the cohort's socioeconomic and |

occupational diversity. Moreover, the exclusive inclusion of Spanish individuals in the PESA cohort and Swedish individuals in the IGT cohort may introduce geographic and population-related bias. As a result, the findings may not fully represent the spectrum of cardiovascular risk or disease presentation seen in more ethnically and socioeconomically diverse or non-European populations. In the IGT cohort, although recruitment was population-based, the exclusion of non-Swedish-born individuals and those unable to understand Swedish may have introduced additional cultural or socioeconomic bias.

Ethics oversight

The Instituto de Salud Carlos III research ethics committee approved the study protocol (CEI PI 32_2018) and all participants were provided with a written informed consent.
All participants gave informed consent, and IGT study was approved by the Ethics Review Board in Gothenburg (560-13)

Note that full information on the approval of the study protocol must also be provided in the manuscript.

# Field-specific reporting

Please select the one below that is the best fit for your research. If you are not sure, read the appropriate sections before making your selection.

☒ Life sciences ☐ Behavioural & social sciences ☐ Ecological, evolutionary & environmental sciences

For a reference copy of the document with all sections, see nature.com/documents/nr-reporting-summary-flat.pdf

# Life sciences study design

All studies must disclose on these points even when the disclosure is negative.

Sample size

To calculate the sample size needed for a study in mice with the given parameters (two-tailed test, unpaired samples, significance level of 0.05, power of 0.8, and detecting at least a 1 standard deviation difference), we use the formula for sample size estimation in a two-sample t-test. These numbers were refined based on our previous knowledge of the reproducibility, balancing statistical robustness and animal welfare, following the reduction criterium. The formula for the sample size (per group) in a two-sample t-test is given by:

$n \approx 2 \cdot (Z1-\alpha/2+Z1-\beta)2 \cdot SD2/d2$

Where:

n: Sample size per group

Z1−α/2: Critical value for significance level (e.g., 1.96 for α=0.05)

Z1−β: Critical value for power (e.g., 0.84 for 80% power)

SD: Standard deviation (assumed equal between groups)

d: Effect size (minimum detectable difference between group means)

For our parameters, we would need approximately 15.7 mice per group to achieve a significance level of 0.05, a power of 0.8, and detect at least a 1 standard deviation difference. We increase the sample group in 1 mouse to be able to discard a mouse where the experimental technique may fail. Total sample size is usually about 17 mice to be tested in (at least) two independent experiments.

For the human cohorts (PESA and IGT), no sample size calculation was conducted, as samples were retrospectively collected from observational studies. Instead, sample sizes were determined based on the availability of well-characterized patients with complete clinical, imaging, and biosamples from ongoing prospective observational studies. The cohorts were assembled with the goal of maximizing biological and phenotypic depth rather than targeting a predefined effect size. The inclusion of two independent cohorts with complementary phenotypes enabled replication and validation across datasets. Post hoc power considerations indicated that the sample size of the derivation cohort (PESA cohort, n=400) was adequately powered at the 0.85 level to detect a minimum 5nMol difference in ImP levels between the group of subjects without atherosclerosis and patients without atherosclerosis. A ratio of 1:3 between patients without and with atherosclerosis was selected to reflect the distribution of AT in the PESA cohort, and measures of dispersion (i.e., standard deviation) were derived from the group of subjects without atherosclerosis in the PESA cohort. Respectively, the IGT cohort was adequately sized to detect with 0.85 power a difference of 2 nMoL in ImP levels between subjects without and with AT. Power considerations were based on the Mann-Whitney test for 2 independent groups. Type I error was prespecified at 0.05 for power calculations. Power analysis was performed with G*Power 3.1.9.6 (University of Kiel., Germany).

Data exclusions

No data were excluded from the analyses shown in the manuscript.

Replication

For mice and primary cell culture experiments, multiple independent biological replicates and independent experiments (at least twice) were performed, as indicated in figure legends. The results from the paper are consistent across multiple experimental approaches performed by different researchers. All attempts at replication obtained consistent data.

Randomization

Mice were homogeneous in terms of age (8 weeks) and randomly assigned to different cages for experimental treatments (antibiotics, imidazole propionate and AGN192403 administration). Human and animal samples were analysed in a randomized fashion on the mass spectrometer.

Blinding

For animal studies and cell-based in vitro studies, numbers were assigned to each experimental sample and analysis was blinded to group allocation during data collection.
For human study, samples were collected by blinded clinical staff and all data were generated by investigators that were blinded to the

metadata. Once data were generated, computational analysis was performed with all of the necessary clinical information to test between groups.

# Behavioural & social sciences study design

All studies must disclose on these points even when the disclosure is negative.

| | |
|---|---|
| Study description | *Briefly describe the study type including whether data are quantitative, qualitative, or mixed-methods (e.g. qualitative cross-sectional, quantitative experimental, mixed-methods case study).* |
| Research sample | *State the research sample (e.g. Harvard university undergraduates, villagers in rural India) and provide relevant demographic information (e.g. age, sex) and indicate whether the sample is representative. Provide a rationale for the study sample chosen. For studies involving existing datasets, please describe the dataset and source.* |
| Sampling strategy | *Describe the sampling procedure (e.g. random, snowball, stratified, convenience). Describe the statistical methods that were used to predetermine sample size OR if no sample-size calculation was performed, describe how sample sizes were chosen and provide a rationale for why these sample sizes are sufficient. For qualitative data, please indicate whether data saturation was considered, and what criteria were used to decide that no further sampling was needed.* |
| Data collection | *Provide details about the data collection procedure, including the instruments or devices used to record the data (e.g. pen and paper, computer, eye tracker, video or audio equipment) whether anyone was present besides the participant(s) and the researcher, and whether the researcher was blind to experimental condition and/or the study hypothesis during data collection.* |
| Timing | *Indicate the start and stop dates of data collection. If there is a gap between collection periods, state the dates for each sample cohort.* |
| Data exclusions | *If no data were excluded from the analyses, state so OR if data were excluded, provide the exact number of exclusions and the rationale behind them, indicating whether exclusion criteria were pre-established.* |
| Non-participation | *State how many participants dropped out/declined participation and the reason(s) given OR provide response rate OR state that no participants dropped out/declined participation.* |
| Randomization | *If participants were not allocated into experimental groups, state so OR describe how participants were allocated to groups, and if allocation was not random, describe how covariates were controlled.* |

# Ecological, evolutionary & environmental sciences study design

All studies must disclose on these points even when the disclosure is negative.

| | |
|---|---|
| Study description | *Briefly describe the study. For quantitative data include treatment factors and interactions, design structure (e.g. factorial, nested, hierarchical), nature and number of experimental units and replicates.* |
| Research sample | *Describe the research sample (e.g. a group of tagged Passer domesticus, all Stenocereus thurberi within Organ Pipe Cactus National Monument), and provide a rationale for the sample choice. When relevant, describe the organism taxa, source, sex, age range and any manipulations. State what population the sample is meant to represent when applicable. For studies involving existing datasets, describe the data and its source.* |
| Sampling strategy | *Note the sampling procedure. Describe the statistical methods that were used to predetermine sample size OR if no sample-size calculation was performed, describe how sample sizes were chosen and provide a rationale for why these sample sizes are sufficient.* |
| Data collection | *Describe the data collection procedure, including who recorded the data and how.* |
| Timing and spatial scale | *Indicate the start and stop dates of data collection, noting the frequency and periodicity of sampling and providing a rationale for these choices. If there is a gap between collection periods, state the dates for each sample cohort. Specify the spatial scale from which the data are taken* |
| Data exclusions | *If no data were excluded from the analyses, state so OR if data were excluded, describe the exclusions and the rationale behind them, indicating whether exclusion criteria were pre-established.* |
| Reproducibility | *Describe the measures taken to verify the reproducibility of experimental findings. For each experiment, note whether any attempts to repeat the experiment failed OR state that all attempts to repeat the experiment were successful.* |
| Randomization | *Describe how samples/organisms/participants were allocated into groups. If allocation was not random, describe how covariates were controlled. If this is not relevant to your study, explain why.* |
| Blinding | *Describe the extent of blinding used during data acquisition and analysis. If blinding was not possible, describe why OR explain why blinding was not relevant to your study.* |

Did the study involve field work? ☐ Yes ☐ No

## Field work, collection and transport

| | |
|---|---|
| Field conditions | *Describe the study conditions for field work, providing relevant parameters (e.g. temperature, rainfall).* |
| Location | *State the location of the sampling or experiment, providing relevant parameters (e.g. latitude and longitude, elevation, water depth).* |
| Access & import/export | *Describe the efforts you have made to access habitats and to collect and import/export your samples in a responsible manner and in compliance with local, national and international laws, noting any permits that were obtained (give the name of the issuing authority, the date of issue, and any identifying information).* |
| Disturbance | *Describe any disturbance caused by the study and how it was minimized.* |

# Reporting for specific materials, systems and methods

We require information from authors about some types of materials, experimental systems and methods used in many studies. Here, indicate whether each material, system or method listed is relevant to your study. If you are not sure if a list item applies to your research, read the appropriate section before selecting a response.

### Materials & experimental systems

| n/a | Involved in the study |
|---|---|
| ☐ | ☒ Antibodies |
| ☐ | ☒ Eukaryotic cell lines |
| ☒ | ☐ Palaeontology and archaeology |
| ☐ | ☒ Animals and other organisms |
| ☐ | ☒ Clinical data |
| ☒ | ☐ Dual use research of concern |
| ☒ | ☐ Plants |

### Methods

| n/a | Involved in the study |
|---|---|
| ☒ | ☐ ChIP-seq |
| ☐ | ☒ Flow cytometry |
| ☒ | ☐ MRI-based neuroimaging |

## Antibodies

Antibodies used

Brilliant Violet 650m anti-mouse CDllc Antibody ;Biolegend;117339; Clone N418 PE anti CDllc;BD bioscience;553802; Clone HL3
PE anti-mouse NK-1.l Antibody ;Biolegend;l56504; Clone S17016D
FITC Anti-Mouse CD3e;Tonbo;35-0031-U500; clone 145-2C11
Anti-mouse B220-FITC;eBioscience;ll-0452-82; clone RA3-6B2
PerCP anti-mouse/human CD45R/B220 Antibody;Biolegend;l03234; Clone RA3-6B2
Anti-Human/Mouse CD45R (B220) PerCP-Cy5.5;eBioscience;45-0452-82; clone RA3-6B2
Brilliant Violet 605m anti-mouse/human CDllb Antibody;Biolegend;l01237; Clone M1/70
anti-mouse CDllb eFluor 660;eBioscience;50-0112-80; Clone M1/70
Anti-Mouse CDllb PerCP-Cyanine5.5;eBioscience;45-0112-82; Clone M1/70
Anti-mouse CD206-eF450 ;eBioscience;48-2069-42; Clone 19.2
PE anti-mouse CD31 Antibody;Biolegend;l02407; Clone 390
Anti-mouse CD4-BV570;Biolegend;l00542; Clone RM4-5
PE/Cy7 anti-mouse CD4 Antibody;Biolegend;l00528 ; Clone RM4-5
Anti-Mouse CD45 APC-eFluor" 780;eBioscience;47-0451-82 ; Clone 30-F11
PE anti-mouse CD49b (pan-NK cells) Antibody;Biolegend;l08908 ; Clone DX5
Anti-mouse CD8-PE;eBioscience;12-0081-83; Clone 53-6.7
CD86 (B7-2) Monoclonal Antibody (Gll), PE-Cyanine7;eBioscience;25-0862-80 ; Clone GL1
CD90.2 Rat anti-Mouse, BUV805, Clone: 53-2.l;BD Biosciences;BDB741908; Clone 53-2.1
BV786 Rat Anti-Mouse CD90.2 Clone 30-H12 (RUO);BD Biosciences; 740841; Clone 53-21
PerCP/CyS.5 anti-mouse F4/80 Antibody;Biolegend;123128; Clone BM8
anti-mouse/rat Foxp3 FITC FJK-16s;eBioscience;ll-5773-82; Clone FJK-16s
Anti-mouse Ly6C-BV711;Biolegend;128037 ; Clone HK1.4
ANTI-MOUSE LY6G PE ;BD PHARMINGEN;551461; Clone 1A8
APC rat anti-Mouse Ly6G ;BD PHARMINGEN;560599; Clone 1A8
anti-Ly6G v450;BD PHARMINGEN;560603; Clone 1A8
Alexa Fluor" 700 anti-mouse I-A/1-E [M5/114.15.2];Biolegend; 107622 ; Clone M5/114.15.2
Anti-mouse MHCII-UV737;BD Biosciences;367-5321-82; Clone M5/114.15.2
Phospho-S6 Ribosomal Protein (Ser235/236) (D57.2.2E) XP® Rabbit mAb;Cell signaling;4858S; Clone D57.2.2.E Anti-Mouse ROR gamma (t) APC;eBioscience;l 7-6981-80 ; Clone B2D
PE Rat Anti-Mouse Siglec-F Clone ES0-2440 (RUO);BD PHARMINGEN;552126; Clone E50-2440
Anti-mouse SiglecH FITC;eBioscience;ll-0333-81; eBIO440c
Anti-mouse T-bet-PECF594;BD Biosciences;562467; Clone O4-46
Mouse VCAM-1/CD106 Alexa Fluor® 594-conjugated Antibody;biotechne;FAB6432T; Clone 112734
Brilliant Violet 78S'M anti-mouse/rat XCRl Antibody;Biolegend;148225 ; Clone ZET

| | |
|---|---|
| Validation | All antibodies are validated by the manufacturer<br><br>https://www.biolegend.com/en-gb/products/brilliant-violet-650-anti-mouse-cd11c-antibody-8840<br>https://www.fishersci.com/shop/products/anti-cd11c-r-pe-clone-hl3bd/BDB553802<br>https://www.biolegend.com/en-us/products/pe-anti-mouse-nk-1-1-antibody-16926?GroupID=GROUP20<br>https://www.citeab.com/antibodies/2204479-35-0031-u500-anti-mouse-cd3e<br>https://www.thermofisher.com/antibody/product/CD45R-B220-Antibody-clone-RA3-6B2-Monoclonal/11-0452-82<br>https://www.biolegend.com/fr-ch/search-results/percp-anti-mouse-human-cd45r-b220-antibody-4266?Clone=RA3-6B2<br>https://www.thermofisher.com/antibody/product/CD45R-B220-Antibody-clone-RA3-6B2-Monoclonal/45-0452-82<br>https://www.biolegend.com/en-us/products/brilliant-violet-605-anti-mouse-human-cd11b-antibody-7637?GroupID=BLG10530<br>https://www.thermofisher.com/antibody/product/CD11b-Antibody-clone-M1-70-Monoclonal/50-0112-82<br>https://www.thermofisher.com/antibody/product/CD11b-Antibody-clone-M1-70-Monoclonal/45-0112-82<br>https://www.thermofisher.com/antibody/product/CD206-MMR-Antibody-clone-19-2-Monoclonal/48-2069-42<br>https://www.biolegend.com/nl-nl/products/pe-anti-mouse-cd31-antibody-122<br>https://www.biolegend.com/nl-be/products/brilliant-violet-570-anti-mouse-cd4-antibody-7379<br>https://www.biolegend.com/en-us/cell-separation/pe-cyanine7-anti-mouse-cd4-antibody-1932<br>https://www.thermofisher.com/antibody/product/CD45-Antibody-clone-30-F11-Monoclonal/47-0451-82<br>https://www.biolegend.com/en-gb/products/pe-anti-mouse-cd49b-pan-nk-cells-antibody-234?GroupID=BLG4768<br>https://www.citeab.com/antibodies/2037994-12-0081-82-cd8a-monoclonal-antibody-53-6-7-pe-eb<br>https://www.thermofisher.com/antibody/product/CD86-B7-2-Antibody-clone-GL1-Monoclonal/25-0862-82<br>https://www.fishersci.com/shop/products/cd90-2-rat-anti-mouse-buv805-clone-53-2-1-bd-biosciences/BDB741908<br>https://www.biolegend.com/en-us/products/percp-cyanine5-5-anti-mouse-f480-antibody-4303?GroupID=BLG5319<br>https://www.citeab.com/antibodies/2041744-11-5773-82-foxp3-monoclonal-antibody-fjk-16s-fitc<br>https://www.biolegend.com/en-us/products/brilliant-violet-711-anti-mouse-ly-6c-antibody-8935?GroupID=BLG7242<br>https://www.citeab.com/antibodies/2410368-551461-bd-pharmingen-pe-rat-anti-mouse-ly-6g<br>https://www.citeab.com/antibodies/2410938-560599-bd-pharmingen-apc-rat-anti-mouse-ly-6g<br>https://www.citeab.com/antibodies/2408945-560603-bd-horizon-v450-rat-anti-mouse-ly-6g<br>https://www.biolegend.com/fr-ch/products/alexa-fluor-700-anti-mouse-i-a-i-e-antibody-3413<br>https://www.bdbiosciences.com/en-ca/products/reagents/flow-cytometry-reagents/research-reagents/single-color-antibodies-ruo/bv786-rat-anti-mouse-i-a-i-e.742894<br>https://www.cellsignal.com/products/primary-antibodies/phospho-s6-ribosomal-protein-ser235-236-d57-2-2e-xp-rabbit-mab/4858<br>https://www.labome.com/product/Invitrogen/17-6981-80.html<br>https://www.citeab.com/antibodies/2411876-552126-bd-pharmingen-pe-rat-anti-mouse-siglec-f<br>https://www.labome.com/product/Invitrogen/11-0333-82.html<br>https://www.bdbiosciences.com/en-de/products/reagents/flow-cytometry-reagents/research-reagents/single-color-antibodies-ruo/pe-cf594-mouse-anti-t-bet.562467<br>https://www.bio-techne.com/p/antibodies/mouse-vcam-1-cd106-alexa-fluor-594-conjugated-antibody-112734_fab6432t<br>https://www.biolegend.com/fr-ch/products/brilliant-violet-785-anti-mouse-rat-xcr1-antibody-16711 |

## Eukaryotic cell lines

Policy information about cell lines and Sex and Gender in Research

| | |
|---|---|
| Cell line source(s) | Mouse aortic endothelial cells (MAECs) were isolated from mouse thoracic aortas as described previously23. Cells were cultured in Medium 199 (Gibco, Invitrogen Life Technologies) + 20% fetal bovine serum + Penicillin/Streptomycin 2 mM + Glutamine 2 mM + HEPES 10 mM + endothelial cell growth supplement 30µg/mL + Heparin 100 mg/mL, all from Sigma–Aldrich, under 5% CO2 at 37ºC.<br><br>Mouse embryo fibroblast (MEF) cell lines were isolated from 13.5 dpc from embryos using standard protocol. Each embryo was dissected into 10 ml of sterile PBS, voided of its internal organs, head, and legs. After 30 min incubation with gentle shaking at 37°C with 5ml 0,1 % trypsin, cells were plated in two 100 mm dishes and incubated for 24-48 h.To establish the immortalized MEF lines, early passage MEFs were seeded in 60 mm plates and infected with 10E5 IU/ml packaged retrovirus carrying the human papillomavirus (HPV) 16 E6/E7 genes. Selection was performed with 400 µg/ml of G418 during 10 days.<br><br>L929 cell line (ATCC® CCL-1TM) used for production of the M-CSF supernatant, was grown on 175 cm2 cell culture flasks (Stemcell) and resuspended in RPMI 1640 (Sigma) supplemented with 10 % heat-inactivated fetal calf serum (FCS, Sigma), 1 mM pyruvate (Lonza, Bassel, Switzerland), 100 µM non-essential aminoacids (Thermo Fisher Scientific, Walthman, MA), 2 mM L-glutamine, 100 U/ml penicillin, 100 µg/ml streptomycin (all three from Lonza) and 50 µM 2-mercaptoethanol (Merck, Darmstad,Germany), herein called R10. Supernatants were obtained by filtering 15-days long cultures through 0.22µm Stericup Filter units (Merck Millipore) and were used to subsequently supplement the medium for the generation of bone marrow derived macrophages.<br><br>Bone marrow derived macrophages (BMDMs) were generated as previously described with some modifications. BM cells from WT C57BL/6J mice were cultured in RPMI 1640 supplemented with 30 % M-CSF obtained from L929 cell line and 10 % FBS, 100 µg/ml penicillin, 100 µg/ml streptomycin, 10 mM HEPES, 1nM sodium pyruvate (all from Gibco) during 5 days in sterile, but not tissue-culture treated, 10-cm Petri dishes. |
| Authentication | L929 were directly purchased from ATCC (ATCC® CCL-1TM). The rest of cells used were primary lines. Primary cell lines were identified by morphology and phenotype characterization by flow cytometry. |
| Mycoplasma contamination | All cells lines were continuously surveyed and tested negative for mycoplasma contamination by PCR. |
| Commonly misidentified lines (See ICLAC register) | No commonly misidentified cell lines were used in the study |

## Palaeontology and Archaeology

| | |
|---|---|
| Specimen provenance | *Provide provenance information for specimens and describe permits that were obtained for the work (including the name of the issuing authority, the date of issue, and any identifying information). Permits should encompass collection and, where applicable, export.* |
| Specimen deposition | *Indicate where the specimens have been deposited to permit free access by other researchers.* |
| Dating methods | *If new dates are provided, describe how they were obtained (e.g. collection, storage, sample pretreatment and measurement), where they were obtained (i.e. lab name), the calibration program and the protocol for quality assurance OR state that no new dates are provided.* |

☐ Tick this box to confirm that the raw and calibrated dates are available in the paper or in Supplementary Information.

| | |
|---|---|
| Ethics oversight | *Identify the organization(s) that approved or provided guidance on the study protocol, OR state that no ethical approval or guidance was required and explain why not.* |

Note that full information on the approval of the study protocol must also be provided in the manuscript.

## Animals and other research organisms

Policy information about studies involving animals; ARRIVE guidelines recommended for reporting animal research, and Sex and Gender in Research

| | |
|---|---|
| Laboratory animals | All mice (Mus musculus) were housed at an ambient temperature around 21-23 C°, humidity of 40-60% and a light dark cycle of 12 hours. Mice were bred and maintained in groups of 5 animals per cage at the CNIC under specific pathogen-free conditions.<br>We used proatherogenic background B6.129P2-Apoetm1Unc/J mice (The Jackson Laboratory,strain 002052, ApoE−/−); and B6.129S7-Ldlrtm1Her/J mice (The Jackson Laboratory, strain 002207, Ldlr−/−) backcrossed with B6.SJL-Ptprca Pepcb/BoyJ mice expressing the CD45.1 congenic marker (The Jackson Laboratory, strain 002014, B6 CD45.1). For initiation of experiments, 6-8 week-old male mice were used.<br>Rag1tm1Mom/J mice (The Jackson Laboratory, strain 002216, Rag1−/−); B6.Cg-Rptortm1.1Dmsa/J mice (The Jackson Laboratory, strain 013188, RaploxP) were mated with B6.129P2-Lyz2tm1(cre)Ifo/J mice (The Jackson Laboratory, strain 004781, Lyz2-Cre) to generate Lyz2ΔRaptor (Cre+) and control Raptorf/f (Cre−) littermates used as controls. Sperm from B6.Nischtm1a(EUCOMM)Hmgu>/H mice (Mary Lyon Centre at MRC Harwell, United, EM:08808) was used for in vitro fertilization of ROSA-Flpe mice (Gt(ROSA)26Sortm1(FLP1)Dym) to generate Nischf/f mice (tm1c). Nischf/f mice were mated with Lyz2-Cre (B6.129P2-Lyz2tm1(cre)Ifo/J) mice to generate Lyz2ΔNisch (Cre+) and control Nischf/f (Cre−) littermates used as controls. |
| Wild animals | No wild animals were used in the study |
| Reporting on sex | Our findings in mouse models include both males and females. The human cohorts also include female participants that account for the 22% and the 54% of the whole PESA and IGT cohorts, respectively. |
| Field-collected samples | No field collected samples were used in the study. |
| Ethics oversight | Animal studies were approved by the local ethics committee. All animal procedures conformed to EU Directive 2010/63EU and Recommendation 2007/526/EC regarding the protection of animals used for experimental and other scientific purposes, enforced by Spanish law under Real Decreto 1201/2005. |

Note that full information on the approval of the study protocol must also be provided in the manuscript.

## Clinical data

Policy information about clinical studies

All manuscripts should comply with the ICMJE guidelines for publication of clinical research and a completed CONSORT checklist must be included with all submissions.

| | |
|---|---|
| Clinical trial registration | The discovery cohort was conducted in a subset of participants from the PESA-CNIC-Santander study (Progression of Early Subclinical Atherosclerosis): NCT01410318 (https://clinicaltrials.gov/ct2/show/NCT01410318).<br>The IGT cohort used for the validation was approved by Ethics Review Board in Gothenburg (IGTM [560-13]) |
| Study protocol | Volunteers were recruited following the inclusion and exclusion criteria of the main PESA-CNIC-Santander study https://clinicaltrials.gov/ct2/show/NCT01410318.<br>Exclusion criteria for the IGT study were: known diabetes, inflammatory diseases (e.g. Crohn's disease, ulcerative colitis, rheumatic diseases), treatment with steroids or immunomodulatory drugs, cancer (unless relapse free for the preceding 5 years), cognitive dysfunction, treatment for infectious diseases and with antibiotics in the past three months, inability to understand written and spoken Swedish as well as subjects born outside Sweden. |
| Data collection | For the PESA study, plasma and faecal samples were collected from December 2018 to May 2021. Metabolomics data were collected and analysed in 2021. 16S gene sequencing data was collected and analysed in 2022.<br>In the IGT cohort, men and women aged 50 to 64 years and born in the region of Gothenburg, Sweden, were screened between 2013 |

and 2018. Metabolomics data were collected and analysed in 2023.

Outcomes

For the PESA ohort, blood and stool samples were collected from the participants followed by targeted mass spectrometry and 16S rRNA gene sequencing, respectively. Subclinical atherosclerosis was assessed by assessed by imaging studies including 2D and 3D vascular ultrasonography of carotid and iliofemoral arteries and presence of coronary artery calcium assessed by CT scan (PMID:24268213). Subjects with subclinical AT underwent a whole body 18F-FDG PET/MRI study to characterize arterial 18F-FDG uptake and bone marrow metabolic activity (PMID:30922468 and PMID: 35567559, respectively). Fasting blood test included biochemistry and determination of high-sensitivity C-reactive protein (hs-CRP). In this study, hypertension (HTN) was as systolic > 130 mmHg and/or diastolic > 85 mmHg and/or subjects taking antihypertensive drugs. Dyslipidaemia was defined as total cholesterol ≥ 240 mg/dL, LDL-cholesterol ≥160 mg/dL, HDL-cholesterol < 40 mg/dL, or use of lipid-lowering drugs. Anthropometry and bioelectrical impedance analysis assessments were performed during the same appointment for each participant. Height and weight were measured using calibrated equipment (Tanita BC-545N,) with participants wearing underwear and barefoot. BMI was calculated as weight (kg) divided by height squared (metre).
For the IGT cohort blood samples were collected from the participants followed by targeted mass spectrometry. Atherosclerosis in the carotid arteries was assessed by ultrasound imaging using a standardized protocol including a Siemens Acuson S2000 ultrasound scanner and by presence of coronary artery calcium assessed by CT scan. Systolic blood pressure (SBP) was measured twice with an automatic device (Omron M10-IT, Omron Health care Co, Kyoto, Japan) and the mean of the measurements was used. A questionnaire was used to collect detailed information on medication and family history. SCORE2 (Systematic Coronary Risk Evaluation) was calculated as previously. Body weight, height waist and hip circumferences were measured on calibrated equipment with subjects dressed in light clothing without shoes and according to current WHO recommendations.

The targeted metabolomics analyses showed that imidazole propionate (ImP), but not histidine or urocanic acid, plasma concentrations were selectively increased in subjects with subclinical atherosclerosis when compared to controls. Linear and nonlinear associations were also observed between ImP concentrations and atherosclerosis and extent of atherosclerosis, respectively. The prevalence of atherosclerosis endpoints and the CAC score also increased across ascending ImP tertiles. These findings were validated in an independent cohort, the IGT cohort. ImP was also found significantly increased in subjects with metabolically active atherosclerosis (FDG+) when compared to inactive atherosclerosis, particularly those with bone marrow activation (FDG+_BM) and systemic inflammation (FDG+_SYS). After adjusting for traditional risk factors in both cohorts, higher ImP levels were independently associated with main atherosclerosis outcomes, suggesting high ImP levels as indicator of heightened atherosclerosis risk. Notably, ImP also showed additive value when added to established blood-derived atherosclerosis biomarkers such as LDL-cholesterol and high sensitive C reactive protein (hs-CRP) in discriminating atherosclerosis prevalence in both cohorts and active atherosclerosis in the PESA cohort. These findings reveal a strong association between ImP and atherosclerosis, particularly active atherosclerosis, suggesting its potential use as an indicator of early active atherosclerosis before other co-morbidities become confounding factors.

## Dual use research of concern

Policy information about dual use research of concern

### Hazards

Could the accidental, deliberate or reckless misuse of agents or technologies generated in the work, or the application of information presented in the manuscript, pose a threat to:

| No | Yes | |
|---|---|---|
| ☐ | ☐ | Public health |
| ☐ | ☐ | National security |
| ☐ | ☐ | Crops and/or livestock |
| ☐ | ☐ | Ecosystems |
| ☐ | ☐ | Any other significant area |

### Experiments of concern

Does the work involve any of these experiments of concern:

| No | Yes | |
|---|---|---|
| ☐ | ☐ | Demonstrate how to render a vaccine ineffective |
| ☐ | ☐ | Confer resistance to therapeutically useful antibiotics or antiviral agents |
| ☐ | ☐ | Enhance the virulence of a pathogen or render a nonpathogen virulent |
| ☐ | ☐ | Increase transmissibility of a pathogen |
| ☐ | ☐ | Alter the host range of a pathogen |
| ☐ | ☐ | Enable evasion of diagnostic/detection modalities |
| ☐ | ☐ | Enable the weaponization of a biological agent or toxin |
| ☐ | ☐ | Any other potentially harmful combination of experiments and agents |

## Plants

Seed stocks

*Report on the source of all seed stocks or other plant material used. If applicable, state the seed stock centre and catalogue number. If plant specimens were collected from the field, describe the collection location, date and sampling procedures.*

Novel plant genotypes

*Describe the methods by which all novel plant genotypes were produced. This includes those generated by transgenic approaches, gene editing, chemical/radiation-based mutagenesis and hybridization. For transgenic lines, describe the transformation method, the number of independent lines analyzed and the generation upon which experiments were performed. For gene-edited lines, describe the editor used, the endogenous sequence targeted for editing, the targeting guide RNA sequence (if applicable) and how the editor was applied.*

Authentication

*Describe any authentication procedures for each seed stock used or novel genotype generated. Describe any experiments used to assess the effect of a mutation and, where applicable, how potential secondary effects (e.g. second site T-DNA insertions, mosiacism, off-target gene editing) were examined.*

## ChIP-seq

### Data deposition

☐ Confirm that both raw and final processed data have been deposited in a public database such as GEO.

☐ Confirm that you have deposited or provided access to graph files (e.g. BED files) for the called peaks.

Data access links
*May remain private before publication.*

*For "Initial submission" or "Revised version" documents, provide reviewer access links. For your "Final submission" document, provide a link to the deposited data.*

Files in database submission

*Provide a list of all files available in the database submission.*

Genome browser session
(e.g. UCSC)

*Provide a link to an anonymized genome browser session for "Initial submission" and "Revised version" documents only, to enable peer review. Write "no longer applicable" for "Final submission" documents.*

### Methodology

Replicates

*Describe the experimental replicates, specifying number, type and replicate agreement.*

Sequencing depth

*Describe the sequencing depth for each experiment, providing the total number of reads, uniquely mapped reads, length of reads and whether they were paired- or single-end.*

Antibodies

*Describe the antibodies used for the ChIP-seq experiments; as applicable, provide supplier name, catalog number, clone name, and lot number.*

Peak calling parameters

*Specify the command line program and parameters used for read mapping and peak calling, including the ChIP, control and index files used.*

Data quality

*Describe the methods used to ensure data quality in full detail, including how many peaks are at FDR 5% and above 5-fold enrichment.*

Software

*Describe the software used to collect and analyze the ChIP-seq data. For custom code that has been deposited into a community repository, provide accession details.*

## Flow Cytometry

### Plots

Confirm that:

☒ The axis labels state the marker and fluorochrome used (e.g. CD4-FITC).

☒ The axis scales are clearly visible. Include numbers along axes only for bottom left plot of group (a 'group' is an analysis of identical markers).

☒ All plots are contour plots with outliers or pseudocolor plots.

☒ A numerical value for number of cells or percentage (with statistics) is provided.

### Methodology

Sample preparation

For blood samples, after erythrocytes lysis buffer, single cell suspensions were stained for 30 min at 4°C with LIVE/DEAD Fixable Aqua Dead Cell Stain Kit (Life Technologies). After washing with PBS, cells were stained in FACS buffer containing anti-CD16/32 (BioXcell), 3 % FBS and 0.05 % EDTA with the corresponding antibody cocktail for 30 min on ice. Cells were stained with a cocktail of antibodies.

For cells infiltrating the in aorta, mice were perfused with 10 ml of Phosphate Buffered Saline (PBS) via cardiac puncture to remove blood contamination from vascular tissue.

The aortas were kept in cold Dulbecco's Modified Eagle Medium (DMEM) to be digested. Perivascular fat was removed and the thoracic aorta with arch was opened longitudinally and cut into smaller pieces that were incubated for 30 min at 37oC in water bath in digestion buffer (Collagenase A (25 mg/ml), (Roche/Sigma #10103586001). Dispase II (25 mg/ml), (Roche/ Sigma #04942078001), DNase I (250µg/ml) (Roche/Sigma #10104159001) elastase (25 µg/ml) and Libersase TL (0.2 Wünsch units/mL) Cat#5401119001. After incubation time the digested tissue was mixed by pipetting, filtered through a 70 µm strainer and spinned at 400g 5 min 4C. Single cells were stained with a cocktail of antibodies.

Instrument

LSRFortessa SORP (BD Biosciences)
FACSymphony (BD Biosciences)
FACSAria Cell Sorter (BD Biosciences)

Software

FlowJo software version 10 (TreeStar)

Cell population abundance

The number of cells is indicated in the respective graph corresponding to each population.

Gating strategy

Gating strategy on blood and aorta tissues:

1. FSC and SSC
2. FSC-H and FSC-A to gate on single cell population
3. Viability to gate on live cells, this is defined as negative cells to staining
4. CD45+ cells
5. CD90 cells for T cells, B220 cell for B cells and non t or b cells as double negative.
6. In CD90-;B220-; was further gated on Ly6C high Monocytes
7. In CD90-;B220-; was further gated on F4/80+CD86+ and F4/80+CD11c+ (Macrophages)
8. CD90 cells was further gated CD4+Rorg-t+ (Th17), CD4+t-Bet+ (Th1), CD4+Foxp3+ (Treg)

Gating strategy on blood to isolated monocytes:

1. FSC and SSC
2. FSC-H and FSC-A to gate on single cell population
3. Viability to gate on live cells, this is defined as negative cells to staining
4. CD45+ cells
5. CD3-, B220-, NK1.1-, LY6G-, CD49-, SiglecF- cells
6. Monocytes was gated as CD11B+ and Ly6C+/-

☒ Tick this box to confirm that a figure exemplifying the gating strategy is provided in the Supplementary Information.

# Magnetic resonance imaging

## Experimental design

Design type

*Indicate task or resting state; event-related or block design.*

Design specifications

*Specify the number of blocks, trials or experimental units per session and/or subject, and specify the length of each trial or block (if trials are blocked) and interval between trials.*

Behavioral performance measures

*State number and/or type of variables recorded (e.g. correct button press, response time) and what statistics were used to establish that the subjects were performing the task as expected (e.g. mean, range, and/or standard deviation across subjects).*

## Acquisition

Imaging type(s)

*Specify: functional, structural, diffusion, perfusion.*

Field strength

*Specify in Tesla*

Sequence & imaging parameters

*Specify the pulse sequence type (gradient echo, spin echo, etc.), imaging type (EPI, spiral, etc.), field of view, matrix size, slice thickness, orientation and TE/TR/flip angle.*

Area of acquisition

*State whether a whole brain scan was used OR define the area of acquisition, describing how the region was determined.*

Diffusion MRI ☐ Used ☐ Not used

## Preprocessing

Preprocessing software

*Provide detail on software version and revision number and on specific parameters (model/functions, brain extraction, segmentation, smoothing kernel size, etc.).*

Normalization

*If data were normalized/standardized, describe the approach(es): specify linear or non-linear and define image types used for transformation OR indicate that data were not normalized and explain rationale for lack of normalization.*

Normalization template

*Describe the template used for normalization/transformation, specifying subject space or group standardized space (e.g. original Talairach, MNI305, ICBM152) OR indicate that the data were not normalized.*

Noise and artifact removal

*Describe your procedure(s) for artifact and structured noise removal, specifying motion parameters, tissue signals and physiological signals (heart rate, respiration).*

Volume censoring

*Define your software and/or method and criteria for volume censoring, and state the extent of such censoring.*

## Statistical modeling & inference

Model type and settings

*Specify type (mass univariate, multivariate, RSA, predictive, etc.) and describe essential details of the model at the first and second levels (e.g. fixed, random or mixed effects; drift or auto-correlation).*

Effect(s) tested

*Define precise effect in terms of the task or stimulus conditions instead of psychological concepts and indicate whether ANOVA or factorial designs were used.*

Specify type of analysis: ☐ Whole brain ☐ ROI-based ☐ Both

Statistic type for inference

*Specify voxel-wise or cluster-wise and report all relevant parameters for cluster-wise methods.*

(See Eklund et al. 2016)

Correction

*Describe the type of correction and how it is obtained for multiple comparisons (e.g. FWE, FDR, permutation or Monte Carlo).*

## Models & analysis

| n/a | Involved in the study |
|---|---|
| ☐ | ☐ Functional and/or effective connectivity |
| ☐ | ☐ Graph analysis |
| ☐ | ☐ Multivariate modeling or predictive analysis |

Functional and/or effective connectivity

*Report the measures of dependence used and the model details (e.g. Pearson correlation, partial correlation, mutual information).*

Graph analysis

*Report the dependent variable and connectivity measure, specifying weighted graph or binarized graph, subject- or group-level, and the global and/or node summaries used (e.g. clustering coefficient, efficiency, etc.).*

Multivariate modeling and predictive analysis

*Specify independent variables, features extraction and dimension reduction, model, training and evaluation metrics.*